USING LOCAL AND REGIONAL AIR QUALITY MODELING AND SOURCE APPORTIONMENT TOOLS TO EVALUATE VEHICLES AND BIOGENIC EMISSION FACTORS

A Dissertation

by

SRI HARSHA KOTA

Submitted to the Office of Graduate and Professional Studies of
Texas A&M University
in partial fulfillment of the requirements for the degree of

DOCTOR OF PHILOSOPHY

Chair of Committee,	Qi Ying
Committee Members,	Bill Batchelor
	Gunnar Schade
	Yunlong Zhang
Head of Department,	Robin Autenrieth

August 2014

Major Subject: Civil Engineering

ABSTRACT

Carbon Monoxide (CO), oxides of nitrogen (NO_x) and volatile organic compounds (VOCs) affect human health, and can also play a significant role in tropospheric ozone and secondary particulate matter formation. Correctly estimating the anthropogenic emission rates of these species is important for their effective control. Additionally, isoprene from biogenic sources also plays a key role in tropospheric ozone and secondary organic aerosol (SOA) formation. In this study, emission factors and inventories of CO, NO_x and VOCs from on-road vehicles estimated by vehicle emission factor models and biogenic emissions of isoprene estimated by a popular biogenic emission model are evaluated using local and regional scale air quality modeling and source apportionment tools supplemented by concentration and flux data collected at surface and in the upper air.

The USEPA's Motor Vehicle Emission Simulator (MOVES) model is evaluated. Local scale analysis indicates over-estimation of NO_x by approximately 15%, based on the curbside data collected near a high diesel traffic rural highway and the predicted NO_x by the TAMU Near-Road Model. The regional scale analysis conducted using the observed NO_x at a number of surface air quality monitoring sites in southeast Texas (ST) and a source-oriented Community Air Quality Model (SCMAQ), a regional chemical transport model, suggests an over-estimation of NO_x emissions by approximately 35-55% using the MOVES-based NEI.

The near-road analysis also reveals that NO_2/NO_x ratio at curbside is approximately 29%, much higher than the generally used 5% ratio. This increase in ratio resulted in predicted 8-hour ozone increase in ST by as much as 6 ppb. While the near-road analysis didn't reveal significant overestimation in CO emissions due to high background concentrations and low emissions, the regional analysis showed that CO emission were overestimated by approximately 60% by the MOVES model.

Finally, VOC emissions estimated by the MOVES model were evaluated using fluxes of 18 VOCs measured on a tall tower in urban Houston during 2008. Vehicle

contributions to the observed flux were determined using the Multilinear Engine (ME-2), a receptor-oriented source apportionment model. Emission factors of vehicle exhaust and evaporative emissions were estimated using a flux footprint model and the contributions resolved by ME-2. The MOVES model estimates vehicle exhaust emissions well, but severely under-estimates evaporative emissions from parked vehicles.

The Model of Emissions of Gases and Aerosol from Nature (MEGAN) estimations of isoprene, the dominant biogenic VOC, in ST were also evaluated using SCMAQ. Comparison of predicted and observed isoprene concentrations at the surface layer and upper layers revealed a significant over-prediction of isoprene in urban areas and necessity of decreasing biogenic emission reduction by 2/3rd. The over-predictions of isoprene had negligible effects on predicted ozone concentrations in ST, but the isoprene generated SOA can be overestimated by as much as 50%.

DEDICATION

I would like to dedicate this work to omnipresent God for treating me as his son and playing several roles not limited to parents, grandparents, siblings, relatives, friends and faculty advisors.

ACKNOWLEDGEMENTS

I would like thank my research advisor Dr. Qi Ying, for his tremendous support and encouragement throughout my graduate school. I will be indebted to him for his efforts. I am also thankful to Dr. Gunnar Schade for his magnanimous patience during the analysis of measured volatile organic compound fluxes. I am honored to have Dr. Bill Batchelor and Dr. Yunlong Zhang as my research committee members. I am also grateful to Dr. Josias Zietsman for attending my final dissertation defense.

I also thank my parents, the United States Environmental Protection Agency and Zachry department of Civil Engineering for their financial support during my doctoral study.

TABLE OF CONTENTS

Page

LIST OF FIGURES

Page

LIST OF TABLES

Page

1. INTRODUCTION

Gaseous air pollutants have significant effects on respiratory (Chauhan et al., 1998; Uysal and Schapira, 2003; Wegmann et al., 2005), digestive (Mandal, 2005), nervous and cardiovascular (Badman and Jaffe, 1996; Burnett et al., 1997; Burnett et al., 1999) and urinary (Chang et al., 2010) systems, and radiative forcing (Daniel and Solomon, 1998; Pacifico et al., 2009). Among the gaseous pollutants, CO, NO_x and Ozone are recognized as criteria pollutants, and several volatile organic compounds (VOCs) fall under hazardous air pollutants category by the United States Environmental Protection Agency (US EPA). While NO_x and VOCs directly involve in the formation of tropospheric ozone (Kleinman et al., 2005; Li et al., 2007), CO plays an important role by changing the abundance of hydroxyl radicals (Isaksen and Hov, 1987). This makes the role of NO_x, CO and VOCs in the atmosphere pivotal.

Southeast Texas which is famous for its high density of industrial facilities located in the Houston-Galveston Bay (HGB) and Beaumont-Port Arthur (BPA) areas, houses Houston, the fourth-largest city in the US. Enormous amounts of NO_x and VOCs in addition to high temperatures, intensive solar radiation and land-sea breeze circulations resulted in frequent violations of National Ambient Air Quality Standards (NAAQS) for ozone in this region (Banta et al., 2005; Kleinman et al., 2002). To design efficient control strategies for ozone, it is necessary to quantitatively evaluate various types of CO, NO_x and VOC emission sources.

Recent studies in Southeast Texas indicated that motor vehicles are significant contributors to CO (Buzcu Guven and Olaguer, 2011; Rappenglück et al., 2013), NO_x (Zhang and Ying, 2011a) and VOCs (Buzcu and Fraser, 2006; Ying and Krishnan, 2010). Estimating emissions from on-road mobile sources, using an emission factor model, is a key factor in studying the influence of motor vehicles on air quality. The estimated emissions are influenced by various parameters including vehicle type, age, speed, road, fuel type, mode of operation and meteorology. Emission factor models can be briefly divided into average speed and modal operation models. While analyzing

signal coordination and traffic congestion planning, a model which considers modes of vehicle operation is more beneficiary. But for studying the regional air quality an average speed model could be sufficient.

In a modal operation model, second by second driving modes of a vehicle i.e. idle, acceleration/deceleration, cruise etc. are used to estimate emissions. For example, Comprehensive Modal Emissions Model (CHEM) (Scora and Barth, 2006) developed by University of California-Riverside is a graphical user interface model which estimates CO, carbon dioxide, NO_x and hydrocarbons using the transient operation modes of vehicles. In this model, the vehicles are classified to normal and high emitting light duty and heavy duty vehicles. Each of the classes is subcategorized based on the engine power, weight, mileage and technology used.

In an average speed model, the emission factors generated would be based on the average speed of vehicle. For example, Emission Factor Model (EMFAC) (CARB, 2007) estimates the emission factors of eleven different pollutants namely total organic gas, reactive organic gases, total hydrocarbon, methane, CO, NO_x, carbon dioxide, PM2.5, PM10, sulfur dioxide and lead. In this model, vehicles are classified based on their weight and fuel type. Similarly, Computer programme to calculate Emissions from Road Transport (COPERT) (EEA, 2007) used by European Environmental Protection Agency is also an average speed model which classifies vehicles based on their vehicle type, fuel, weight and technology used.

The US EPA used MOBILE model, an average speed model, to estimate the emission factors for regulatory purposes. MOBILE classifies vehicles based on their weight and fuel used (USEPA, 2003). The US EPA has replaced MOBILE series with MOVES (USEPA, 2010b) which classifies vehicles based on their activity. MOVES apart from being an average speed model, can also be used as a modal operation model to estimate emission factors based on the transient operation of a vehicle. These emission factor models use data collected during chassis and engine dynamometer testing carried in controlled conditions. Thus, evaluating the performance of MOVES in real world conditions is necessary.

Tunnel, on-road and remote sensing studies were used in past to evaluate vehicle emission factor models. For example, Kirchstetter et al. (1996) estimated light duty vehicle emission factors using measurements at Caldecott tunnel. Results indicated that EMFAC model does a decent job in estimating VOC/NO_x but over-estimates CO/NO_x emission factors. Kuhns et al. (2004) compared CO emission factors estimated using a remote sensing system with MOBILE6 estimations and concluded that MOBILE6 over-estimates the emissions by a factor of two. Weiss et al. (2011) used on road portable emission measurement system in Europe and concluded that COPERT under estimates NO_x emissions from diesel vehicles by 60%. Even though, these methods give actual data regarding real-world behavior of vehicles, they are less precise than dynamometer tests, due to additional factors such as environmental, traffic and driver conditions (Franco et al., 2013). Additionally, their conclusions might be confined to the study area.

Vehicle emission inventories can also be indirectly evaluated using near-road air quality models. Near-road air quality modeling has aided monitoring studies in past for congestion mitigation, traffic planning (Boriboonsomsin and Barth, 2007) and epidemiological studies on traffic exposure (Lee et al., 2012). Near-road models differ with other air quality models in their representation of pollutant dispersion processes like vehicle induced turbulence (Kalthoff et al., 2005; Kastner-Klein et al., 2000) and level of treatment of chemical and physical transformation of pollutants. Even though MOBILE emissions were used in the past (Cook et al., 2008; Vardoulakis et al., 2003; Wang et al., 2013), no studies using MOVES in near-road air quality modeling are reported.

Another way of studying vehicle emission inventories is by using regional air quality models to comparing the predicted and observed pollutant concentrations at monitoring sites. The USEPA uses National Emission Inventories (NEI) which includes temporal and spatial emission estimates from different sources. For example,Parrish (2006) compared the MOBILE generated vehicle emissions in NEI with a fuel based emission inventory, and concluded that MOBILE over-estimates CO by a factor of 2. Another way of evaluating is by using regional air quality models which use NEI. For example, Miller et al. (2008) used a lagrangian model and concluded that the emission inventories

overestimate the CO emissions atleast by a factor of 2. Castellanos et al. (2011) analyzed Community Multiscale Air Quality Model (CMAQ) performance in Eastern United States during morning rush hours and concluded that the NEI overestimates NO_x emissions. However, this assumption of using morning rush hour peaks to evaluate vehicle emission inventories might not be correct due to other factors like weekday/weekend vehicle fleet differences, and influence of other emission sources during rush hours.

In addition to methods discussed above, vehicle emission factor models can be evaluated is using source apportionment techniques. For example in receptor oriented source apportionment, the total species concentration measured at a receptor location is attributed to the contributions of different sources in the locality. Kim et al. (2005) used Positive Matrix Factorization (PMF) to study the VOCs measured at three sites in Houston and concluded that vehicles contributed to 5-25% of total VOC mass measured at those sites. Buzcu and Fraser (2006) used PMF to analyze 54 VOC species collected at three sites in Houston, and concluded that fuel evaporation contributed to 29 and 17% of the total VOC mass measured at two of the locations. However, no clear vehicle exhaust profiles were observed at any of the sites, which might be due to the presence of these sites closer to largest industrial complexes in the Houston Ship Channel (HSC). Xie and Berkowitz (2006) used PMF to study VOC data from four PAMS stations near HSC and concluded that vehicle exhaust contributed to 1-10% of total VOC mass at three of the sites. Results also indicated that fuel evaporation contributed to 7-19% of the total VOC mass at the four sites analyzed. Luchner and Rappenglück (2010) used PMF modeling to study the VOC data collected during TexAQS II Radical and Aerosol Measurement Project (TRAMP) and concluded that vehicle exhaust and fuel evaporation contribute to 15 and 14% respectively to the total VOC mass. Buzcu Guven and Olaguer (2011) analyzed the TRAMP data and concluded that vehicle exhaust contributed to 11-16%, while fuel evaporation contributed to 21-22% at the monitoring sites. While these studies are useful in understanding sources of VOCs in the atmosphere, their fundamental assumption of species being non-reactive in nature constrains the method

mainly to primary species. Additionally, as these calculations are based on observed VOC concentrations, they cannot be related to the actual emission rates of VOCs.

In addition to vehicles, plants emit isoprene, monoterpenes, sesquiterpenes, diterpenes etc., which account to major fraction of global VOC emissions (Guenther, 1995; Guenther et al., 2006; Laothawornkitkul et al., 2009). Isoprene represents, 40-60% of total vegetation emissions (Guenther et al., 2006). However its share in total VOCs varies with location. For example, Buzcu and Fraser (2006) used PMF to analyze 54 VOC species collected at three sites in Houston, and concluded that biogenic emissions (dominated with isoprene) contributed to less than 4% of the total VOC mass measured at two of the locations. Guo et al. (2007) used principal component analysis and estimated that biogenic isoprene contributed to a maximum of 4% in Hong Kong.

Most studies till date in Southeast Texas either use USEPA's BEIS (Pierce and Waldruff, 1991), with BEIS3.13 as latest version, or global biosphere emissions and interactions system (GloBEIS3) (Yarwood et al., 2002), or Model of Emissions of Gases and Aerosols from Nature (MEGAN) (Guenther et al., 2006). Temperature, photo synthetically active solar radiation and water availability (Alessio et al., 2008; Fuentes et al., 2000; Harley et al., 1996, 1997; Sharkey et al., 1999; Tingey et al., 1979) are major environmental factors effecting basal isoprene emission rates from plants in these models. Additionally, these models also require inputs from land use/land cover databases, leaf area index and biomass density.

Texas Commission of Environmental Quality (TCEQ) is thinking of using MEGAN to generate isoprene emissions in Texas, for regulatory purposes. However, MEGAN has not been evaluated properly as yet in Southeast Texas. Generally above canopy flux measurements have been used to evaluate these emission factor models in forest areas (Geron et al., 1997; Guenther and Hills, 1998). For example, Potosnak et al. (2014) used measured isoprene fluxes in a deciduous forest, and concluded that while MEGAN does a good job in predicting light and temperature effects on isoprene emissions, its response to drought is not accurate. Another way of evaluating these emission factor models is by using regional air quality models. As discussed earlier, this can be achieved by

comparing predicted isoprene concentrations, using emissions generated by MEGAN, with observed concentrations. For example, Carlton and Baker (2011) used MEGAN generated emissions in CMAQ model and observed over predictions of isoprene concentrations. However, most of these validation studies are under taken in rural environments. The presence of other sources of isoprene (Song et al., 2008) along with heterogeneous distribution of vegetation makes urban/sub-urban regions quite different from a rural/forested region. But these models have not been sufficiently evaluated in urban regions.

The first objective of this research is to test the feasibility of using MOVES to generate necessary emissions for near-road air quality modeling based on simple traffic count data. To carry out this objective, a three dimensional Eulerian air quality model, TAMNROM-3D (Kota et al., 2010) will be used to predict the gaseous pollutants near a rural freeway at Austin, Texas. This objective will aid the validation of MOVES in estimating CO, NO, NO_2 and air toxics concentrations in a near-road environment.

The second objective of this study is to apply the source-oriented regional air quality modeling approach to track emissions of CO and NO_x from on-road vehicle sources separately to directly evaluate the accuracy of the on-road vehicle emission inventories. A source oriented CMAQ model, which explicitly tracks CO and NO_x from on-road vehicles will be developed. This model will be applied to study summer time concentrations of CO and NO_x in Southeast Texas. This will suggest modifications to future versions of MOVES in predicting CO and NO_x emissions.

The third objective of this research is to estimate vehicle emission factors using simultaneous VOC fluxes in an urban environment, and compare with MOVES predictions. Simultaneous fluxes of 18 VOCs, measured on the top of a tall tower in Houston, will be used in a receptor oriented source oriented model to quantify the source profiles and contributions of vehicle exhaust in the locality. The predicted contributions along with flux footprints will be used to estimate the VOC emission factors from vehicles. The comparison of estimated emission factors in this study with MOVES predictions will aid the evaluation of MOVES in terms of VOC emissions.

The fourth objective is to evaluate the performance of MEGAN model in estimating isoprene emissions in Southeast Texas. A source oriented CMAQ model, which explicitly tracks isoprene from vegetation, will be used during a relatively dry summer ozone episode. This study will aid in estimating uncertainties in the predicted isoprene concentrations due to soil moisture, the plant functional types (PFTs) and leaf area index (LAI).

In conclusion, this study will aid in determining the potential short comings and benefits of using MOVES in generating CO, NO_x and VOC emissions. Additionally, the evaluation of MEGAN will help in understanding the important factors in accurately predicting isoprene emissions in urban regions. Overall, this study will facilitate governing agencies in designing effective strategies for different sources in Southeast Texas for avoiding NAAQS violations and control radiative forcing.

2. SIMULATING NEAR-ROAD REACTIVE DISPERSION OF GASEOUS AIR POLLUTANTS USING A THREE-DIMENSIONAL EULERIAN MODEL*

In this study, the TAMNROM-3D model, a 3D Eulerian near-road air quality model with vehicle induced turbulence parameterization and a MOVES based emission preprocessor, is tested using near-road gaseous pollutants data collected near a rural freeway with 34% heavy duty vehicle traffic. Exhaust emissions of gases from the vehicles are estimated using a lumped vehicle classification scheme based on the number of vehicle axles and the default county-level MOVES vehicle fleet database. The predicted dilution of CO and NO_x in the downwind direction agrees well with observation, although the total NO_x emission has to be scaled to 85% of its original emission rate estimated by the MOVES model. Using the atmospheric turbulent diffusion coefficient parameterization of Degrazia et al. (2000) with variable horizontal turbulent diffusion coefficient (K_{xx}) leads to slightly better predictions than a traditional non-height-dependent K_{xx} parameterization. The NO_2 concentrations can be better predicted when emission of total NO_x is split into NO and NO_2 using the NO_2 to NO_x ratio of 29% measured near the road. Simulations using the SAPRC99 photochemical mechanism do not show significant changes in the predicted NO and NO_2 concentrations near the road compared to simulations using a simple three-reaction mechanism that involves only NO_x and O_3. A regional air quality simulation in Houston, Texas during a high O_3 episode in August 2000 shows that using the NO_2 to NO_x ratio of 29% instead of the traditional 5% leads to as much as 6 ppb increase in 8-hour O_3 predictions.

---

* *Reproduced with permission from:* Kota, S.H., Ying, Q., Zhang, Y., 2013. Simulating near-road reactive dispersion of gaseous air pollutants using a three-dimensional Eulerian model. Science of the Total Environment 454-455, 348-357. Copyright 2013, Elsevier Ltd.

2.1 Introduction

Elevated concentrations of carbon monoxide (CO), oxides of nitrogen (NO_x) and air toxics are frequently observed in the vicinity of a roadway compared to their background ambient levels (Parrish, 2006). Health studies have indicated an increase in lung and respiratory related diseases (Gauderman et al., 2007; Kim et al., 2004), premature mortality (Finkelstein et al., 2004), and hypertension and cardiac problems (Hoffmann et al., 2006) due to exposure to traffic emissions. Near-road air quality models are necessary to aid air quality monitoring programs to provide required data for traffic planning, congestion mitigation and epidemiology studies of traffic pollution exposure.

Although significant progress has been made in numerical simulations of near-road air pollution, most of the well-accepted near-road models (e.g. CALINE4) are based on steady-state solutions of the atmospheric turbulent dispersion equation. However, in many studies it is demonstrated that vehicle-induced-turbulence (VIT) significantly affects near-road pollutant dispersion (Eskridge and Hunt, 1979; Kota et al., 2010; Sahlodin et al., 2007). VIT is usually treated empirically, for example, using the mixing zone concept (Held et al., 2003; USEPA, 2010a). To overcome this limitation, Rao et al. (2002) formulated ROADWAY-2, a two-dimensional (2D) Eulerian model that treats VIT more realistically. Wang et al. (2011) incorporated VIT into a computational fluid dynamics (CFD) model and demonstrated that it yields better near-road predictions of NO_x than CALINE4, using data collected near urban and rural freeways in Texas. The CFD approach, however, is complex to implement and is extremely computationally intensive due to millions of grid cells used in the solution processes. Another potential problem in the near-road modeling is that current near-road models typically use relatively simple atmospheric chemistry that includes mainly NO, NO_2 and O_3. The effect of organic peroxy radicals (RO_2) on NO to NO_2 conversion is either neglected entirely (as in ROADWAY-2) or accounted for using representative RO_2 species from simple VOCs (Wang et al., 2011). However, these simple approaches have not been evaluated against a more complete atmospheric chemical mechanism.

Kota et al. (2010) developed a 3D Eulerian model, the TAMU Near-Road Model (TAMNROM-3D), to simulate near-road dispersion and chemical transformation of pollutants. The TAMNROM-3D model predicts vehicle induced turbulent kinetic energy in each grid cell to determine the magnitude of VIT using a parameterization scheme suggested by Bäumer et al. (2005). This allows it to include more mechanistic treatments of the chemical and physical processes that affect near-road pollutant concentrations. The capability of this model to predict the dispersion of a non-reactive tracer was already evaluated using the SF_6 dataset collected at the General Motor's testing track (Kota et al., 2010). It has been demonstrated that TAMNROM-3D performs better than CALINE4 and ROADWAY-2 on that dataset. However, the ability of the model to simulate dispersion and transformation of reactive air pollutants has not been evaluated.

Emissions from on-road mobile sources are key input parameters to near-road and regional air quality models. The US EPA developed the MOBILE model to estimate on-road vehicle emission factors. Recently, US EPA has suggested the replacement of the MOBILE model with the MOVES (Motor Vehicle Emission Simulator) model (USEPA, 2010b). Although there are studies that directly evaluate MOVES emission factors with observed vehicle emission data, indirect evaluation of the MOVES model through near-road air quality modeling using vehicle traffic count data has not been previously reported.

Thus, the aim of this study is to (i) test the feasibility of using MOVES to generate necessary emissions for near-road air quality modeling based on simple traffic count data and (ii) to further evaluate the TAMNROM-3D performance on predicting averaged concentrations of reactive gaseous pollutants collected in the field.

2.2 Model Description

The detailed formulation and solution procedures of the TAMNROM-3D model can be found in Kota et al. (2010) and are not repeated here. In the following sections, the photochemical mechanism, the microphysics modules, and the MOVES based emission preprocessor are described.

2.2.1 Photochemical mechanism

Unlike other near-road air quality models that use simplified representations of NO to NO_2 conversion in near-road environments (Kenty et al., 2007; Kukkonen et al., 2001; Rao, 2002), the TAMNROM-3D model includes a relatively complete description of atmospheric gas phase chemistry based on the SAPRC-99 photochemical mechanism, which is one of the most widely used photochemical mechanism families for both regulatory and research applications (Carter, 1994; Czader et al., 2008). This is necessary because in real atmosphere peroxy radicals (RO_2 or HO_2) also convert NO to NO_2. In addition, some radicals can react with NO_2 to form relatively stable products, acting as a sink to NO_x. Neglecting or unrealistically treating these processes may lead to errors in NO and NO_2 predictions. The detailed treatment of the gas phase chemistry can be used as a reference to evaluate other simplified gas phase mechanisms of NO to NO_2 conversion in near-road models. Emission and photochemical degradation of several air toxics can also be simulated in the mechanism. The original SAPRC-99 mechanism already treats formaldehyde as an explicit species. In this study, the SAPRC-99 mechanism is enhanced to explicitly simulate five additional air toxics from mobile sources: benzene, 1,3-butadiene, acetaldehyde, acrolein and Methyl Tertiary Butyl Ether (MTBE) using the reaction rate coefficients and products designations from Carter (2000). Using a relatively complete chemical mechanism allows the concentrations of OH to be estimated mechanistically, which is essential to model the photochemical decomposition of air toxics. The production of formaldehyde, acetaldehyde and acrolein from other VOCs are also more realistically represented in the model.

2.2.2 Emission processing using the MOVES model

Emissions from the on-road vehicular traffic for the TAMNROM-3D model are estimated using an emission preprocessing program based on vehicle count data and the MOVES model (version 2010a). The MOVES model uses detailed vehicle classifications based on vehicle uses and fuel types. Since most automatic traffic

counters measure vehicle velocity and the number of axles when vehicle make and model information is not directly available, it is convenient to classify vehicles into lumped classes based on the number of axles only. In this study, three lumped vehicle classes are used: Class A (two axles, light duty vehicles), Class B (more than 2 axles, heavy duty vehicles) and Class C (motorcycles). Class A includes passenger cars (MOVES ID: 21), passenger trucks (ID: 31) and light commercial trucks (ID: 32). Class B comprises of refuse trucks (ID: 51), single unit short haul trucks (ID: 52), single unit long haul trucks (ID: 53), combination short haul trucks (ID: 61), combination long haul trucks (ID: 62), motor homes (ID: 54) and buses (ID: 41-43). More strictly speaking, some two axles commercial trucks with 6 tires belong to the heavy duty vehicle category (FHWA, 2001), and are grouped into the vehicle class B. Moreover, MOVES does not treat two axles 6 tires vehicles separately, but places them in refuse trucks and motor homes.

The emission factors predicted for each MOVES vehicle type and fuel combinations are vehicle population averaged to generate emission factors (EF, g mile^{-1} for moving vehicles and g hr^{-1} for parked or idling vehicles) for an average vehicle in these three lumped classes using equation (2.1):

$$EF_j = \frac{\sum_{m=1}^{M_j}\sum_{f=1}^{2}\sum_{y=1}^{N} g_{m,f,y}\,p_{m,f,y}}{\sum_{m=1}^{M_j}\sum_{f=1}^{2}\sum_{y=1}^{N} p_{m,f,y}} \qquad (2.1)$$

where j is the lumped vehicle class index (A, B or C), M_j is the number of MOVES vehicle classes in a lumped vehicle class j, f is the fuel type (gasoline and diesel) index, y is the vehicle age index, N is the total number of years in a vehicle fleet, p is the number of vehicles, and g is the emission factor (g mile^{-1} for moving vehicles and g hr^{-1} for parked or idling vehicles) for a specific vehicle year, fuel and class. The vehicles can also be electric or CNG driven but their numbers are small (zero in the current modeling domain based on the MOVES default database) and thus are not considered in the current study. County specific g and p values are extracted from the MOVES default database. With the population-averaged EFs, the emission rate (E, g s^{-1}) of species i from a lumped vehicle class j at each model grid cell can be calculated using equation (2.2):

$$E_{i,j} = 1609.3 N_j V_j EF_{i,j} / 3600 \quad (2.2)$$

Where N_j and Vj are vehicle density and velocity (mph) in each grid cell, respectively. The coefficients 1609.3 and 3600 convert emission rate to the designated units. Obviously, equation (2.2) can only be applied to moving vehicles. For emissions of parked or idling vehicles, the population averaged parking or idling EFs (in g hr^{-1}) are used along with the number of parked/idling vehicles in the grid cell to calculate the emissions.

As an example that demonstrates how the averaged EFs are calculated, table 1 shows the 2007 vehicle population data for the vehicle fleet in Travis County, Texas and the NO_x EFs from the MOVES default county level database. The MOVES vehicle fleet database has a cut-off vehicle age of 30 years (i.e. N=30 in equation (2.1)). Based on the data, the vehicle population weighted NO_x EF for a Class A vehicle moving at 35 mph in year 2007 is 1.13 g $mile^{-1}$. The lumped EFs generally change slowly with average vehicle speed. However, in the MOVES model, certain types of vehicles such as combination short and long-haul trucks, motor homes, and buses have EFs increasing rapidly as speeds decrease below approximately 20 mph. The lumped EFs for Class B vehicle will show significant sensitivity especially at these low speeds (see Figure A1 in Appendix A). Uncertainty of the predicted emissions and concentrations due to uncertainty in vehicle speed should be explored when modeling slow moving vehicles.

Table 1 NO_x emission factor (EF, g $mile^{-1}$) for passenger car (PC), passenger truck (PT) and light commercial truck (LCT) moving at 35mph in Travis county, Texas based on 2007 vehicle fleet data in MOVES.

Model Year	No.of gas. PC	EF of gas. PC	No.of diesel PC	EF of diesel PC	No.of gas. PT	EF of gas. PT	No.of diesel PT	EF of diesel PT	No.of gas. LCT	EF of gas. LCT	No.of diesel LCT	EF of diesel LCT
1977	235	1.978	3	1.093	377	4.091	5	4.037	122	3.940	5	5.275
1978	221	1.977	3	1.092	347	4.126	5	4.078	113	3.981	5	5.326
1979	295	1.964	9	1.085	432	4.105	6	4.055	140	3.955	6	5.297
1980	388	1.926	19	1.064	544	4.089	7	4.034	164	3.930	20	3.841
1981	473	1.927	39	0.899	551	4.091	10	4.001	174	3.952	13	5.101
1982	596	1.944	39	0.906	698	4.160	29	4.070	190	4.004	53	4.462

Table 1 Continued

Model Year	No.of gas. PC	EF of gas. PC	No.of diesel PC	EF of diesel PC	No.of gas. PT	EF of gas. PT	No.of diesel PT	EF of diesel PT	No.of gas. LCT	EF of gas. LCT	No.of diesel LCT	EF of diesel LCT
1983	936	2.349	30	0.808	976	4.412	21	4.067	265	4.258	68	4.654
1984	1416	2.374	27	0.817	1450	4.480	21	4.134	419	4.314	73	4.673
1985	2005	2.387	24	0.651	1901	4.493	33	4.037	581	4.327	65	4.684
1986	2767	2.123	0	0.000	2208	3.710	50	4.204	693	3.628	61	4.213
1987	3257	2.098	0	0.000	2534	3.744	27	4.256	804	3.631	52	5.542
1988	4387	1.871	0	0.000	2987	3.381	15	4.318	925	3.307	78	5.018
1994	14530	1.494	0	0.000	6909	3.168	126	5.041	2110	3.010	240	5.612
1995	16349	1.506	0	0.000	7485	3.209	113	5.090	2236	3.053	303	5.479
1996	17697	1.012	0	0.000	8588	1.603	173	5.222	2667	1.636	260	5.456
1997	18022	1.016	0	0.000	9542	1.571	181	5.404	2807	1.590	442	4.707
1998	18481	0.879	0	0.000	10922	1.392	110	4.408	3546	1.422	140	4.747
1999	20488	0.880	0	0.000	12529	1.419	297	4.420	3571	1.456	714	4.452
2000	22136	0.775	0	0.000	14226	1.171	337	4.017	4269	1.230	596	4.454
2001	21508	0.477	83	0.668	15470	0.931	204	4.541	4331	1.052	906	3.939
2002	21087	0.349	81	0.668	15974	0.684	210	4.334	4558	0.751	849	4.268
2003	20089	0.328	78	2.477	16797	0.724	221	4.972	4929	0.787	756	4.831
2004	20123	0.087	78	2.483	17934	0.258	236	4.985	4972	0.350	1099	4.843
2005	20735	0.068	80	2.483	18037	0.217	238	4.985	5440	0.312	666	4.843
2006	21078	0.067	81	0.243	16851	0.188	400	3.731	5311	0.287	453	3.717
2007	20599	0.054	79	0.243	16582	0.178	393	1.624	5181	0.278	491	1.613

In order to drive the SAPRC-99 photochemical mechanism, predicted emissions need to be speciated properly. NO_x emissions can be split into NO and NO_2 using a user-specified NO_2 to NO_x ratio or the internal NO_2 to NO_x ratio specified by the MOVES model. Two user-specified NO_2 to NO_x ratios and the MOVES internal NO_2 to NO_x ratio will be tested in this study (see Section 4.1.3). The VOC profiles for light duty gasoline and heavy duty diesel vehicles, extracted from EPA's SPECIATE 4.2 speciation profile database, are used to speciate total VOC estimated from Class A and B vehicles, respectively. It would be more accurate if heavy duty gasoline and diesel vehicle profiles are population-averaged to generate a more representative VOC emission profile for Class B vehicles, but the change in the emission of speciated VOCs is expected to be minor as the VOC speciation profiles for heavy duty diesel and gasoline engines are quite similar.

2.3 Model Application

2.3.1 Description of field measurements and model setup

The model was applied to study the concentrations of CO, air toxics, and NO_x downwind of a roadway. The data used in this paper was collected at Farm to Market 973 (FM973) in Austin, Travis County, Texas in July, 2007. The experimental study is described elsewhere (Clements et al., 2009; Zhu et al., 2009) and only briefly summarized here. FM973 is a two-lane surface roadway with a width of 4.25 m/lane. It has a significant amount of heavy duty vehicle traffic (approximately 34%). NO, NO_2 and CO measurements were taken from up to 68 m upwind to 13-105 m downwind of the roadway using a mobile platform. Wind data and carbonyls concentrations were measured at 80 m upwind and 15 m downwind at stationary locations. Observed NO_x concentrations were taken from Wang et al. (2011) for the same model episode. In this study, data collected in the afternoon of July 13, 2007, during which Wang et al. (2011) did the analysis and the wind was mostly perpendicular of the roadway, was used to supply boundary conditions and evaluate model performance. The average CO concentrations were not reported in Wang et al. (2011) for that specific day, thus the concentrations were taken from Clements et al. (2009), which are based on data collected on July 12-14 under perpendicular wind. A simulation of the concentrations of NO_x under parallel wind conditions was also conducted and briefly discussed in the Supplementary Materials (see figure A2 and associated discussions in Appendix A). Generally speaking, the model can also predict the NO_x concentrations reasonably well in that case, but the results are sensitive to the selection of mean wind direction.

The model domain was divided into 100×40 grids horizontally with a grid size of 4.25×4.25 m so that the entire lane width could fit into a single grid cell. The vertical domain was divided into 11 layers extending to 40 m above surface, which is identical to the vertical extent used in Kota et al. (2010). The vertical spacing of grid cells varies from 1 m near the surface to 10 m at the top. Figure 1 shows an overview of the model domain and the measurement locations. The 8.5 m wide two-lane highway is placed at 67.5 m from the left boundary as shown in inner panel of figure 1. As illustrated in

figure A3 (Appendix A), predicted NO_x concentration profiles from a higher grid resolution simulation are almost identical to the base case results.

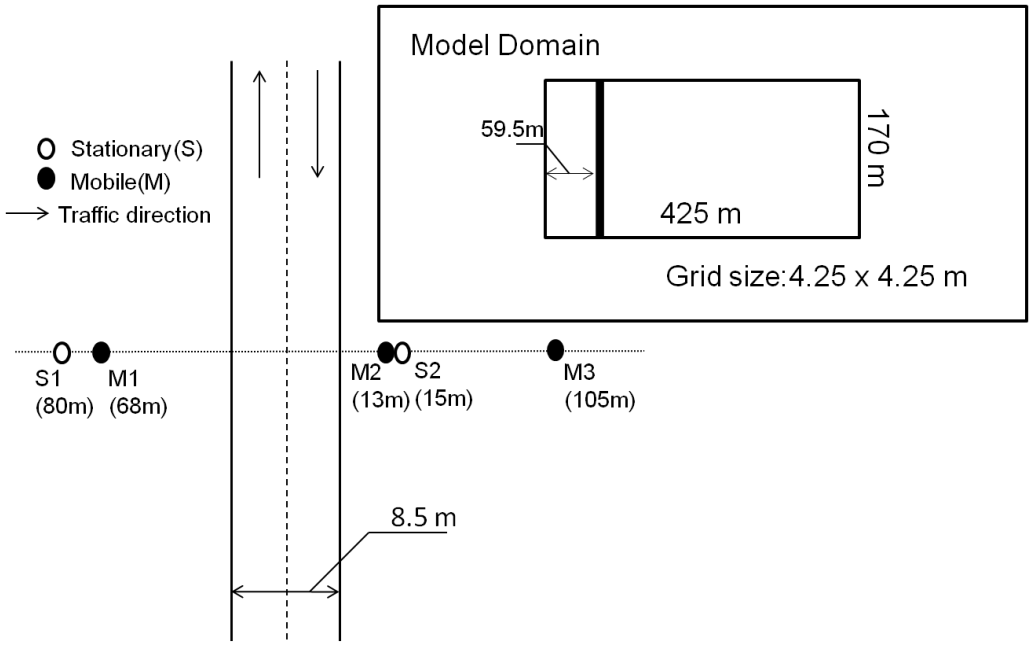

Figure 1 Schematic for FM973 and the relative position of the stationary (S) and mobile (M) stations to the roadway. The stationary stations measure carbonyls and wind data and the mobile stations measure other gas phase species concentration. M1 station measures concentrations immediately upwind till 68 m perpendicular to the road, M2 station measures from immediate downwind to 15 m, and M3 station moves up to 105 m downwind for concentrations of gaseous species.

The emissions from roadways were calculated based on an average traffic volume of 17.34 vehicles per minute (34% of which, reported as heavy duty vehicles, are considered as Class B vehicles) moving at speed of 35 mph during the model episode (Clements et al., 2009). Even though, less than 3 axle vehicles were treated as light duty in the experimental study, vehicles with 2 axles and 6 tires were treated as Class B in this study, due to the reasons discussed earlier. The vehicle population averaged EF for Class A and B vehicles at Travis County, Texas is shown in table 2. A clear increase in EF from Class B compared to Class A vehicles is observed for all species, ranging from

1.3 times for CO to 9.3 times for NO_x. This indicates that the percentage of Class B vehicles in a fleet could significantly affect, and sometimes dominate, the concentrations of pollutants measured near a roadway. EFs of NO_x were scaled by 0.85 from the values shown in table 2 for both Class A and Class B vehicles in this study to minimize the difference between predicted and observed NO_x concentrations. This less-than-unity scaling factor qualitatively agrees with a previous report that the MOVES model over estimates NO_x emissions from older vehicles (Choi and Koupal, 2011). It is also in agreement with previous assessments that the MOBILE model (version 6, or MOBILE6) slightly over estimates NO_x EFs when compared to observations (CRC, 2004), and the MOVES model predicts even higher NO_x EFs than MOBILE6 (Kota et al., 2013b). Figure A4, in Appendix A, depicts the difference predicted NO_x concentrations due MOVES predicted NO_x emissions and 75% and 85% scaled MOVES emissions. Results indicate that 85% scaled case is slightly better than the other two cases, and thus is used as base case in this study.

Table 2 Vehicle fleet averaged EFs for Class A and B vehicles at 35 mph. Units are g $mile^{-1}$.

Species	Class A	Class B
CO	11.00	14.71
NO_x*	1.13	10.49
VOC	3.09×10^{-1}	1.14
Acetaldehyde	2.79×10^{-3}	2.26×10^{-2}
Acrolein	2.52×10^{-4}	3.33×10^{-3}
Formaldehyde	5.71×10^{-3}	5.86×10^{-2}
Benzene	1.50×10^{-2}	2.95×10^{-2}
1,3-Butadiene	2.45×10^{-3}	7.64×10^{-3}

*Actual emission factors of NO_x used in calculating on-road emissions are reduced by 85%.

The photolysis rates were calculated for 1500 CST, July 13, 2007 as the actual data were collected during 1320-1715 CST. The temperature within the domain was assumed

to be a uniform value of 25.5 ^{o}C based on the averaged measurements. Measured average wind speed of 2.17 m s^{-1} at 3 m above surface was extrapolated to mid-level model layer height based on the velocity profile above rough surfaces as suggested by Seinfeld and Pandis (2006) with a surface roughness length of 0.1 m. A convective planetary mixing layer height of 2200 m, which is typical for summer time, was used in atmospheric turbulent diffusivity calculations. The surface bulk turbulent parameters such as surface friction velocity, convective velocity scale and Monin-Obukhov length were estimated using the parameterizations described in Garratt (1994). The horizontal and vertical atmospheric turbulent diffusion coefficients are calculated using the parameterization of Degrazia et al. (2000). More discussion on this can be found in Section 2.5.1.

Boundary conditions for CO (60 ppb), NO (0.9 ppb), NO_2 (1.9 ppb), acetaldehyde (0.5 ppb), formaldehyde (0.7 ppb) and acrolein (0.04 ppb) were from the upwind location measurements. The boundary conditions of O_3 (26 ppb) was taken from Wang et al. (2011). The boundary conditions for the remaining model species were extracted from a 4 × 4 km^2 grid cell which contains the roadway in a regional air quality simulation for August 2006.

2.4 Results

2.4.1 CO

The performance of the model in terms of dilution of a tracer species is shown in figure 2 using CO as a representative species. The observed concentrations agree best with the predictions for the case with a boundary concentration of 60 ppb. The predictions are sensitive to the ±25% change of the boundary conditions because of the low emission rate of CO from a rural road but the dilution rate of the tracer can still be accurately predicted. In order to evaluate the sensitivity of the model predictions to the emission rate, the emission rate of CO is changed by ±25% in two sensitivity runs. Only small variations to the base case emission rates are predicted, again due to low vehicle density during the simulated episode.

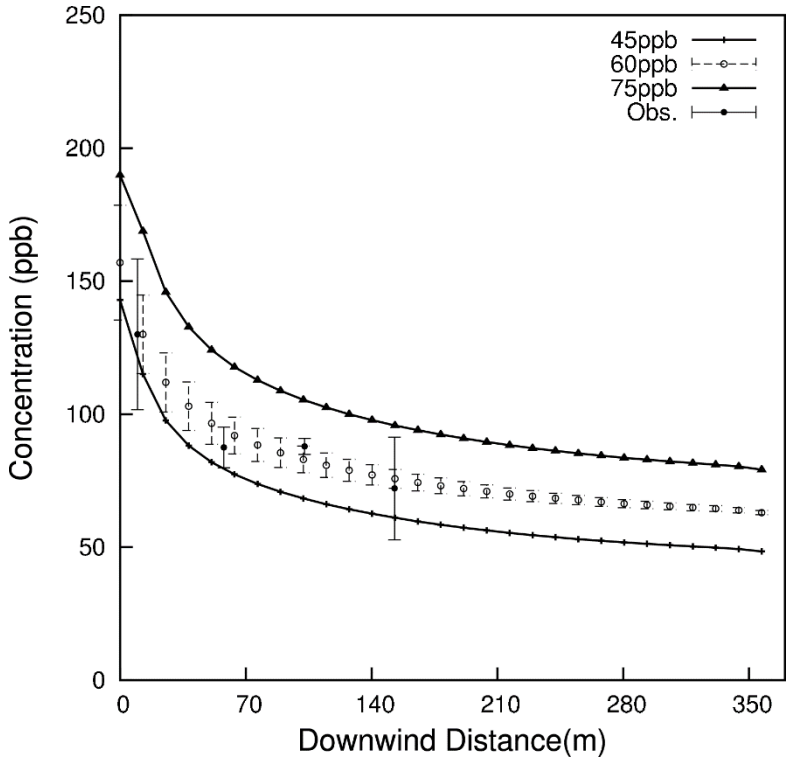

Figure 2 Predicted and observed CO concentrations as a function of downwind distance. The predictions are for cases with different boundary concentration values of 30, 60 and 75ppb. The sensitivity of model results to variability of vehicle density (±25%) is also shown for the case with boundary condition of 60 ppb.

2.4.2 Air toxics

Predictions of acetaldehyde, acrolein, formaldehyde, benzene and 1,3-butadiene at the roadway and 15 m downwind of the roadway are shown in table 3, along with observations of acetaldehyde, acrolein and formaldehyde at 15 m downwind and 55 m upwind. (i.e. the boundary conditions used in the simulation). As expected, the air toxics concentrations at the roadway are higher than the upwind concentrations due to emissions from vehicles. The predictions at 15 m downwind usually agree well with the observations for acetaldehyde and acrolein. For formaldehyde, the reported concentration at 15 m downwind is lower than the upwind concentration. This disagrees

with the model prediction, which shows an increase in the concentration. The reported lower concentration of formaldehyde in the downwind is in contrast with the measurements at the State Highway 71 and Interstate Highway 35, which show clear increase in the formaldehyde concentrations in the downwind vicinity of the roadways (Clements et al., 2009). This leads to speculations that the observed decrease in the formaldehyde concentrations at FM973 could be an error in the measurements.

Table 3 Observations and predictions of air toxics near the roadway (units: ppb).

Species	Observations		Predictions	
	-80 m	15 m	0 m	15 m
Acetaldehyde	0.495	0.527	0.556	0.534
Acrolein	0.037	0.041	0.042	0.039
Formaldehyde	0.703	0.205	1.020	0.938
Benzene	NA	NA	0.062	0.036
1,3-Butadiene	NA	NA	0.019	0.010

* 'NA' indicates data is unavailable.

2.4.3 NO_x

In traditional regional air quality modeling, the estimated NO_x emissions are split into NO and NO_2 assuming a NO_2 to NO_x ratio of 5% (Berkowicz, 2000). The MOVES model has the capability of predicting NO_2 directly. The predicted NO_2 to NO_x ratio is approximately 10% for Class A vehicles and 7% for Class B vehicles in this study, yielding an average ratio of approximately 9%. The NO_2 to NO_x ratio predicted by the MOVES model does not vary much with vehicle speed. Carslaw et al. (2005) reported a clear continuous increasing trend of NO_2 to NO_x ratio near roadways in London from 5% in 1997 to 17% in 2003. Wang et al. (2011) reported that a fixed NO_2 to NO_x ratio of 29% at the roadway is needed to make model predicted downwind concentrations agree with measurements.

In this section, the impact of initial NO_2 to NO_x ratio (5% vs. 29%) and the level of details in the gas phase chemistry (no chemistry vs. simple NO_x-O_3 conversions vs. full SAPRC-99 mechanism) to the predictions of NO and NO_2 in the model are tested. The simple NO_x-O_3 chemistry has only three reactions, as listed in (1.R1)-(1.R3) below:

$$NO_2 + hv \rightarrow NO + O,\ j_1=7.05\times10^{-3}\ s^{-1} \quad (1.R1)$$

$$NO + O_3 \rightarrow NO_2 + O_2,\ k_2=1.81\times10^{-14}\ cm^3\ s^{-1} \quad (1.R2)$$

$$O + O_2 + M \rightarrow O_3,\ k_3=5.79\times10^{-34}\ cm^6\ s^{-1} \quad (1.R3)$$

The implication of a possible higher NO_2 to NO_x ratio in regional air quality simulations are further explored in Section 2.5.4.

Figure 3 (a) shows that the three simulations with NO_2 to NO_x ratio of 29% have similar concentrations of NO near the vicinity of the roadway, while the simulation with NO_2 to NO_x ratio of 5% predicts higher NO concentrations. At further downwind distances (approximately 25 m), the concentrations from different simulations become quite similar. The effect of NO_2 to NO_x ratio is more significant in the predictions of NO_2 concentration, as demonstrated in figure 3 (b). When using an NO_2 to NO_x ratio of 5%, the model under-predicts NO_2 concentrations in the immediate downwind of the roadway. It also predicts a slight increase in the NO_2 concentration from 0 to 100 m, before the concentration starts to decrease with distance. This does not agree with observations, which show a monotonous decrease of NO_2 from the roadway. The predictions agree with observation much better when a NO_2 to NO_x ratio of 29% is used. An additional simulation that uses the MOVES predicted NO_2 to NO_x ratios shows similar results as the 5% ratio case. These results are in general agreement with Wang et al. (2011), in which the same FM973 roadway was simulated. However, the methodologies used in the two studies are quite different. In this study, concentration of pollutants are predicted based on calculated emission rates using lumped vehicle categories and the MOVES emission model as discussed in Section 2.2, which is different from Wang et al. (2011) where concentrations of all pollutants at the roadway are fixed using concentrations measured at the nearest downwind site.

Figure 3 (a) also shows that the simulation with no chemistry predicts higher NO concentrations as it does not account for NO to NO_2 conversion due to O_3, HO_2 and RO_2. The difference between the simple chemistry and the full chemistry cases is small because of the low peroxy radical concentrations as predicted by the SAPRC99 mechanism (see figure A5 in Appendix A). Figure 3 (b) shows that the difference due to chemistry is more noticeable for NO_2, with an increase of approximately 10% when full chemistry is applied. This conclusion is similar to that of Wang et al. (2011), which suggests that peroxy radicals do not significantly alter NO_2 concentrations at FM973. The effects of using a more detailed chemical mechanism on NO and NO_2 are further explored in Section 2.5.3 for different emission scenarios.

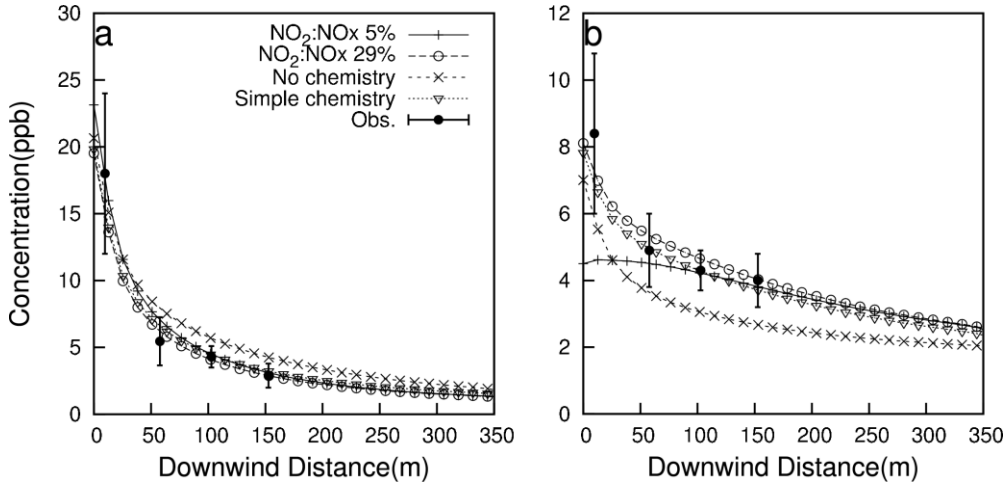

Figure 3 Predicted and observed (a) NO and (b) NO_2 concentrations as a function of downwind distance for the cases with NO_2 to NO_x ratio of 5% and 29 % (both with full SAPRC-99 gas phase chemistry) and with different treatment of gas phase chemistry (both with NO_2 to NO_x ratio of 29%).

2.5 Discussions

2.5.1 Atmospheric and vehicle induced turbulent diffusion

One of the problems in applying a finer grid size in studying the transport of pollutants using an Eulerian approach is the formulations of vertical and lateral atmospheric

diffusion coefficients. It has been suggested that the parameterizations used in regional air quality models might not be suitable for grid sizes less than 4 km (Byun and Schere, 2006). However, our previous study shows that these parameterizations might be sufficient for concentrations averaged over 20-30 minutes (Kota et al., 2010). In this study, the atmospheric diffusion coefficients are calculated using the parameterization developed by Degrazia et al. (2000). This scheme gives continuous transitions of the turbulent diffusion coefficients when the atmospheric stability class changes. In addition, it also gives height dependent horizontal diffusion coefficients (K_{xx}). It has been successfully applied and evaluated in several trajectory and Eulerian modeling studies (e.g. see Costa et al. (2006) and Carvalho et al. (2007)) of atmospheric tracer dispersion experiments, including the Prairie Grass (Barad, 1958) and the Copenhagen dataset (Gryning and Lyck, 1984).

The NO_x results using this parameterization are compared with results based on the vertical turbulent diffusion parameterization as described in Jacobson (1998) and horizontal turbulent diffusion parameterization in Seinfeld and Pandis (2006), as used in Kota et al. (2010). The K_{zz} values predicted by the two parameterization schemes are very similar while the Degrazia et al. (2000) parameterization predicts much lower K_{xx} near the surface (figure 4). As shown in figure 5, the Degrazia et al. (2000) parameterization gives higher predictions when it is very close to the roadway and the difference between the two parameterizations becomes less significant further downwind. Although the differences are small, this new parameterization gives predictions that are slightly closer to the observations.

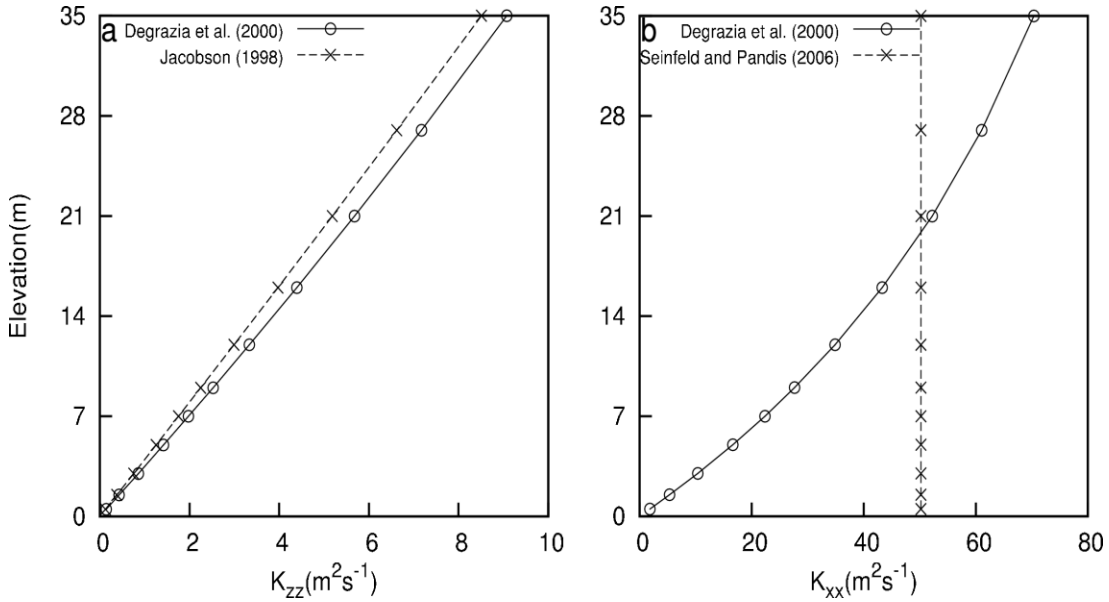

Figure 4 Simulated (a) vertical turbulent diffusion coefficient (K_{zz}) using Degrazia et al. (2000) and Jacobson (1998) parameterizations, and (b) horizontal turbulent diffusion coefficient (K_{xx}) using Degrazia et al. (2000) and Seinfeld and Pandis (2006) parameterizations.

The AERMOD model, which is recommended by the US EPA for regulatory purposes, is also used to predict NO_x concentrations. In this study the FM973 roadway was treated as an area-polygon source with a length of 170 m and width of 8.5 m. These dimensions are selected to correspond with the simulated roadway in this study. A mixing zone height is taken to be 2.8 m i.e. 1.7 times (USEPA, 2010a) the population weighted vehicle height of 1.6 m. AERMOD over-predicts NO_x concentration near the roadway but under-predicts at further downwind distances. This indicates that using a mixing zone of 2.8 m might lead to under-prediction of the effect of VIT on pollutant dispersion in this case. The impact of the vehicle induced turbulent diffusivities on roadway is also shown in figure 5. The sensitivity simulation neglecting VIT (no VIT case) also leads to a slight overestimation of surface NO_x concentrations.

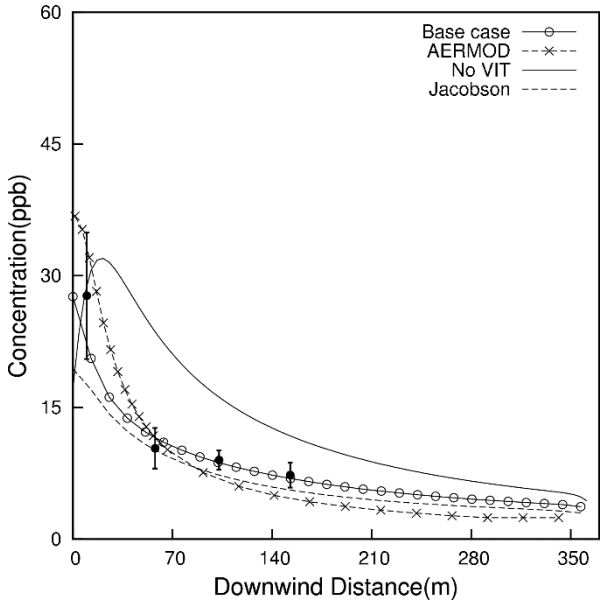

Figure 5 Change in NO_x decay for cases with Jacobson (1998) + Seinfeld and Pandis (2006) and Degrazia (2000) parameterizations of atmospheric diffusivity; and without vehicle induced turbulence as a function of distance from the freeway. AERMOD predictions are also included for comparison purposes. Filled circles are averaged observations. Units are ppb.

2.5.2 Year of fleet and heavy duty vehicle fraction

The emissions used in the previous sections are estimated based on average vehicle EFs for lumped Class A and B vehicles for the 2007 vehicle fleet in Travis County, and the traffic count data and heavy duty fraction of vehicles in the experimental study. The sensitivity to the selections of the year of vehicle fleet and the fraction of heavy duty vehicles on the roadway is studied in detail in figure 6. Figure 6(a) shows the predicted NO_x concentrations for vehicle fleet years of 2000 and 2015 along with the base year 2007 for the Travis County, based on the data from the MOVES model. The heavy duty vehicle fraction (i.e. Class B vehicles) is still kept at 34%, as used in the base case simulations. As expected, using emissions based on fleet year 2000 predicts higher NO_x concentrations while using the 2015 fleet predicts much lower concentrations. The predicted concentrations of NO_x from roadway decrease by approximately 50% by 2015

from 2000. This is expected due to newer vehicle technologies (Roy et al., 2009) introduced to meet stringent US EPA regulations.

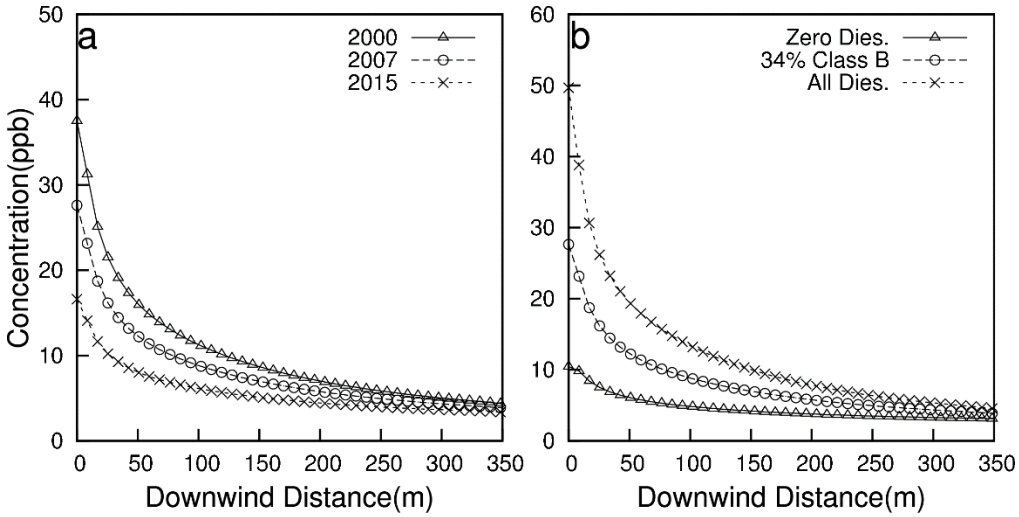

Figure 6 Sensitivities of predicted NO_x concentrations due to (a) vehicle fleet year (2000, 2007 and 2015) and (b) fraction of heavy duty vehicles (0%, 34% and 100%). NO_x is units of ppb.

Figure 6(b) shows the predicted NO_x concentrations for different fractions of heavy duty vehicles. Apart from the base case results (34% class B vehicles), two additional simulations are included, one with all vehicles treated as class B vehicles and one with all vehicles treated as Class A vehicles. The simulations show an increase in predicted concentrations of NO_x with an increase of the heavy duty vehicle fraction in the vehicle fleet. This is because in the MOVES modeled diesel vehicles generally produce more NO_x when compared to gasoline driven vehicles, and most of the heavy duty vehicles in the vehicle fleet are diesel powered. Although the results are affected by the Class B fractions, uncertainties in the estimation of heavy duty fractions are not expected to significantly change the simulation results. Using the reported heavy duty vehicle fraction based on the number of axles and lumped MOVES classes with county specific average vehicle emission, reasonable results can be achieved in this study.

2.5.3 Impact of full chemistry on near-road NO and NO_2 predictions

In Section 2.4.3, it is demonstrated that using the SAPRC99 photochemical mechanism does not significantly alter the predictions of NO and NO_2 near roadways. However, the simulations were for a rural road with high diesel fraction with low vehicle traffic compared to more busy urban freeways (for example see Zhu et al. (2002)). Since gasoline vehicles typically emit more VOCs than diesel vehicles but less NO_x, it is necessary to evaluate if the conclusion drawn in Section 2.4.3 is still applicable under high traffic volume and gasoline faction scenarios. Figure 7(a) and 7(b) illustrate the change in NO and NO_2 concentrations near-road predicted by simple and full chemistry with the base case (17.34 vehicles min^{-1}) and 10 times of the vehicle density, all with a 100% gasoline vehicle fleet. Same boundary conditions used in the base case are used in the simulations. Similar to figure 3, only slight changes in predicted concentrations of NO and NO_2 are predicted in the full chemistry cases compared to the simple chemistry cases.

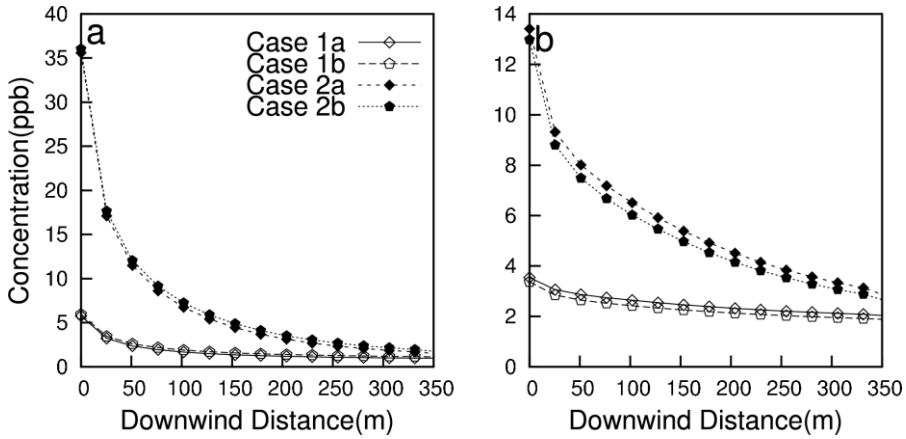

Figure 7 Predicted NO (a) and NO_2 (b) using simple and full chemistry under higher vehicle density (173 vehicles min^{-1}) and 100% gasoline passenger vehicle fleet. Case 1a: full chemistry with original vehicle density; Case 1b: simple chemistry with original vehicle density; Case 2a: full chemistry with higher vehicle density; Case 2b: simple chemistry with higher vehicle density.

Another sensitivity study is conducted by increasing boundary conditions of O_3 (from 26 ppb in the base case to 55 ppb) and VOCs (from 3.2 ppb in the base case to 20 ppb). The higher boundary concentrations were extracted from a grid representing urban Houston in a regional air quality simulation using the CMAQ model with SAPRC99 mechanism. Again there is only small difference from the simple chemistry case when full SAPRC99 chemistry is used. These simulations indicate that the three-reaction mechanism is sufficient in predicting near-road NO and NO_2 concentrations.

2.5.4 Regional impact of NO_2 to NO_x ratio

In the previous section, it is demonstrated that the assumption of NO_2 to NO_x ratio of 5% can leads to erroneous estimation of NO_2 near roadway. The potential impact of a higher NO_2 to NO_x ratio in regional air quality modeling has not been discussed in detail. In this study EPA's Community Multiscale Air quality Model CMAQ (version 4.7.1) (Byun and Schere, 2006) is used to study the impact of a higher NO_2 to NO_x ratio (29% based on this study) instead of the commonly used ratio of 5% on air quality predictions in Southeast Texas. The simulation episode is from August 16th to September 5th 2000, which is part of the Texas Air Quality Study 2000. Details of the modeling episode, model inputs and model evaluation can be found in several previous model studies (Ying and Krishnan, 2010; Zhang and Ying, 2011a, b) and thus are not included here. Two different simulations with different NO_2 to NO_x ratio of 5% and 29% were used to split the total NO_x emissions from on-road emissions. The results of the simulations are presented in figure 8.

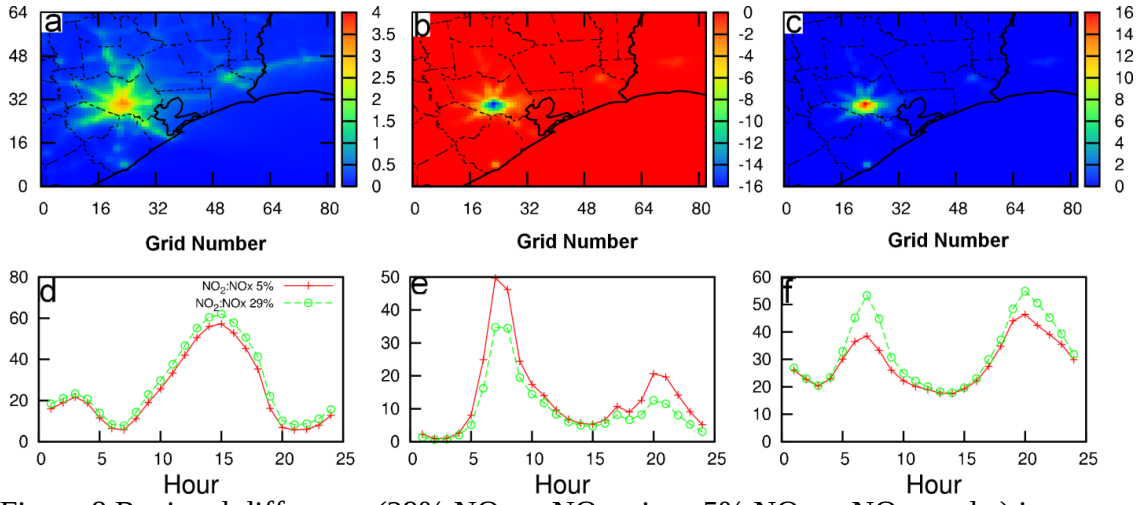

Figure 8 Regional difference (29% NO_2 to NO_x minus 5% NO_2 to NO_x results) in episode averaged CMAQ predictions of (a) 8-hr O_3, (b) NO at 1900 CST and (c) NO_2 at 1900 CST. The episode averaged diurnal variation of (d) O_3, (e) NO and (f) NO_2 at grid cell (22,31) where the differences are most significant are also illustrated. While the yaxis denotes grid number in panels (a)-(c), they denote concentration (ppb) in panels (d)-(f). Units are ppb for all the panels.

Figure 8(a) shows that in the urban Houston area where vehicle emissions are highest, episode-average 8-hr (1100-1800CST) O_3 concentrations are increased by approximately 3-4 ppb due to the increased NO_2 fraction in the NO_x emission. The maximum increase can be as high as 6 ppb. Figure 8(b) and 8(c) show a decrease of peak-hour NO (0700CST) and an increase in peak-hour NO_2 concentrations in the case with 29% ratio compared to the 5% ratio case. Higher NO_2 concentrations lead to less O_3 loss due to $NO+O_3$ titration reaction, thus explaining the predicted higher O_3 concentrations. Figure 8(d), (e) and (f) show the predicted episode average concentrations of O_3, NO and NO_2 from the two cases as a function of hour of a day in a grid cell in Houston where maximum differences are observed. A decrease in NO and an increase in NO_2 and O_3 is observed at all hours in the case with 29% ratio compared to the case with 5% ratio. A rush hour peak where the maximum NO and NO_2 concentrations and minimum O_3 concentrations is observed at 0700 hrs.

Although the differences are significant, they are based on a uniform change in the emission NO_2 to NO_x ratio in the entire model domain. The actual change in the NO_2 to

NO_x ratio is expected to be significantly affected by the fraction of diesel vehicles, the age of the vehicles and types of emission control equipment. The 29% ratio based on a fleet of 34% of heavy duty vehicle fraction might represent a higher estimation for regions where more light duty vehicles are expected. Thus, the values reported in this sensitivity study should be considered as a possible upper limit of the impacts on ambient O_3, NO and NO_2 levels.

2.6 Conclusions

The TAMNROM-3D model with the SAPRC-99 photochemical mechanism can reasonably predict the concentrations of gaseous and particulate matter concentrations near a rural roadway with significant fraction of heavy duty vehicle traffic. Emissions from on-road vehicles for near roadway air quality studies can be easily estimated with the MOVES model, using population-averaged EFs for three lumped vehicle classes based on the number of axles and vehicle count data that differentiate vehicles by axles or by weight (as light and heavy duty vehicles). Results from the NO_2 simulations imply that both the traditional 5% NO_2 to NO_x ratio and the MOVES predicted NO_2 to NO_x ratio (~9%) under-represents the actual NO_2 concentrations near roadways. A much higher NO_2 to NO_x ratio (29%) in the emissions might be needed to match the predicted and observed downwind NO_2 concentrations. This higher NO_2 to NO_x ratio also has significant implication in regional air quality modeling and attainment demonstration as the regional air quality simulation in Southeast Texas suggests that using an NO_2 to NO_x ratio of 29% instead of the traditional 5% can lead to higher 8-hour O_3 predictions by more than 6 ppb.

From a near-road modeling perspective, NO_2 concentrations are not significantly affected by RO_2 radical concentrations generated from VOC emissions. This study indicates that the dominant pathway of conversion of NO to NO_2 is its reaction with O_3 and complex radical reactions can be neglected.

As it has been demonstrated in the study, the MOVES EF model still has significant uncertainties for NO_x and is likely to overestimate total NO_x emissions and

underestimate NO_2 fraction for modern-day vehicles. More studies are needed to constrain the uncertainties of the MOVES model. For example, source typed regional air quality models like CMAQ can be used to study the performance of MOVES in predicting the observations at vehicle influenced cases (Kota et al., 2013b). Moreover, the MOVES predicted emission factors can be compared with emission factors estimated using observations collected near tunnel (Fujita et al., 2012). Care should be taken when MOVES is applied in near-road modeling studies without sufficient observation to constrain the model predictions, as the results may have large uncertainties especially in NO_2 predictions.

3. ESTIMATION OF ON-ROAD VEHICLE CO AND NO_X NATIONAL EMISSION INVENTORIES USING AN URBAN-SCALE SOURCE-ORIENTED AIR QUALITY MODEL*

The MOBILE6.2 model was replaced by the Motor Vehicle Emission Simulator (MOVES) in 2012 as an official tool recommended by the United States Environmental Protection Agency (US EPA) to predict vehicular pollutant emission factors. In this study, on-road vehicle emission inventories of CO and NO_x for Southeast Texas generated by MOVES and MOBILE6.2 in two versions of the 2005 National Emission Inventory (NEI) were studied by comparing predicted CO and NO_x using the EPA's Community Multiscale Air Quality (CMAQ) Model incorporated with a source-oriented gas phase chemical mechanism with measurements made at six urban and industrial sites in Southeast Texas. The source tracing technique allows direct determination of contributions of on-road vehicles to overall CO and NO_x concentrations and identification of ambient concentration measurements which are mostly impacted by vehicle emissions.

By grouping the fractional bias (FB) values of the hourly predictions based on vehicle contributions to total CO or NO_x concentrations, clear trends in the FB were observed, indicating systematic biases in the emission inventory for these species. Data points dominated by vehicle emissions suggest that surface CO concentrations due to vehicle exhaust are significantly over-estimated by a factor of 2 using either MOVES or MOBILE6.2. NO_x concentrations are overestimated by approximately 20-35% and 70% by using the MOBILE6.2 and MOVES emissions, respectively. Emission scaling runs show that a domain-wide reduction of MOBILE6.2 CO emissions by 60% and NO_x

---

* *Reproduced with permission from:* Kota, S.H., Zhang, H., Chen, G., Schade, G.W., Ying, Q., 2014. Evaluation of on-road vehicle CO and NOx National Emission Inventories using an urban-scale source-oriented air quality model. Atmos. Environ. 85, 99-108. Copyright 2014 Elsevier Ltd.

emissions by 15-25% leads to better model performance of exhaust CO and NO_x concentrations in the current study.

3.1 Introduction

The United States Environmental Protection Agency (US EPA) develops National Emission Inventories (NEI) to aid air quality studies by providing temporal and spatial emission estimates from different sources across the nation. Air pollution control agencies use NEI and other emissions inventories to model air quality and to formulate air quality attainment plans that will meet federal and local standards. Motor vehicles are significant contributors to air pollution (Harley et al., 1993; Schauer et al., 1996; Ying and Kleeman, 2006; Zavala et al., 2006; Zhang and Ying, 2011a), global climate change Wegmann et al., 2005 and public health problems (Brunekreef et al., 1997; Gauderman et al., 2007; Hoek et al., 2002; Samet et al., 2000) by directly emitting significant amounts of criteria pollutants, including carbon monoxide (CO) and nitrogen oxides (NO_x), among others. Many of these emissions also contribute to the formation of secondary pollutants such as ozone and secondary particulate matter. To evaluate the impact of vehicle traffic on these issues, an accurate estimation of pollutant emissions from a vehicle fleet is essential.

The US EPA used the MOBILE model in the past to estimate the vehicle emission factors for regulatory purposes. The MOBILE6.2 model (the latest version in the MOBILE series) is a fuel based emission factor model that broadly classifies vehicles into gasoline motorcycles, diesel and gasoline powered cars, trucks and buses. In addition, there are multiple classes of trucks based on their weight. Recently, the US EPA requested replacement of the MOBILE6.2 model with the MOVES (Motor Vehicle Emission Simulator) model (USEPA, 2010b) as the official model for estimating on-road vehicle emissions. MOVES uses an activity based approach and classifies vehicles based on their utilities (passenger cars, passenger trucks, light commercial trucks, refuse trucks, single unit short-haul trucks, single unit long-haul trucks, combination short-haul trucks, combination long-haul trucks, motorcycles, motor homes and buses). In this

model, each vehicle type can be combined with one of several fuel types (diesel, gasoline, natural gas, electric, etc.) to estimate their emission factors. While both MOBILE6.2 and MOVES include a regional emission component to support the development of national and regional emission inventories, MOVES also includes a project-level emission component to local-scale emission and air quality modeling.

Several previous studies have investigated the differences between NO_x emissions estimated by these two models and reached generally consistent results. For example, Vallamsundar and Lin (2011) showed that NO_x emissions from the MOVES (version 2010a; MOVES hereafter) model was approximately 20% higher than MOBILE6.2 estimations with identical input data for Cook County, IL. Fujita et al. (2012) compared MOVES and MOBILE6.2 estimated NO_x using vehicle data collected in a traffic tunnel in California and concluded that MOVES predictions were approximately 10% higher than MOBILE6.2 predictions. Kota et al. (2012) also demonstrated that MOVES predicts higher emissions factors of NO_x and the differences are more significant for heavy-duty vehicles at all speeds and for passenger vehicles at low speeds. Differences between MOVES and MOBILE6.2 in CO predictions have also been reported. For example, Fujita et al. (2012) reported that CO concentrations in the traffic tunnel predicted by MOVES were lower than those predicted by MOBILE6.2 by approximately 30%. Kota et al. (2012) found that MOVES-predicted passenger car CO emission factors are approximately 12-34% lower than MOBILE6.2 predictions using the national average vehicle fleet of 2007. However, CO emission factors for heavy duty vehicles predicted by MOVES can be as much as 63% higher than MOBILE6.2 predictions.

As MOVES and MOBILE6.2 predictions can vary significantly, it is essential to evaluate these predictions against measured ambient concentrations. A direct evaluation was made by Fujita et al. (2012) to compare predicted CO and NO_x concentrations with observations made in a tunnel in California dominated by passenger car traffic. It was concluded that both MOVES and MOBLIE6.2 significantly over-predicted measured NO_x concentrations by 30-45% although MOVES predictions were closer to the

observations. CO concentrations were also over-predicted significantly by both models and MOVES predictions were better.

While the traffic tunnel measurements provided excellent direct data to evaluate the emission factor models, the evaluations were limited by vehicle fleet composition which might not be representative for other areas. However, many regional air quality monitoring sites measure CO and NO_x concentrations simultaneously over much longer periods of time with hourly resolution, which can provide additional data to evaluate the emission factor models. Wallace et al. (2012) observed that CO/NO_x ratios predicted by MOVES were better than MOBILE6.2 at a freeway-influenced regional air quality monitoring site in Idaho, although both models significantly over-predicted the observed ratios. The Wallace et al. (2012) study assumed CO/NO_x ratio measured at the air quality site during morning traffic hours were dominated by CO and NO_x from vehicle emissions, which might not be valid for many other surface air monitoring sites because other local or regional sources could also contribute to NO_x and CO concentrations. Most of the studies to this date evaluated vehicle related emission inventories by selecting morning rush hours at urban sites as representative data for the analyses (Parrish, 2006; Wallace et al., 2012; Zavala et al., 2009), assuming pollutant concentrations during these hours were dominated by emissions from vehicles. This assumption, however, is not always correct as many factors such as vehicle fleet differences on weekday and weekends, and other emission sources could affect the predicted concentrations during rush hours.

Another approach that utilizes the ambient monitoring data is to use regional air quality models, with MOVES or MOBILE6.2 based regional emission inventories, to predict CO and NO_x concentrations at air quality monitoring sites. By comparing the predicted and observed concentrations, an indirect evaluation of the underlying emission factor model can be performed. McKeen et al. (2009) reported that CO emissions in 1999 NEI might be significantly overestimated, based on comparisons of air quality model predicted and emission inventory reported CO/NO_y ratios. Brioude et al. (2011) applied an inverse modeling technique and determined that 2005 NEI-based CO

emissions in the Houston urban area were overestimated by 41%. Kim et al. (2011) compared predicted NO_x with satellite observations in Texas and concluded that NOx emissions from urban Houston were reasonably represented. However, none of these studies have been able to clearly separate vehicle emissions from other emission sources. Simon et al. (2011) used the Community Multiscale Air Quality (CMAQ) Model in the northeastern United States with two different versions of the 2005 NEI, and concluded that MOVES predicted higher NO_x than MOBILE6.2 with smaller biases at urban areas during morning rush hour peaks. However, the conclusion is sensitive to the selection of the meteorology model. Kota et al. (2012) showed that CMAQ NO_x and ozone predictions using MOVES agreed better with observations at 7 out of 11 surface observation sites in Southeast Texas during the 2006 Texas Air Quality Study. However, since the predicted concentrations by traditional regional air quality models are affected by a combination of different sources, direct comparison of predicted and observed concentrations does not provide a direct evaluation of the underlying emission factor models either.

Recently, source-oriented versions of the CMAQ model have been developed to directly determine contributions of different sources to predicted air quality by tracking emissions from multiple sources simultaneously as well as their transport, transformation and removal in the atmosphere. The source-oriented models have been applied in the past to determine contributions of different sources to VOCs and NO_x in Southeast Texas (Ying and Krishnan, 2010; Zhang and Ying, 2011a), among other applications in Texas and California. The objective of this study is to apply the source-oriented air quality modeling approach to track emissions of CO and NO_x from on-road vehicle sources separately to directly evaluate the emission inventories of these two compounds based on MOBILE6.2 and MOVES generated emission factors.

3.2 Model Description

The SAPRC99 (S99) photochemical mechanism (Carter, 2000) was modified to include additional source-specific species and reactions, and incorporated into the CMAQ model

(version 4.7.1) to determine source contributions to CO and NO_x from on-road vehicles and other sources. The CMAQ model is a three-dimensional regional air quality model developed by the US EPA that simulates the emission, transport, transformation and removal of gas and particulate air pollutants in the atmosphere. It has been widely used in both regulatory and research applications (Simon et al., 2012). More details of the CMAQ model can be found in Byun and Schere (2006), Foley et al. (2010) and Carlton et al. (2010).

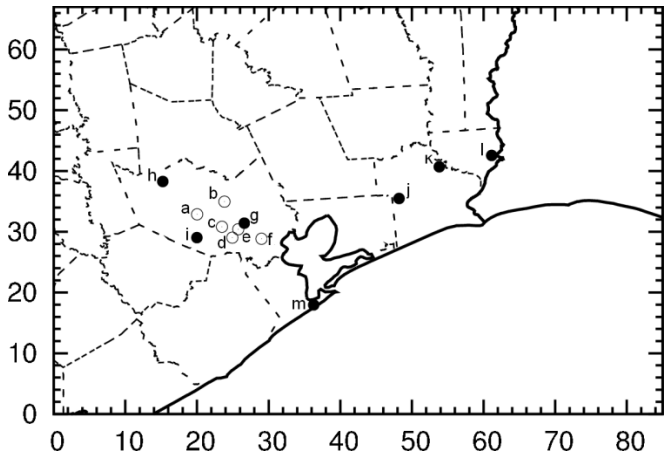

Figure 9 The Southeast Texas model domain with locations of air monitoring stations. Stations 'a-f' have both CO and NO_x observations available, while stations 'g-m' have only NO_x observations. Grid cell index for the 4 km domain are shown on x and y axis.

To determine the contribution of vehicle sources to overall CO concentrations, CO emissions from on-road vehicles are represented in the emission input files as CO_X1 while CO emissions from other sources, including initial and boundary conditions, are combined and represented as CO. The S99 mechanism is modified so that any reaction that involves CO as a reactant is expanded into two reactions. For example, CO oxidation reaction with OH is expanded into two reactions as shown in reaction set 3.R1,

$$\begin{aligned} &CO + OH \rightarrow HO_2 \\ &CO\_X1 + OH \rightarrow HO_2 \end{aligned} \qquad (3.R1)$$

where CO_X1 and CO represent concentrations due to on-road and all other sources, respectively. Modifications to the reactions that generate CO are not necessary as the produced CO is automatically grouped with the emitted CO from other sources. Similarly, CO entering the model domain as boundary conditions is also represented as other CO species. Modifications to the NO_x chemistry to determine contributions due to on-road vehicle sources are similar. In the emission input files, NO_X1 and NO_2_X1 are used to represent emissions from on-road vehicle sources and NO and NO_2 are used to represent emissions from all other sources and from upwind sources through boundary conditions. Reactions that involve reactive nitrogen species are expanded to include reactions for NO_X1, NO_2_X1 and other typed nitrogen species. More details of expanding the NO_x chemistry in S99 can be found in Zhang and Ying (2011a).

3.3 Model Application

Details of the model episode, domain and input data have been described previously (Kota et al., 2012; Zhang and Ying, 2012) and are briefly summarized below. In this work, the modified CMAQ 4.7.1 with the source-oriented S99 mechanism, described in the previous section, was applied to predict concentrations of CO and NO_x due to on-road vehicle emissions in Southeast Texas during a 2.5 week long episode (August 28 to September 15, 2006). The simulations were conducted using a three-level nested domain with the inner most 4-km resolution Southeast Texas domain centered on the Houston metropolitan area. The nested-domain setup is based on that used by the Texas Commission on Environmental Quality (TCEQ), and has been documented in detail in a previous study (Zhang and Ying, 2011b). Simulation results of the third-level 4-km resolution domain (figure 9), which covers Houston-Galveston-Brazoria (HGB) and Beaumont-Port Arthur (BPA) areas, is discussed in detail in this study.

The US EPA's NEI for 2005 (2005 NEI) was used to generate anthropogenic emissions of CO, NO_x, SO_2, NH_3 and VOCs. The US EPA's Sparse Matrix Operator Kernel Emissions (SMOKE) emission processing model (version 2.5) was used to process the NEI emission inventory to generate the gridded, speciated and temporally

allocated emission rates for the CMAQ model. NEI assumes monthly time resolution of meteorology and source activity. Modifications were made to the SMOKE model so that emissions from on-road vehicles are saved separately from other sources in the final emission files (Ying and Krishnan, 2010). Two versions of the 2005 NEI were acquired from the US EPA: NEI v4, which uses the MOVES model to generate on-road vehicle emissions, and NEI v2, which uses the MOBILE6.2 model to calculate emissions from on-road mobile sources. The 2005 NEI v2 uses county-specific vehicle fleet information and vehicle miles travelled (VMT) data based on default database in the EPA's National Mobile Inventory Model (NMIM) and state-supplied data set to directly generate emissions of gases at county level. Emissions from the State of Texas were based on Texas-specific data provided by TCEQ. The 2005 NEI v4 uses state level MOVES simulations and allocates the emissions to county-level using the county-specific data used in NEI v2. These county-level emissions generated by the state-month approach were then spatially allocated using SMOKE into model grid cells. More details about the 2005 NEI v2 and v4 can be found at the US EPA Clearinghouse for Inventories and Emissions Factors (CHIEF) website (http://www.epa.gov/ttn/chief/index.html). Emissions from other anthropogenic activities for the two NEI inventories are identical. Biogenic emissions were generated using the biogenic emission inventory system version 3 (BEIS3) imbedded in the SMOKE model.

Table 4 Predicted average-day emissions of CO and NO_x (10^3 kg day^{-1}) in the 4-km CMAQ model domain for August 2006.

	CO		NO_x	
	MOBILE6.2	MOVES	MOBILE6.2	MOVES
LDGV	1053.4	977.3	77.2	130.9
LDGT	503.7	816.0	42.4	103.1
HDGT	44.5	50.5	11.2	7.0
MC	3.5	5.1	0.2	0.2
LDDV	0.2	0.1	0.2	0.3
LDDT	0.2	1.0	0.3	1.6
HDDT	45.9	78.7	156.1	232.5
BUS	2.3	3.0	7.5	8.7
Total	1653.8	1931.6	295.1	484.3

Note: LDGV = Light duty gasoline vehicles; LDGT = Light duty gasoline trucks; HDGT = Heavy duty gasoline trucks; MC = Motorcycles; LDDV = Light duty diesel vehicles; LDDT = Light duty diesel trucks; HDDT = heavy duty diesel trucks; BUS = buses.

The provided EPA emission inventories were formatted for regional air quality modeling purposes, and MOVES emissions were internally mapped to MOBILE6.2 classifications. Table 4 summarizes the predicted CO and NO_x emissions in Texas for a representative weekday (August 31, 2006). The differences in the underlying emission factors used in the two emission models are likely the fundamental cause of the observed regional emission differences. First of all, MOVES incorporates more recent vehicle emission testing data. For example, NO_x emission rates for heavy-duty diesel trucks in MOVES were based on emission data collected for vehicle model years 1994-2006 while the MOBILE6.2 emission rates were based on vehicles from mid to late 1990s.Secondly, the algorithms used by the two models to interpolate the experimental data can also cause differences. For example, MOVES needs vehicle specific power, which is affected by vehicle conditions as well as driver behavior, in the vehicle emission factor estimations. Uncertainty analysis is needed to evaluate the error of vehicle emission inventory estimations due to uncertainties in these additional inputs.

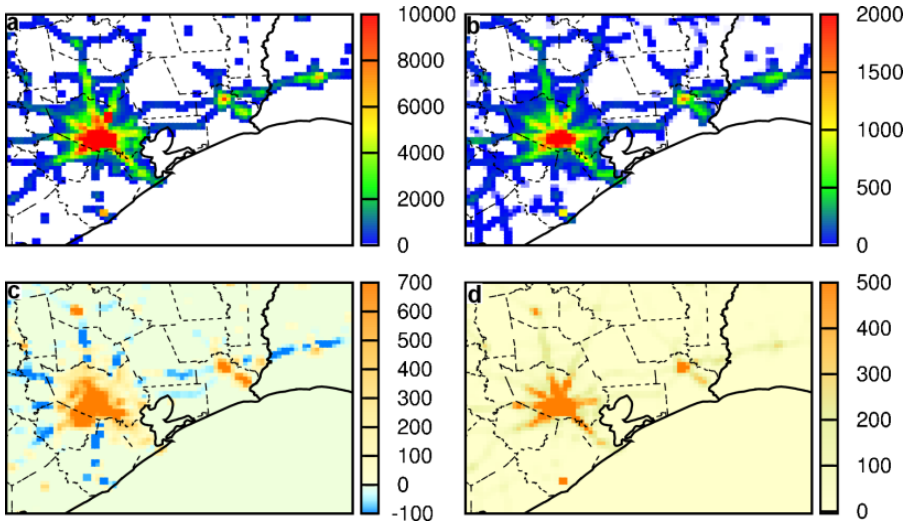

Figure 10 Episode average emission rates of CO (a) and NO_x (b) from on-road vehicle sources based on MOBILE6.2, and the differences of the episode average emission rates between MOVES and MOBILE6.2 for CO (c) and NO_x (d) in the 4-km domain. The difference plots are calculated using MOVES case - MOBILE case. Units are kg day^{-1} (per grid cell). Ranges are scaled to better illustrate spatial distribution.

Regional average emission rates of CO and NO_x from on-road vehicles in the Southeast Texas domain and differences between the MOVES and MOBILE6.2 emission estimates are illustrated in figure 10. Overall, the MOVES model predicts higher emissions of CO and NO_x, with a higher percentage difference for NO_x.

As it has been shown in a previous study that different meteorology models affect air quality model's prediction of NO_x concentrations (Simon et al., 2011), two sets of meteorological inputs were used in this study to drive the model simulations. The first set of meteorological files was generated by the TCEQ using the Penn State/UCAR mesoscale model (MM5) and was extensively evaluated in a previous study (Ngan et al., 2012). The second set of meteorology inputs were generated in-house using the Weather Research and Forecasting (WRF) Model following the same domain configurations as the MM5 simulations. The initial and boundary conditions for the WRF simulations were prepared using the 1°×1° resolution (National Centers for Environmental Prediction) FNL (Final) Operational Global Analysis dataset (available at http://rda.ucar.edu/datasets/ds083.2/). The land use/land cover and topographical data were from the 30 sec resolution default WRF input dataset. The performance of the MM5 and WRF model for 10-m wind speed and wind direction is shown in table 5. Both models over-predict wind speed but MM5 predictions are generally lower and closer to observation at all but one station. The two models have similar performance in wind direction.

Table 5 Mean Fractional bias (MFB) of predicted wind speed and direction by MM5 and WRF at different TCEQ operated meteorological stations.

		Wind Speed (m/s)					Wind Direction				
	Site	AO*	AS*	MFB	MFE	RMSE	AO	AS	MFB	MFE	RMSE
MM5	Aldine	1.98	2.49	0.22	0.37	1.09	119.93	103.58	-0.12	0.65	102.69
	NW Harris	1.86	2.61	0.33	0.45	1.29	165.67	143.11	-0.17	0.63	120.17
	Bayland park	2.21	2.29	0.04	0.39	1.11	151.40	138.25	-0.12	0.61	116.57
	Park Place	2.00	2.49	0.19	0.42	1.22	160.59	135.39	-0.18	0.70	130.71
	Houston East	1.67	2.57	0.41	0.46	1.24	133.81	106.54	-0.20	0.64	105.83
	Clinton drive	1.95	2.37	0.19	0.37	1.01	141.95	118.20	-0.11	0.71	124.30
	Deer Park	2.01	2.58	0.25	0.39	1.17	154.90	132.70	-0.19	0.70	129.60
	Galveston	3.62	3.49	-0.03	0.31	1.23	149.78	142.73	-0.03	0.35	78.35
	Conroe	2.77	3.29	0.20	0.37	1.34	199.92	146.75	-0.29	0.51	124.95

Table 5 Continued

		Wind Speed (m/s)					Wind Direction				
	Site	AO	AS	MFB	MFE	RMSE	AO	AS	MFB	MFE	RMSE
WRF	Aldine	1.99	2.54	0.21	0.48	1.42	118.77	123.64	-0.01	0.68	115.66
	NW Harris	1.87	3.40	0.51	0.64	2.25	168.66	136.85	-0.24	0.74	135.55
	Bayland park	2.19	2.66	0.17	0.51	1.55	154.88	153.08	-0.03	0.62	117.22
	Park Place	1.98	2.86	0.33	0.53	1.63	159.03	156.61	-0.04	0.70	127.17
	Houston East	1.67	2.61	0.38	0.52	1.51	135.33	107.54	-0.22	0.70	115.38
	Clinton drive	1.95	2.74	0.32	0.49	1.44	142.76	130.52	-0.06	0.69	121.58
	Deer Park	2.01	2.91	0.34	0.51	1.60	158.62	137.53	-0.18	0.66	121.04
	Galveston	3.61	3.36	-0.07	0.39	1.78	148.86	145.37	-0.08	0.59	118.57
	Conroe	2.75	3.77	0.30	0.47	1.88	210.07	160.67	-0.29	0.56	128.25

* AO and AS denote average observation and simulation respectively.

Two sets of simulations, one with the on-road emissions based on the MOVES emission factors (MOVES case hereafter) and another with on-road emissions based on the MOBILE6.2 emission factors (MOBILE case hereafter), are carried out in this study. In each set of simulations, two simulations were conducted, one each using MM5 and WRF meteorological inputs to drive the air quality simulations.

3.4 Results and Discussion

3.4.1 Model performance of overall CO and NO_x

Figure 11(a) and 11(b) show the relative differences between the MOVES and MOBILE6.2 (using MM5 meteorology) predicted episode-average regional CO and NO_x concentrations. As expected, higher NO_x emissions from MOVES resulted in higher predicted concentrations compared to the MOBILE case. The urban Houston area shows the biggest difference in predicted emissions and ambient concentrations. The maximum percentage difference of surface CO and NO_x concentrations is approximately 16% and 43%, respectively. Table 6 shows the list of air quality monitoring stations and the mean fractional bias (MFB) for predicted CO and NO_x using different combinations of emissions (MOVES or MOBILE6.2) and meteorological inputs (MM5 or WRF). The observation data at those stations were acquired from the US EPA Air Quality System (AQS). Simulations using MM5 generally show better model performance than WRF

simulations using the same emission inputs because of better wind speed predictions. Simulations using MOVES generated vehicle emissions show better model performance of CO and NO_x than their counterparts using MOBILE6.2 emissions, if WRF meteorology inputs are used. When MM5 meteorology inputs are used, there is no clear indication of improvement in model performance using MOVES emissions.

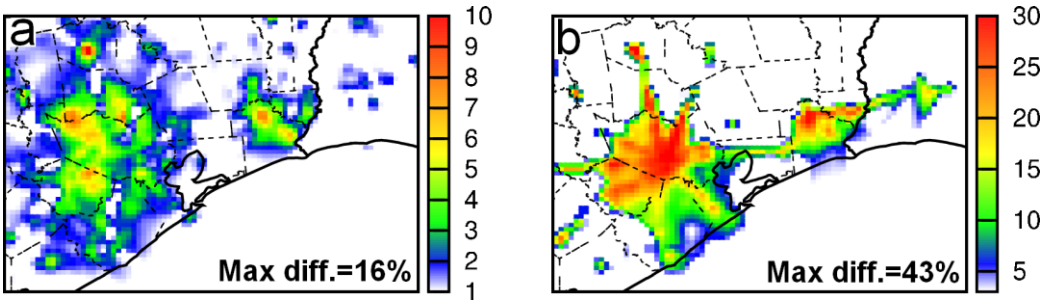

Figure 11 Relative differences of episode average (a) CO and (b) NO_x concentrations (ppb) from on-road vehicles in Southeast Texas. The relative difference is calculated as (MOVES case–MOBILE case)/MOVES case×100%. Ranges are scaled to better illustrate spatial distribution.

Table 6 Mean Fractional Bias (MFB*) of CO and NO_x at different air quality monitoring sites in Southeast Texas.

	CO				NO_x			
	MOVES	MOBILE	MOVES	MOBILE	MOVES	MOBILE	MOVES	MOBILE
Site	MM5		WRF		MM5		WRF	
(a) Lang	-0.22	-0.26	-0.52	-0.55	-0.01	0.36	-0.69	-0.90
(b) Aldine	-0.20	-0.22	-0.54	-0.55	0.05	-0.24	-0.77	-1.00
(c)Texas Avenue	-0.07	-0.09	-0.45	-0.47	0.55	0.29	-0.06	-0.31
(d) Park Place	0.52	0.51	0.06	0.05	0.47	0.23	-0.08	-0.29
(e) Clinton drive	0.34	0.33	-0.21	-0.22	0.68	0.53	0.18	0.04
(f) Deer Park	-0.42	-0.44	-0.65	-0.67	0.87	0.80	0.64	0.59
(g) Houston East	-	-	-	-	-0.07	-0.25	-0.5	-0.65
(h) NW Harris	-	-	-	-	-0.38	-0.55	-0.89	-1.03
(i) Bayland Park	-	-	-	-	0.40	0.13	-0.27	-0.52
(j) Hamshire	-	-	-	-	-0.98	-1.12	-0.99	-1.10
(k) Beaumont	-	-	-	-	0.64	0.54	0.22	0.14
(l)West orange	-	-	-	-	-0.23	0.37	-0.78	-0.88
(m) Galveston	-	-	-	-	-0.23	-0.32	-0.91	-0.99

*$MFB=2/N*\Sigma(P_i-O_i)/(P_i+O_i)$, where N is the total number of data points, P is prediction, O is observations and subscript i represents the i^{th} data point.

Based on the overall FB values, it is hard to determine if vehicle CO and NO_x emissions are correctly estimated by the emission factor models, and whether MOVES-based NEI gives better emission estimates than MOBILE6.2-based NEI. CO and NO_x concentrations at receptor locations are not only influenced by vehicle emissions and meteorology but also emissions from other sources. For example, Zhang and Ying (2011a) showed that industries, coal combustion and natural gas are also important sources of ambient NO_x in the Southeast Texas region. Although CO is predominantly from vehicle emissions in urban areas, other combustion sources, such as industrial combustion sources in the area could also contribute to CO concentrations in the ambient air. Another potential error in CO is the allocation of off-road start exhaust emissions, which was allocated to roadways on the basis of VMT. This led to temporal and spatial misallocation of off-road vehicle emissions, as they were not related to on-road VMT activity. Errors in the emission estimations of these sources as well as the meteorological inputs might be compensated by errors in the vehicle emissions. This could lead to apparently better model performance even though the vehicle emissions were shifted towards a wrong direction.

3.4.2 CO and NO_x performance as a function of vehicle contributions

The advantage of the source-oriented model in this study is its capability of directly resolving contributions of on-road vehicle sources to total CO and NO_x concentrations. This allows a more detailed analysis of the model results to evaluate vehicle emission inventories. Six stations with both CO and NO_x measurements were used for further analysis (figure 9).

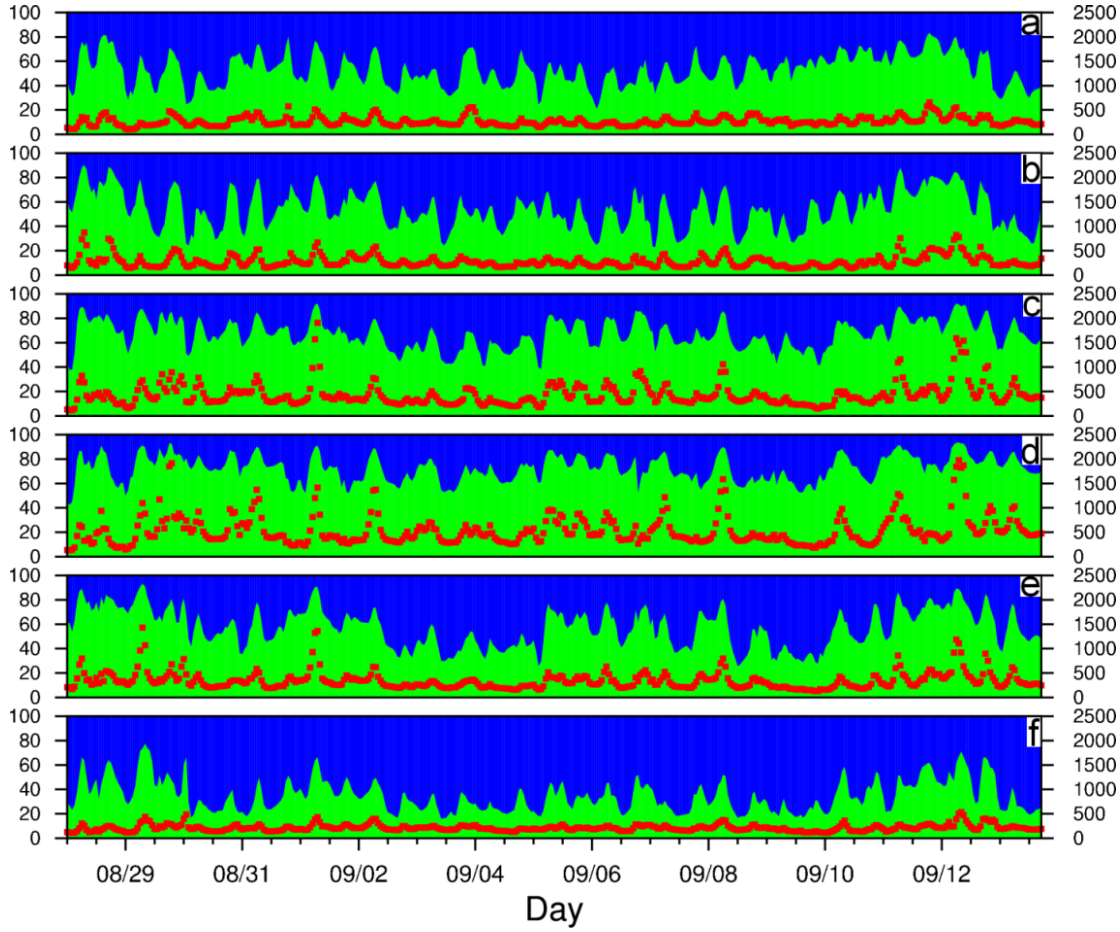

Figure 12 Time series of relative source contributions (percent of vehicles and other sources are indicated by green and blue, respectively) to total CO at stations shown in figure 9. The red dots indicate total predicted CO concentrations (ppb) from MM5/MOBILE6.2 (secondary y-axis).

Figure 12 shows the predicted time series of CO using MM5/MOBILE6.2 and relative contributions due to vehicles and other sources at the six stations. There are clear diurnal and episodic variations in the vehicle contributions to total CO concentrations. For example, the Park Place site (figure 12c) shows highest level of vehicle influence while the Deer Park site (figure 12f) shows the lowest influence. Figure 13 shows the predicted time series of NO_x using MM5/MOBILE6.2 and the relative contributions due to vehicles and other sources at the six stations. There are obvious variations in the vehicle influence among different stations. Relative contributions of NO_x due to vehicles are lower at Clinton Drive (figure 13e) and Deer Park (figure 13f), and higher at Aldine

(figure 13a) and Lang (figure 13b). Unlike CO, high concentrations of NO_x do not always correspond to higher vehicle contributions, suggesting that other sources can also be significant contributors to NO_x concentrations. In fact, the Clinton Drive and Deer Park sites are closer to the Houston Ship Channel (HSC) area and are more influenced by NO_x emissions from natural gas combustion (Zhang and Ying, 2011a).

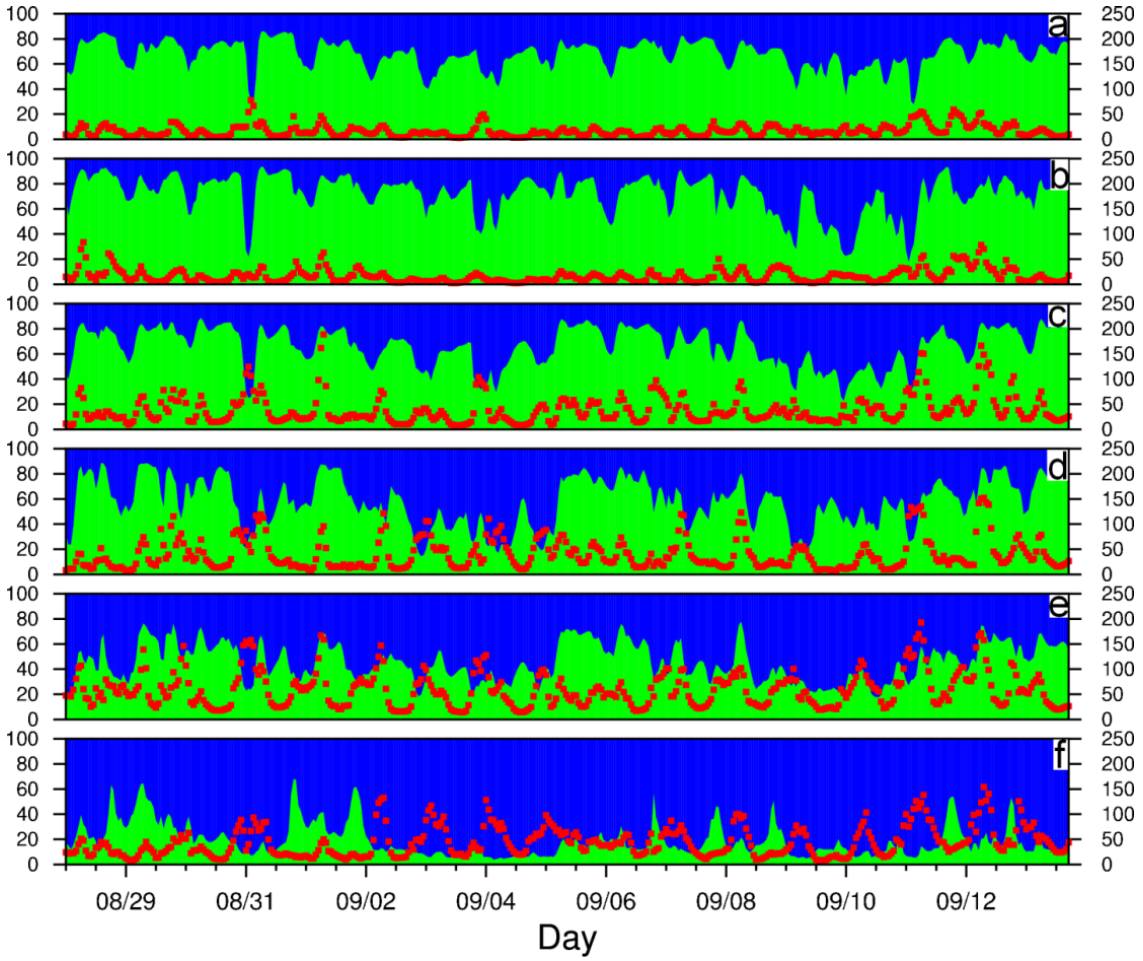

Figure 13 Time series of relative source contributions (vehicles and other sources are indicated by green and blue, respectively) to total NO_x at stations shown in figure 9. The red dots indicate total predicted NO_x concentrations (ppb) from MM5/MOBILE6.2 (secondary y-axis).

With the source-oriented CMAQ results, it is now possible to further evaluate the impact of vehicle emissions on model performance. Figure 14 shows the fractional bias (FB) of CO and NO_x as a function of relative contributions of on-road vehicles to total concentrations using all available hourly data at the six stations. FB is chosen because it is a bounded measure, and is unbiased regarding under and over-predictions (Seigneur et al., 2000). The vehicle contributions are grouped into 10 bins with a bin width of 10%. For CO (figure 14a), when the vehicle contributions are less than 50%, the FB values are generally below zero with a relatively stable median value of -0.5. This indicates that CO from some other sources is likely under-predicted in the emission inventory. For data points with higher vehicle contributions, FB increases. The median FB value is close to zero with 60-70% vehicle contributions, and exceeds 0.5 in the 90-100% range bin. The FB values of CO using MOVES-based NEI are similar to those using MOBILE6.2-based emissions. This clearly indicates that concentrations of CO due to vehicles are significantly overestimated by both MOVES-based NEI and MOBILE6.2-based NEI. Taking the median FB value of 0.6 from the 90-100% vehicle contribution bin in the MOVES case, predicted CO concentrations due to on-road vehicles are approximately 1.85 times higher than the observed values.

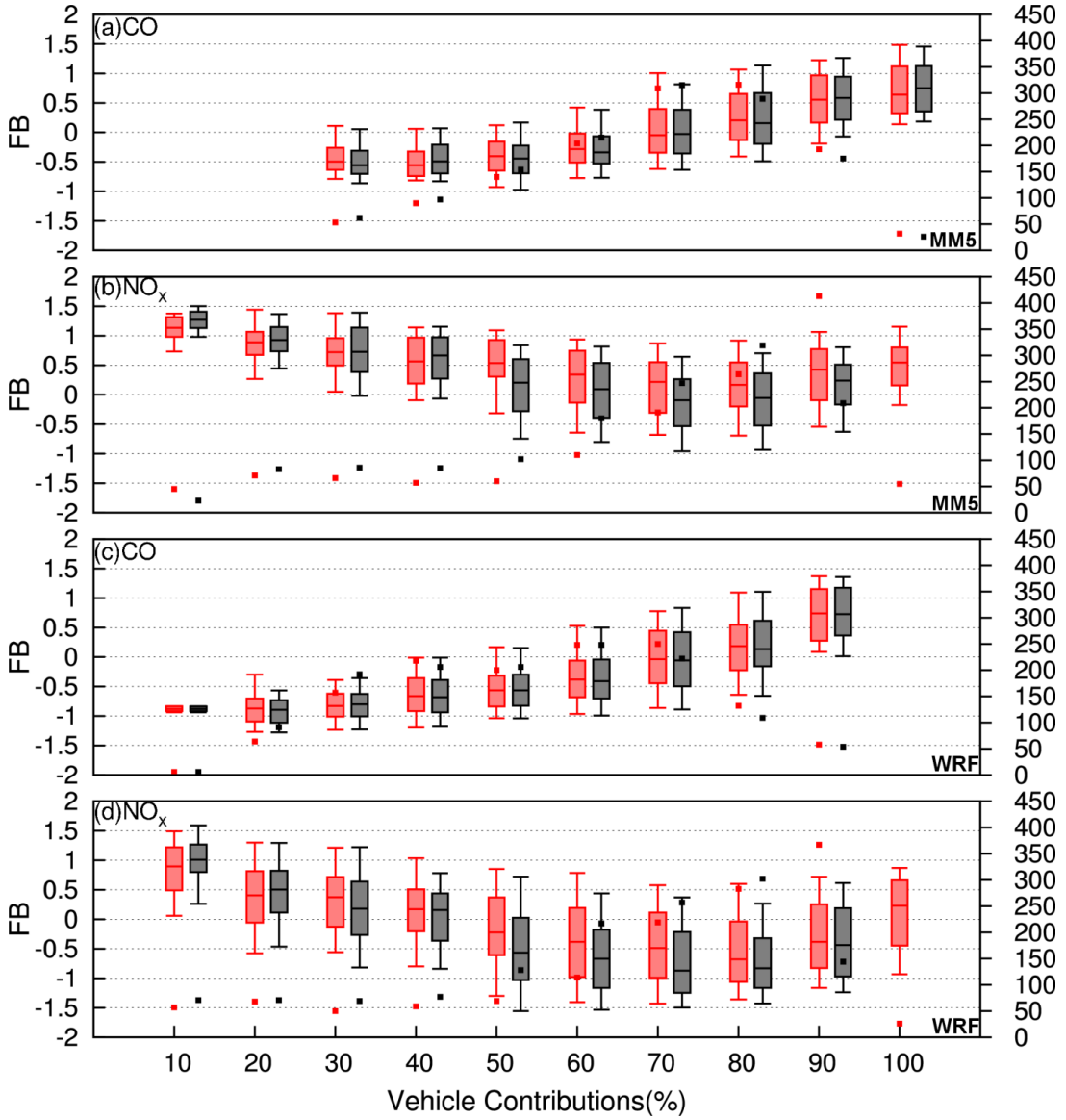

Figure 14 Fractional bias (FB) of CO (a,c) and NO_x (b,d) as a function on-road vehicle contributions to the total CO and NO_x. Simulations are conducted using MOVES (red) and MOBILE6.2 (grey) emissions with MM5 (a,b) and WRF (c,d) meteorology. The Box-Whisker plot shows the maximum, minimum, upper and lower quartiles and the median of the FB within each vehicle contribution bin. FB=2*(P-O)/(O+P), where O and P represents observation and predictions, respectively. The small squares indicate the number of data points for each vehicle contribution bin (secondary y-axis).

Figure 14(b) shows the FB of NO_x initially decreasing from large positive values when vehicle fraction increases. This suggests that emissions from some other NO_x

sources are likely overestimated and error in the vehicle emissions is lower. If NO_x emissions from vehicle sources were accurately estimated, one would expect that the decreasing trend in FB would slow down and approach a relatively constant value as vehicle contribution increases. In fact, if the meteorology inputs were perfect, the FB would approach zero. However, this is not clearly reflected in figure 14(b). Instead, the median FB value reaches its minimum at approximately 60-70% vehicle contributions but starts to increase when vehicle contributions further increase. The increasing trend in the FB suggests that, overall, vehicle emissions of NO_x are likely overestimated by both emission models. The difference between MOVES and MOBILE6.2 cases are more obvious for vehicle contributions of more than 50%, reflecting the larger differences in the NO_x emissions between MOBILE6.2-based NEI and MOVES-based NEI (figure 10). The median FB for the MOVES case at 90-100% vehicle contributions is 0.5, which corresponds to an overestimation of 1.67 times (67% higher) the ambient NO_x concentrations. There are no data points within the 90-100% vehicle contribution range, but it would be approximately 0.2-0.3 (22-35%) higher based on differences in the FB values between 50-90% vehicle contribution ranges. Based on the MM5 meteorological inputs, NO_x emissions from MOBILE6.2-based NEI are more accurate than MOVES-based NEI.

Ranges of FB values as a function of time of the day were also investigated. High vehicle contributions to CO occur more often during early morning hours (5AM-8AM) when the mixing height is low and vehicle emissions are high due to commute traffic. However, there is no significant difference in the ranges of FB for early morning, rest of the day (9AM-7PM) and nighttime hours (8PM-4AM). For NO_x, high vehicle contributions occur throughout daytime hours and ranges of FB do not differ significantly between early morning and rest of the daytime hours. This suggests that error in dispersion rates and emission rates does not vary significantly throughout the day.

Figure 14(c) and 14(d) are similar to figure 14(a) and 14(b) but are based on simulations using the WRF meteorology. Relatively poorer WRF model performance is

clearly reflected in the larger FB ranges. Similar trends can be observed for CO and NO_x model performances. FB for CO increases monotonically from negative values, indicating underestimation of the emissions from other sources, to positive values, indicating overestimation of on-road vehicle emissions. This is generally consistent with the conclusions based on MM5 meteorology, although the amount of overestimation does not appear as high as it is in the MM5 case. FB for NO_x decreases from large positive to negative values and then increases again as vehicle contributions increase. This is also consistent with results based on MM5. However, NO_x emissions from both MOBILE6.2-based NEI and MOVES-based NEI could be concluded as underestimated based on the WRF results; and MOVES-based NO_x emissions would appear to be more accurate than MOBILE6.2-based emissions because the FB values are more close to zero. However, the better overall NO_x performance using MOVES-based NEI emissions, as shown in table 6, is likely because higher NO_x emissions from MOVES-based NEI compensate the errors to the overall concentration caused by over-predicted wind speed.

Since the MM5 wind speed predictions are better than the WRF predictions in this study, and are over-predicted (table 5), the conclusions drawn from this study should be based on the simulations using MM5 instead of WRF. In the following sections, only simulations based on MM5 meteorology inputs are used in the analysis.

3.4.3 Estimating the amount of CO and NO_x emission overestimations

Since the predicted to observed CO and NO_x ratios do not necessarily reflect the amount of overestimation in the emission inventory, a series of simulations were conducted by systematically reducing the vehicle emissions of CO and NO_x emissions in the MOBILE6.2 case. CO emissions from on-road vehicles were reduced by 40%, 60% and 80%; and NO_x emissions from on-road vehicles were reduced by 5%, 15% and 25% in a series of simulations using MM5 meteorology. As shown in figure 15(a), a 60% CO emission reduction from on-road vehicle exhaust is needed to reduce the FB of CO closer to zero, when vehicle contributions approach 100%. Figure 15(b) showed that 15-

25% reductions of on-road vehicle NO_x emissions are necessary to better match the observations with predictions.

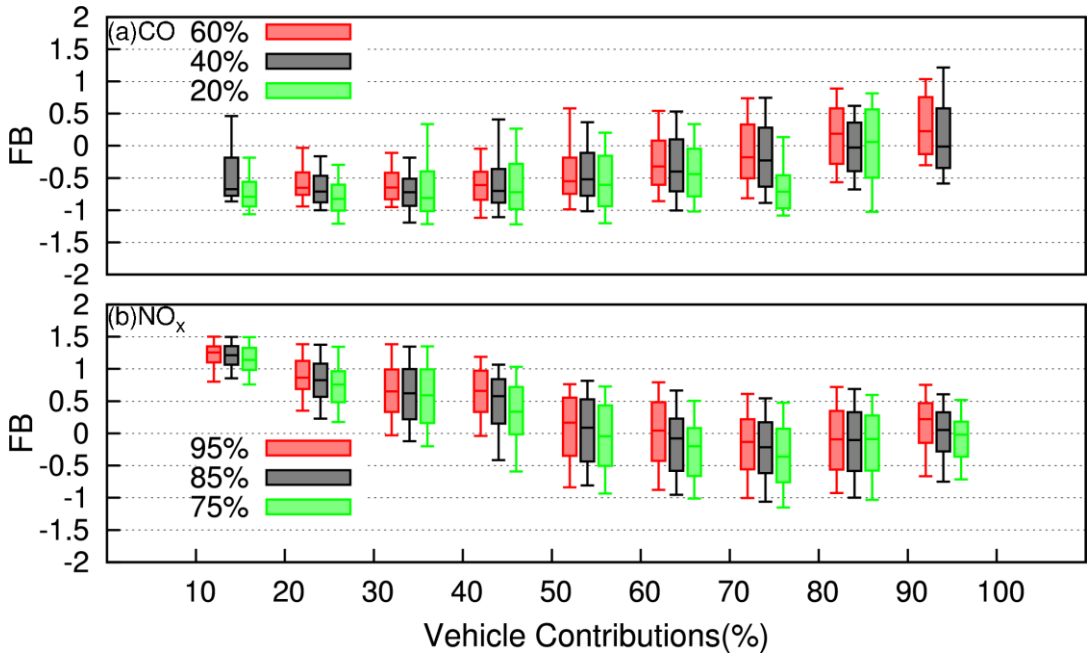

Figure 15 Fractional bias (FB) of CO (a) and NO_x (b) as a function of on-road vehicle contributions to the total CO and NO_x under different emission reduction scenarios. For CO, emissions of on-road vehicles were reduced to 60%, 40% and 20% of the base case emission rates; and for NO_x, the emissions were reduced to 95%, 85% and 75% of the base case emission rates.

The meteorology models in this study appear to over-predict dispersion by overestimating wind speed (see table 5). Wind speed predicted by WRF is even higher than MM5, leading to even lower predicted concentrations of CO and NO_x (see table 6 and figure 14). This suggests that if the models had predicted wind speed correctly, the predicted CO and NO_x concentrations would have been even higher than what is currently predicted by MM5. Thus the overestimation of CO and NO_x under high vehicle contributions is likely due to emission overestimations, and the amount of

overestimation we proposed based on emission scaling using MM5 meteorology might be a lower limit and the actual overestimation might be even higher.

3.4.4 Differentiating diesel vs. gasoline vehicle emissions

Theoretically, the method described in the previous section can allow a further detailed evaluation of diesel and gasoline vehicle emissions separately. An additional simulation that tracks the diesel emissions was conducted using MOBILE6.2 and MM5. However, almost all vehicle exhaust CO is generated from gasoline vehicles (table 4). None of the stations has any data points where diesel emitted CO dominates the total CO concentration, thus a detailed analysis of diesel CO emission is not possible in this study. The conclusions regarding CO emissions drawn from the above analysis should only be applied to gasoline vehicle emissions.

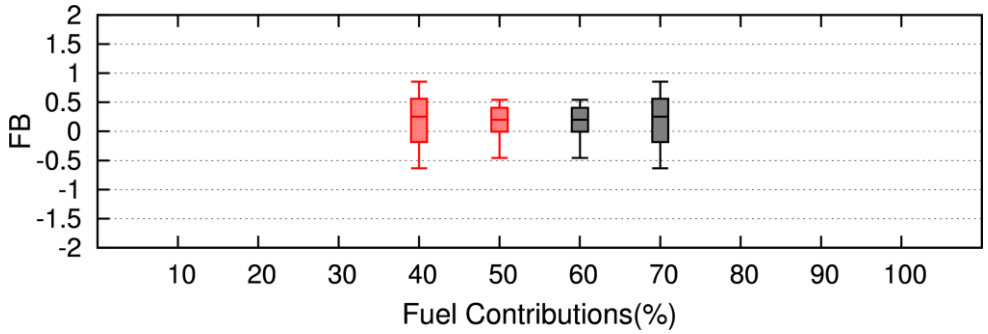

Figure 16 Fractional bias (FB) of NO_x as a function of gasoline (red) and diesel (grey) contributions to total vehicle NO_x using MM5 meteorology and MOBILE6.2 inputs. Only data points with more than 80% of NO_x from vehicle emissions are included in the analysis. Diesel contributions are always more than 50% while gasoline contributions are always less than 50% of total vehicle NO_x, thus there is no overlap in the data points.

Diesel vehicles can, however, be a significant contributor of NO_x because of significantly higher NO_x emission than gasoline vehicles on a per-vehicle basis. Data points with vehicle NO_x contributions greater than 80% were selected for further analysis. The FB values of these data points were grouped based on the ratio of diesel

NO_x to total vehicle NO_x concentrations. However, at all NO_x monitoring sites, variations of the diesel contributions to vehicle NO_x were narrowly distributed between 50 and 70%. The high diesel contributions are in agreement with NOx emissions from diesel and gasoline vehicles reported in table 4 and in Kite (2011). This lack of variation in the diesel contributions in predictions makes it difficult to quantitatively determine the error in the diesel vs. gasoline emissions. Nevertheless, as shown in figure 16, the range of the FB values increases as diesel contributions increase, suggesting that diesel NO_x emissions are likely not as accurate as gasoline NO_x.

3.5 Conclusions

In this study, on-road vehicle emission inventories of CO and NO_x in the 2005 NEI for Southeast Texas based on the MOVES and MOBILE6.2 emission factor models were evaluated by comparing predicted CO and NO_x using a source-oriented CMAQ model with observations to directly determine the contributions from on-road vehicles to CO and NO_x concentrations. The source tracing technique allows direct determination of contributions of on-road vehicles to overall CO and NO_x concentrations and identification of ambient concentration measurements which are mostly impacted by vehicle emissions. Clear trends in the fractional bias (FB) values of the hourly predictions can be observed when they are grouped by vehicle contributions to total CO or NO_x, indicating systematic biases in the emission inventory for these species. For vehicle emissions dominated data points, surface CO concentrations are significantly over-estimated by a factor of 2 using either MOVES-based NEI or MOBILE6.2-based NEI. In turn, NO_x concentrations are overestimated by approximately 30% and 70% by using the MOBILE6.2-based and MOVES-based NEI emissions, respectively. Additional simulations in this study indicated that a domain-wide reduction of 60% and 15-25% in CO and NO_x vehicle emissions, respectively, are necessary for better performance of the MOBILE6.2 case.

The quantitative results derived from this study can be affected by the accuracy of the meteorological inputs. The MM5 meteorological inputs provided by the TCEQ were

more accurate than the in-house meteorological simulation using a standard WRF model. Although both MM5 and WRF inputs lead to the conclusion that CO emissions are overestimated by both emission factor models, they led to a different assessment of NO_x emissions. Further studies using the source-oriented technique to evaluate emission inventories should carefully evaluate and improve the meteorological model results to minimize uncertainty in the subsequent source contribution analysis. Also, long-term simulations that provide more temporal and spatial coverage are needed to evaluate the performance of the vehicle emission factor models under different meteorological and vehicle fleet conditions for both gasoline and diesel vehicles. Many other sources including air quality model configuration (e.g. horizontal and vertical grid resolution), parameterization of dispersion processes (e.g. vertical turbulent diffusion coefficient), emissions processing (e.g. spatial and temporal allocation of emission) and vehicle fleet information (e.g. regional variation of vehicle fleet composition, especially high emitters), could affect the modeling results. The effects of the potential error sources on the evaluation of the accuracy of MOBILE and MOVES-based regional and national emission inventories need to be further studied.

4. ESTIMATION OF VOC EMISSION FACTORS FROM FLUX MEASUREMENTS USING A RECEPTOR MODEL AND FOOTPRINT ANALYSIS*

Fluxes of eighteen volatile organic compounds (VOCs) collected during May to July 2008 from a tower platform 60 m above the ground surface in an urban Houston residential area were analyzed using a receptor-oriented statistical model and an analytical flux-footprint model to resolve daytime source specific emissions rates. The Multilinear Engine version 2 (ME-2) was used to determine that five sources were responsible for the measured flux at the tower: (i) vehicle exhaust, (ii) a foam plastics industrial source with significant pentane emissions, (iii) consumer and commercial solvent use emissions, (iv) a biogenic emissions source dominated by isoprene, and, (v) evaporative fuel emissions. The estimated median daytime (0700-1900 CST) hourly emission rate from the foam plastics industry was 15.7±3.1 kg h^{-1}, somewhat higher than its permitted hourly emission rates. The median daytime vehicle exhaust volatile organic compounds emission rate of 14.5±2 g h^{-1} $vehicle^{-1}$, was slightly higher than our estimation using the Motor Vehicle Emission Simulator (MOVES) with a county-representative vehicle fleet of year 2008 (11.6±0.2 g h^{-1} $vehicle^{-1}$). The median daytime evaporative fuel volatile organic compounds emission rate from parked vehicles was 2.3±1 g h^{-1} $vehicle^{-1}$, which is higher than MOVES estimations and could not be explained by the age of the vehicle fleet, indicating either locally higher VOC evaporative emission sources in the footprint or an underestimation of evaporative emissions by MOVES, or both.

---

* *Reproduced with permission from:* Kota, S.H., Park, C., Hale, M.C., Werner, N.D., Schade, G.W., Ying, Q., 2014. Estimation of VOC emission factors from flux measurements using a receptor model and footprint analysis. Atmos. Environ. 82, 24-35.

4.1 Introduction

Volatile organic compounds (VOCs) play a prominent role in photochemical reactions that lead to the formation of ozone and secondary particulate matter, thus directly affect regional air quality and global climate (Atkinson, 2000; Kroll and Seinfeld, 2008). A number of VOCs are also classified as hazardous air pollutants by the US EPA due to their adverse health effects. Although significant efforts have been devoted in the past to develop and improve VOC emission inventories, large uncertainties and biases remain (Brown et al., 2004; Buzcu and Fraser, 2006; Reid et al., 2000). Under-reported or unreported anthropogenic emissions in VOC emission inventories are one of the major factors that affect air quality models and forecasts, particularly for ozone (Nam et al., 2006) in metropolitan areas. In urban areas, vehicle emissions account for a large fraction (e.g. approximately 30% in the Houston metropolitan area) of the anthropogenic VOC emissions (Ying and Krishnan, 2010), but the accuracy of the emissions depends largely on the vehicle emission factor models used in the estimations. The uncertainty in the VOC emission inventory can thus significantly affect the evaluations of VOC emissions on air quality, human health, climate and the design of effective control strategies to mitigate adverse effects.

Ozone and particulate air quality in Houston, the 4th largest metropolitan area in the United States (US) with a population of over 2.2 million, is significantly influenced by the VOC emissions from petrochemical, industrial and motor vehicle sources (Kim et al., 2011; Vizuete et al., 2008; Ying and Krishnan, 2010). This complex mixture of VOCs has led to a number of studies to quantify the contributions of different sources to the observed VOC concentrations in the area. Fujita et al. (1995) used Chemical Mass Balance (CMB) modeling to study the VOC data from Photochemical Assessment Monitoring Stations (PAMS) and concluded that refineries are the dominant VOC source in the Houston Ship Channel (HSC). Henry et al. (1997) used a multivariate receptor model to study data collected during the Coastal Oxidant Assessment for Southeast Texas (COAST) study, and showed that self-reported emissions by various industries in the HSC area were unreliable. Kim et al. (2005), Buzcu and Fraser (2006), and Luchner

and Rappenglück (2010) applied the Positive Matrix Factorization (PMF) technique to study VOC sources in Houston, and concluded that refineries, petrochemical industries, vehicle emissions and biogenic sources are all important contributors to the ambient VOC abundance. While these receptor-oriented source apportionment studies are useful in understanding sources of VOCs in the atmosphere, the calculations are based on measured VOC concentrations and thus are not directly related to the actual emission rates of VOCs from various sources.

Instead of using ambient concentrations, VOC fluxes calculated from micrometeorological and VOC gradient measurements have been used in the past to estimate biogenic emission fluxes from forest areas (Karl et al., 2001; Langford et al., 2010a; Lee et al., 2005; Spirig et al., 2005). Recently, micrometeorological flux measurements have also been applied to measure emission rates of anthropogenic and biogenic VOCs in urban environments (Karl et al., 2009; Langford et al., 2009; Park et al., 2010; Velasco et al., 2009). The urban fluxes, usually measured from tall towers, are used to directly infer the emission rates of pollutants from upwind areas using footprint models (Langford et al., 2010b). The results of footprint modeling, resulting in apparent surface fluxes, can be used in conjunction with an analysis of land use/land cover and/or traffic count data to infer specific emission rates for different sources included in the footprint areas (Park et al., 2011). Although this technique is useful, it is not straightforward to identify responsible sources within the footprint area due to the high spatial heterogeneity of emission sources in typical urban environments. In addition, different sources are likely responsible for different groups of VOCs, while a typical footprint analysis applies to a homogeneous source distribution.

In this study, simultaneous fluxes of 18 VOCs are used in receptor-oriented statistical analyses to resolve sources of measured VOC fluxes in an urban environment. Results of the source attribution analysis are used alongside flux-footprint modeling to determine the emission rates of VOCs from the different sources. To the knowledge of the authors, this is the first time such a combination of VOC flux measurements and

receptor-oriented source apportionment analyses is applied to resolve source specific emission rates of VOCs in urban locations.

Table 7 List of measured VOCs and their abbreviations.

IUPAC name (common name)	Abbreviation	Method Detection Limit (MDL), ppt
butane*	C4	12.0
2-methyl 1,3-butandiene (Isoprene)	C5H8	10.0
n-pentane	C5H12	10.0
2-methylbutane (Isopentane)	IC5H12	10.0
Benzene	BENZ	8.0
Ethylbenzene	EBENZ	6.0
n-hexane	NC6H14	8.0
2-methylpentane	M2PEN	8.0
3-methylpentane	M3PEN	8.0
methylbenzene (toluene)	TOLU	7.0
n-heptane	NC7H12	7.0
2-methylhexane (Isoheptane)	M2HEX	7.0
2,2-dimethylpentane (neoheptane)	NEOH	7.0
1,3- and 1,2-dimethylbenzene (m/p-xylene)	MPXYL	6.0
1,2-dimethylbenzene (o-xylene)	OXYL	6.0
2-methylprop-2-enal (methacrolein)	MACR	16.0
butenone (methyl vinyl ketone)	MVK	16.0
butanone (methyl ethyl ketone)	MEK	16.0

* Note: includes n-butane and 2-methylpropane (isobutane).

4.2 Methodology

4.2.1 Data and data uncertainties

The experimental setup and data collection have been described in detail in Park et al. (2010) and are only briefly summarized here: Meteorology data and concentration and flux of 18 VOCs (see table 7 for the list of the VOCs) were measured at 60 m above ground level (agl) from a tall communication tower owned by the Greater Houston Transportation Company (hereinafter referred as the Yellow Cab Tower, or YCT) in an older neighborhood 3-4 km north of downtown Houston (Northside Village area; Figure

B3 in Appendix B) from May 23 to July 27, 2008. The area surrounding the tower is mostly residential, with several multi-lane roadways and a light industrial area surrounding YCT. It was estimated that 29% of the surrounding areas are covered by trees and shrubs, among which a mature oak tree population results in significant emissions of isoprene as reported in Park et al. (2011). Figure 17 shows a schematic view of the area surrounding the flux measurement site, including the locations of YCT, major through-traffic roadways, two YC parking lots, and some other potentially contributing sources that are mentioned in this manuscript.

The VOC concentrations were measured using a dual channel gas chromatograph with flame ionization detectors (GC-FID) and the fluxes were determined using a relaxed eddy accumulation (REA) setup. In summary, the REA setup measures the concentration of a VOC species in atmospheric updrafts (C_{up}) and downdrafts (C_{down}) over an averaging time period of 30 minutes. The resultant flux (F) is calculated using equation (4.1):

$$F = \beta \sigma_w \left(C_{up} - C_{down} \right) \tag{4.1}$$

where β is a flux correction factor (in this study β=0.335, see Park et al. (2011) for details) and σ_w is the standard deviation of vertical wind speed of each 30 min sampling period. At the top of each hour a 30-minute sample was taken and it was assumed to represent the average flux of that hour. Species specific method detection limit (MDL) of the concentration measurements is included in table 7. Flux MDL (species and sample specific) was based on regular (every 30th run) GC-FID channel intercomparisons by obtaining identical air samples into the Teflon bags. The 95% confidence limit (95%CI) of the difference in concentration between these samples (excluding outliers) was used as the error of the concentration difference measurement (equation 4.1) for each VOC. Sample specific flux $MDL_{i,j}$ (MDL for the ith sample and jth species) is calculated by $MDL_{i,j} = \beta\, \sigma_{w,i} \times (95\%CI)_j$.

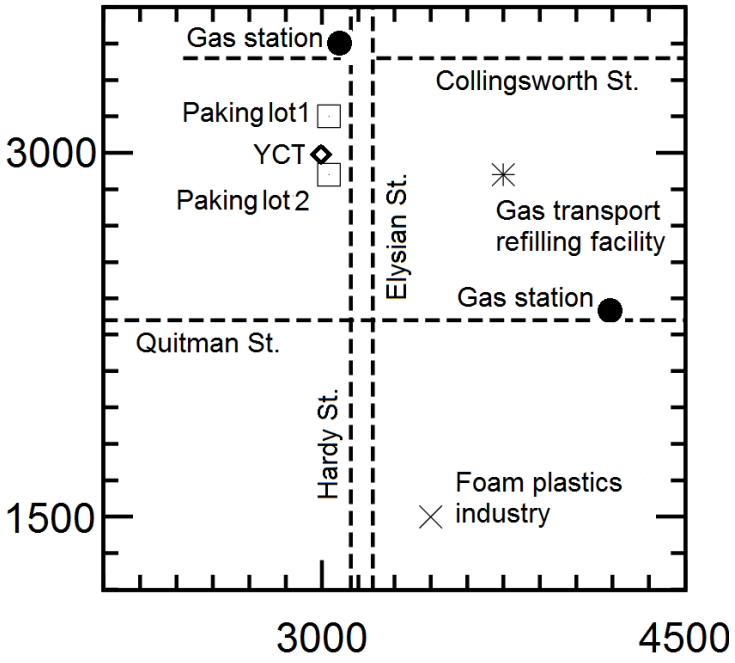

Figure 17 A schematic showing the positions of the Yellow Cab Tower (YCT), nearby major roadways (Collingsworth St., Quitman St., Hardy St., and Elysian St.), surface parking lots near YCT, a foam plastics industry site, a gasoline transport refilling facility and two refueling stations. Numbers on the x and y axes represent distance in m from the origin of the flux footprint model domain.

Prescreening was performed to eliminate data obtained under low turbulence and non-stationary flux conditions: Flux and concentration data obtained under friction velocities, $u^{*}<0.2$ m s^{-1} or 60-m agl wind speed less than 2 m s^{-1} were not retained (Park et al., 2011). This particularly reduced the amount of nighttime data, when turbulence was weaker. Furthermore, periods with questionable stationarity of high frequency CO_2 and low frequency CO data, following the standard deviation technique used by Foken and Wichura (1996), were removed. For the remaining samples (760 30-minute samples), data below $MDL_{i,j}$ were replaced with $0.5MDL_{i,j}$, and missing data were set to the median concentration of the species (Polissar et al., 1998). A species was marked as missing in the flux data set if one or both of the two GC-FID channels had a concentration below MDL.

The uncertainty (σ) associated with each sample for receptor-oriented source apportionment analyses was estimated using equation (4.2) when the concentration or absolute value of flux was less than or equal to $MDL_{i,j}$ or otherwise using equation (4.3) (Polissar et al., 2001):

$$\sigma_{i,j} = \frac{1}{2}\overline{MDL}_j + \frac{1}{3}MDL_{i,j} \tag{4.2}$$

$$\sigma_{i,j} = \sqrt{\mu_{i,j}^2 + MDL_{i,j}^2} \tag{4.3}$$

$$\mu_{i,j} = \sqrt{\left(0.01 \times \frac{\left(C_{up,i,j}^2 + C_{down,i,j}^2\right)}{\left(C_{up,i,j} - C_{down,i,j}\right)^2}\right) + 0.0025} \tag{4.4}$$

where $\mu_{i,j}$ is the absolute analytical uncertainty of the measured concentration or flux. A relative precision of 10% for concentrations based on internal standard variability was used to calculate the absolute uncertainty (see Park et al., 2010 for further details). However, for fluxes equation (4.4), derived using error propagation of equation (4.1) and accounting for 5% uncertainty in σ_w, was used to estimate absolute analytical uncertainty. The uncertainties for missing data in concentration analysis were set to five times the median concentration. For fluxes if both updraft and downdraft concentrations are missing then missing flux is replaced by median with an associated uncertainty of 5 times median. However, if only one channel concentration is missing, then the sample is treated as below MDL.

4.2.2 Source apportionment of fluxes

The Multilinear Engine version 2 (ME-2) (Norris, 2009), the underlying solver for the United States Environmental Protection Agency Positive Matrix Factorization (PMF) version 3.0 model (USEPA, 2008; downloaded from http://www.epa.gov/heasd/products/pmf/pmf.html), was used to solve the source apportionment problem for both concentration and flux data. ME-2 can be used to solve the least-square problem from many types of factor analysis (including PMF) and has been applied before in a number of air pollution source apportionment studies (Amato et

al., 2009; Kim et al., 2003; Ramadan et al., 2003; Wu et al., 2007). One of the features of ME-2 that is useful for this study is that it can be configured to allow negative source contributions (Norris, 2009), which is natural for the flux data as the measured net flux can be a superposition of gross positive and negative fluxes from different sources and sinks. In this study, for the concentration data source apportionment, ME-2 was configured to use non-negativity constrains for source profiles and contribution matrices, and to allow an unconstrained solution for the contribution matrices when it was applied to determine source contributions for the flux data. For both concentration and flux source apportionment, 100 bootstrap runs with a block size of 16 and a minimum correlation R-value of 0.6 were conducted to ensure proper solutions and to estimate the uncertainties to the estimated profiles.

4.2.3 Automatic identification of source profiles

To attribute the ME-2 resolved source profiles (mg mg^{-1}) to a specific source, the profiles were compared with renormalized VOC profiles (including only the 18 species analyzed in this study) from the SPECIATE 4.2 database (Hsu and Divita, 2008), a VOC and PM speciation profile data base maintained by the US EPA, using equation (4.5):

$$\theta = \frac{\sum_{i=1}^{N} f_i s_i}{\sqrt{\sum_{i=1}^{N} f_i^2}\sqrt{\sum_{i=1}^{N} s_i^2}} \tag{4.5}$$

where f_i and s_i are the i^{th} matching component in the ME-2 resolved source profile and the SPECIATE 4.2 profile, respectively. θ is bounded between 0 and 1, where 1 indicates perfect agreement. Top 20 matching SPECIATE profiles were then manually checked to determine the source type for the ME-2 source profile.

4.2.4 Emission rate estimation

The source-apportioned VOC fluxes at YCT were used to estimate the VOC emission rates of the identified sources using the analytical footprint model described by Kormann and Meixner (2001). Generally, the flux measured at a certain height, $F(0,0,z_m)$, can be related to upwind surface fluxes, as described by equation (4.6),

$$F(0,0,z_m) = \int_{-\infty}^{+\infty} \int_{0}^{+\infty} F(x,y,0)\phi(x,y,z_m)dxdy \quad (4.6)$$

where the two-dimensional flux-footprint probability density function ϕ represents the probability of a unit flux at (x,y,0) that reaches the flux measuring location (0,0,z_m). The Kormann and Meixner model assumes a homogeneous underlying surface and well-defined atmospheric turbulence regimes. It is attractive due to the limited amount of input parameters required, providing a symmetric flux footprint function with results similar to a more sophisticated model (Kljun et al., 2004; Kljun et al., 2002). However, it has not yet been rigorously tested in a turbulently more complex urban environment, which is heterogeneous both in terms of roughness length (due to different building and vegetation heights) and heat flux/stability. In addition, the analytical footprint model strictly only provides the flux footprint function at the displacement height, which may vary between 5 and 13 m at this site.

The flux footprint model output option of EdiRe flux processing software (http://www.geos.ed.ac.uk/abs/research/micromet/EdiRe/) was used to calculate the 2D gridded flux-footprint probability function φ (i.e. ϕ integrated within each grid cell) in a domain of 6×6 km^2, i.e. using a square grid of 30 m, with the YCT at the center of the domain. Hourly flux footprint probability values used in the following analyses were calculated by averaging the 30-min footprint values within a given hour. If flux F(0,0,z_m) is known, the calculated footprint probabilities can be used to estimate the surface emission fluxes by inverting a discrete form of equation (4.5). For the emission rate analysis in Section 3.2, individual periods were removed from the analysis if the domain sum of the flux probability φ was less than 0.7 to ensure that a sufficient amount of the flux footprint lies within the computation domain. Nighttime data (2000 – 0600 CST) were completely excluded to further reduce uncertainty. This resulted in a total removal of 363 samples before source specific criteria were specified for the emission rate analysis.

4.3 Results and Discussion

Analysis of the concentration data are described in greater detail in the Appendix B (figure B1-B2). In summary, measured concentrations were generally well-reproduced by ME-2 with five factors, representing consumer and commercial solvent use emissions, an industrial source dominated by pentane emissions (referred to as the "foam plastics industry" emissions hereafter), vehicle exhaust, evaporative emissions and a biogenic emissions source. While this is an expected result in line with previous work, the additional flux dimension can provide further insight, wherefore in the following analyses we focus on the flux data. A comparison of the source profiles and relative source contributions derived from concentration and flux data can be found in figure B3 and Table B6 in Appendix B.

4.3.1 Source apportionment of flux data

Results generated by ME-2 assuming 4, 5 and 6 factors (sources) were explored. The value of the sum-of-squares objective function Q to its expected (or theoretical) value $Q_{expected}$, $Q/Q_{expected}$, for 4, 5 and 6 factors were 1.4, 1.15 and 1.1, respectively. The 5 and 6 factor solutions had similar correlation coefficients (r^2) for the total VOC mass (0.935 vs. 0.941), and the amount of total VOC represented (84% vs. 85%). However, the 6-factor solution resulted in two very similar consumer and commercial solvent use emission factors. Similar results were also achieved for ME-2 analysis of the concentration data (see Supplementary Materials). Thus, the 5-factor solution, with rotational parameter FPEAK of 4 (Norris, 2009) (see Tables B2 and B3 for more information), was used in the following analyses.

Figure 18 shows the predicted source profiles, which are determined to represent (1) consumer and commercial solvent use emissions, with C4 as the dominant species (43% of the VOCs in the profile, θ=97%), (2) a foam plastics industry emissions source, with pentane as the dominant species (60% of the VOCs in the profile), (3) vehicle tailpipe exhaust emissions, dominated by TOLU and MPXYL (19% and 24% of the VOCs in the profile, θ=92%), (4) evaporative emissions, dominated by IC5H12 (30% of the VOCs in

the profile, θ=94%), and (5) biogenic emissions, dominated by isoprene (44% of the VOCs in the profile, θ=91%). Table B4 in the supplementary materials lists the top matching profiles in the SPECIATE 4.2 database. Figure 18(a) shows the consumer and commercial solvent use emissions factor, which apparently does not represent fugitive evaporative fuel emissions from vehicles because butane, primarily used as aerosol propellant, is the dominate species in that profile, and it does not have a significant contribution from IC5H12 (less than 5%). Rubin et al. (2006) reported that IC5H12 (26.6%) is much more important than n-butane (8.0%) among the most abundant components in evaporative fuel emissions, which agrees much better with the profile shown in figure 18(d). The profile shown in figure 18(a) more closely resembles several consumer and commercial profiles in the SPECIATE 4.2 data base than the closest vehicle fuel evaporation profiles (θ=93%). Figure 18(b) was determined to be a foam plastics industry source based on the directional dependence of the factor (figure 21) and a survey of the surrounding area as described later in this section. Another observation from this study is the absence of pentane in vehicle exhaust and evaporative emissions source profiles predicted by ME-2. This is in contrary to previous studies which reported an isopentane to pentane ratio of 1.5-2.5 and 2-3 from evaporative emissions and vehicle exhaust respectively (Gentner et al., 2009; Leuchner and Rappenglück, 2010; McGaughey et al., 2004). This could be due to presence of strong foam plastic source, with pentane as the dominant species, in the direction of major road traffic, taking up all the variation of this species. Figure C3 in Appendix C shows a comparison of the profiles based on concentration and flux data. The two profiles are very similar and no consistent trend of the major species could be found.

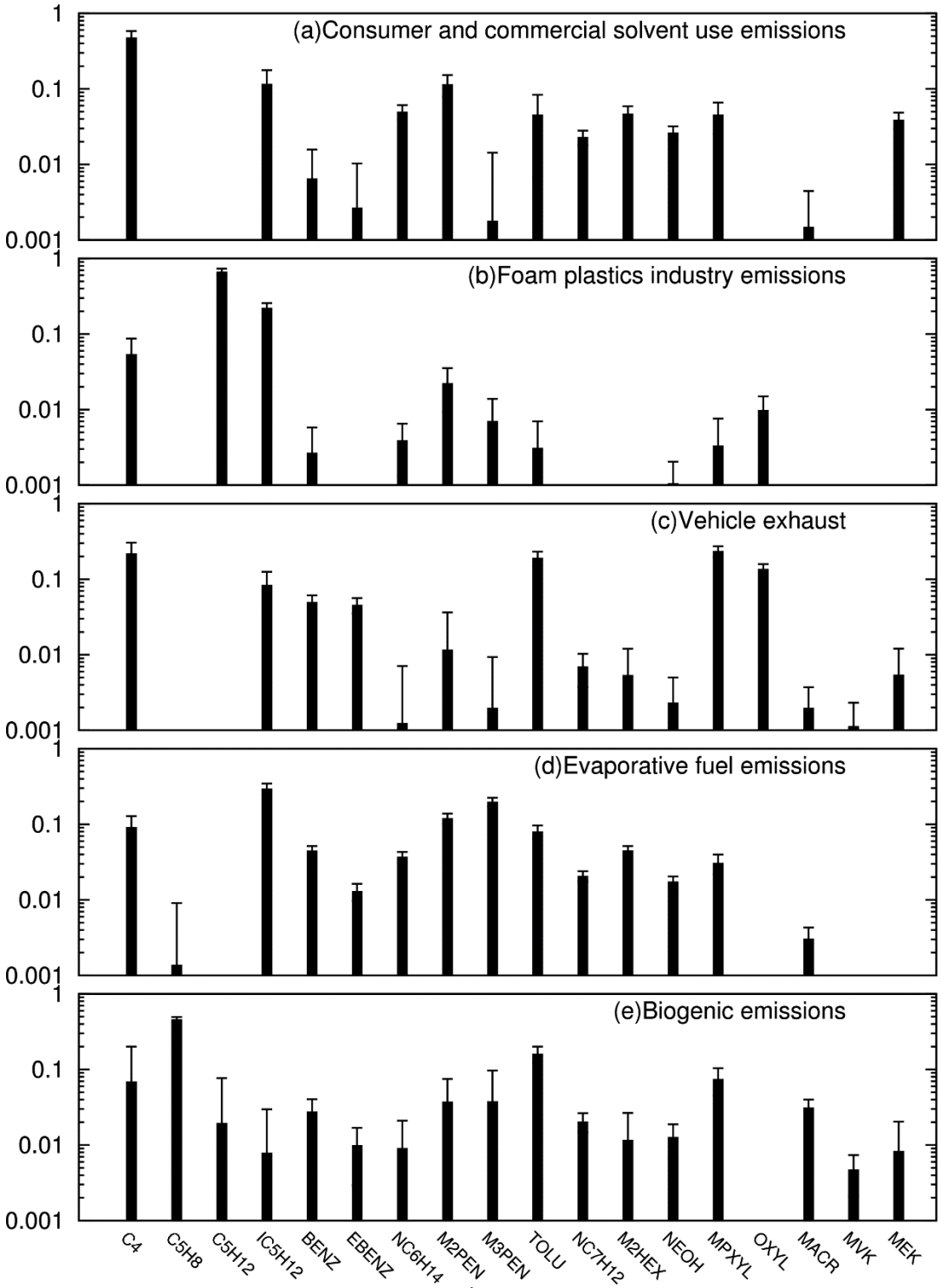

Figure 18 Predicted source profiles (mg mg^{-1}) by ME-2 based on the flux data. Error bars are standard deviations estimated using bootstrap analyses.

Figure 19 shows that ME-2 predicted VOC fluxes generally agreed well with observations except for few species such as MACR, MVK and MEK. Normalized mean bias factor (NMBF) and Normalized mean absolute error factor (NMAEF), calculated using Gustafson and Yu (2012), for the species were in the range of -0.37 to -0.06 and 0.43 to 0.75 for most species, as shown in Table B5. MACR and MVK are oxidation products of isoprene, and MEK is an oxidation product of n-butane and isopentane. The receptor-oriented statistical methods typically do not work as well for these compounds because the ratio of these products to their precursor changes as they are transported towards the receptor.

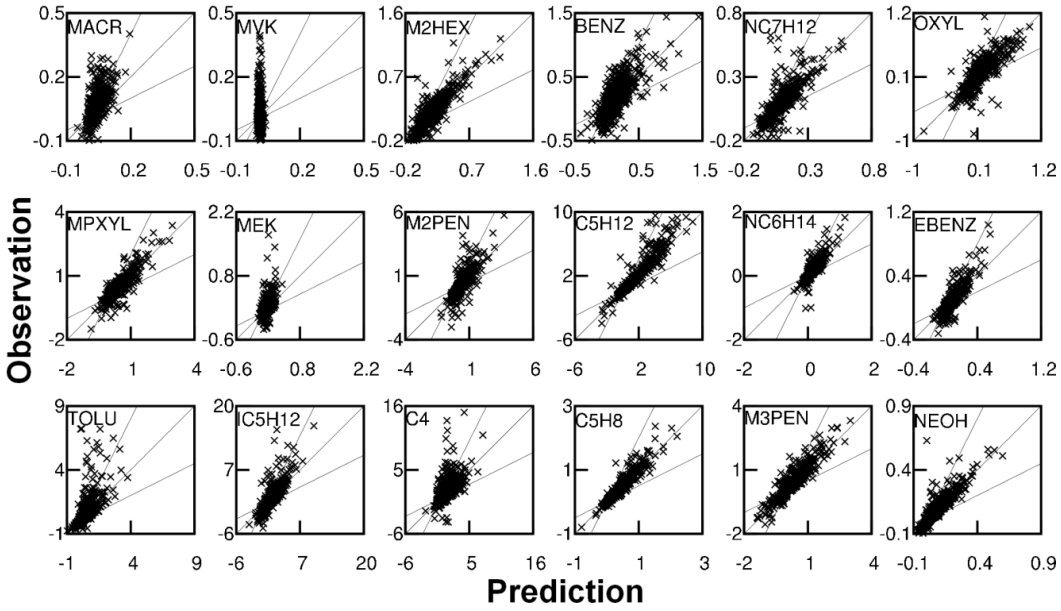

Figure 19 Observed and reconstructed fluxes of VOC species measured at the Yellow Cab Tower. Thin solid lines represent 1:1, 1:2 and 2:1 ratios. Units are mg m^{-2} h^{-1}. Note that the data points with missing observations replaced by median values are not shown in the plot.

The diurnal variation of the contribution of each source to the measured total VOC flux is presented in figure 20. Figure 20(a) shows that VOC flux due to consumer and commercial solvent use emissions is higher during the day, with a maximum median

flux of 1.6 mg m^{-2} h^{-1}. Contributions at late night until early morning were comparatively smaller, possibly due to lower temperature as well as decreased activities associated with the emissions of these VOCs. Figure 20(b) indicates a clear diurnal pattern of contributions from the foam plastics industry source, with a maximum median flux of 1.2 mg m^{-2} h^{-1} during the late afternoon. Contributions were lower during the night as emissions of this source are also largely driven by ambient temperatures and work activity. Figure 20(c) shows a clearly higher daytime than nighttime contribution from vehicle exhaust with a clear morning rush hours peak around 0700-0900 CST (average median flux of 0.76 mg m^{-2} h^{-1}), which was 50% higher than the surrounding hours' (0600-0700 and 0900-1000 CST) median fluxes. The morning peak coincided with the weekday rush hours observed on Hardy St., the nearest major thoroughfare near the sampling site (See Table B7). More discussions of the nearby roadways can be found in Section 3.2.2. Figure 20(d) indicates that contributions from evaporative emissions were slightly higher (maximum median flux of 1.5 mg m^{-2} h^{-1}) than vehicle exhaust at the YCT but the factor did not display an as significant rush hour peak signature as observed in Figure 20(c). This suggests that the evaporative VOC emissions source was likely not dominated by running losses from vehicles on the nearby roadways. Lastly, Figure 20(e) indicates that the highest biogenic isoprene contributions from the surrounding oak tree population occurred in the early afternoon due to an optimum radiation and temperature environment at that time of day (Park et al., 2011). Biogenic isoprene contributions peaked at 1200 to 1400 CST, with a maximum median flux of 2.1 mg m^{-2} h^{-1}.

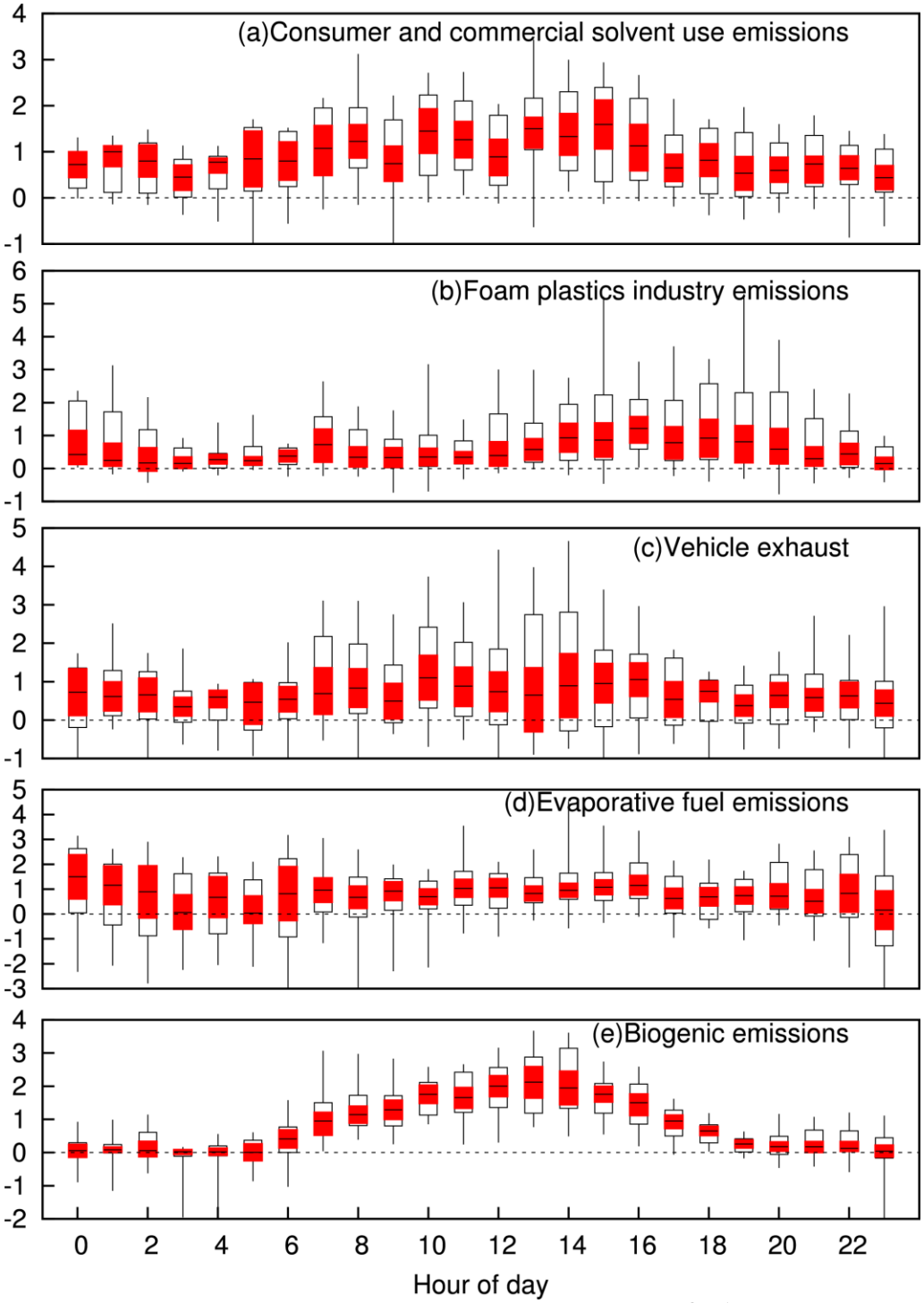

Figure 20 ME-2 predicted average hourly source contributions (mg m^{-2} h^{-1}) to the measured VOC fluxes at the Yellow Cab Tower. The box-and-whisker plot shows the median, min, max and interquartile range of the data for each hour. 95% confidence intervals of the median are shown in red.

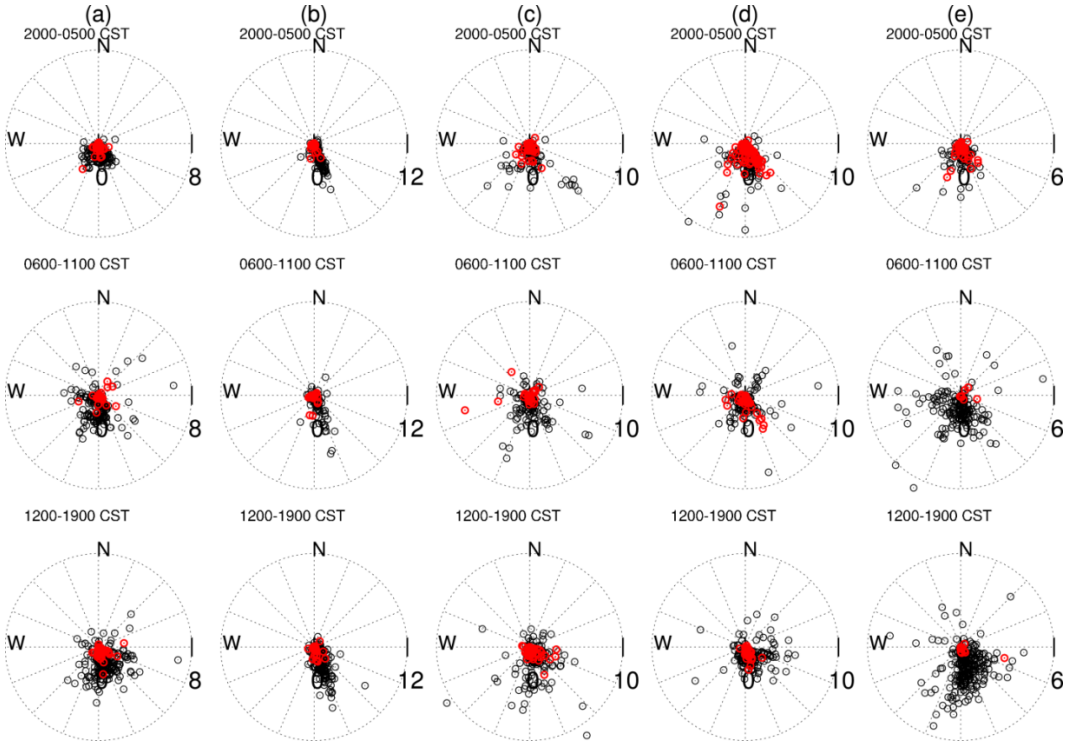

Figure 21 Wind direction dependence of the ME-2 apportioned fluxes of measured VOCs. Units are mg m^{-2} h^{-1}. Negative fluxes are shown in red.

Figure 21 shows the wind directional dependence of the fluxes from the different resolved sources. Approximately 75% of the time during the analysis, the receptor was under the influence of southerly winds. Figure 21(a) indicates that most of the contributions from consumer and commercial solvent use source were from south to southeast directions of the tower without a strong directional dependence. This suggests that this is a regional source rather than a collection of a few point sources. In contrast, the contribution of the foam plastics industry emissions source, figure 21(b), is almost exclusively from the south-southeast direction throughout the day. This strong wind direction dependence suggests contributions from a well-defined source. A survey of the area southeast of YCT revealed this potential source to be an industry specializing in foam plastics approximately 1.6 km southeast of the receptor location (figure 17), noting that pentane is used as an expansion agent in many foam plastics industries (Mills,

2007). As the source is relatively far away from YCT, unidentified non-stationary flux conditions could explain the occasional negative fluxes shown in the figure.

The vehicle exhaust contributions, depicted in figure 21(c), are from all directions as the tower is surrounded by roadways. However, two directions stand out slightly: Southeast, likely due to optimum overlap of the flux footprint with the major thoroughfare Hardy/Elysian roads, and south-southwest due to significant traffic surrounding two major schools in that direction in approximately 1 km distance from YCT. As the sampling site is amidst the parking lots of the Yellow Cab Co., which operates around 1400 vehicles (Mike Spears, Houston Yellow Cab Co., personal communication, May, 2011), many of which are parked at different directions from the tower, observed contributions of evaporative emissions from all directions, figure 21(d), can be expected. Comparison of figures 21(c) and 21(d) indicates that evaporative emissions contributions followed a different wind direction pattern compared to vehicle exhaust, which supports the earlier discussion that evaporated gasoline from parked vehicles rather than running vehicles are responsible for most of the observed fluxes. This presumption of attributing evaporative emissions dominantly to parked vehicles will be discussed in detail in later sections. Lastly, the presence of oak trees in the surrounding neighborhood resulted in contributions of biogenic emissions from all directions, shown in figure 21(e). Details have been published by Park et al. (2011). Negative fluxes due to biogenic emissions occurred mostly during nighttime, with a strong direction dependence pointing towards the HSC area, again suggesting a contribution from non-stationary conditions due to emissions from sources advected from outside the footprint domain.

4.3.2 VOC emission rates using footprint analysis

Figure 22 shows the gridded flux footprint probability φ between hours 0700-1200 (374 individual ½ hours) and 1300-1900 CST (678 individual ½ hours). During both morning and afternoon hours, the dominant wind direction was southerly so that high values of the footprint function occurred in that direction. Thus, sources to the south of the tower

contributed most to the fluxes measured at the tower. Maximum footprint values generally occurred close to YCT and decreased rapidly towards the border of the domain. This suggests that, on average, the footprint model area is sufficient to include the influence of major sources. In the following sections, emission rates for the foam plastics industry, vehicle exhaust and evaporative fuel emissions are discussed. The calculation of isoprene emission factors was discussed by Park et al. (2011) and is not repeated here. Emission rates of VOCs from consumer and commercial solvent use cannot be directly estimated as the unit area emission rate from residential and commercial areas are different. An optimization step is needed to estimate the emission rates for those two different sources. Many factors also affect the unit area emission rates such as the type of commercial facilities and products. Due to limitations of manuscript length, an analysis of the VOC emission rates from this source will be discussed elsewhere.

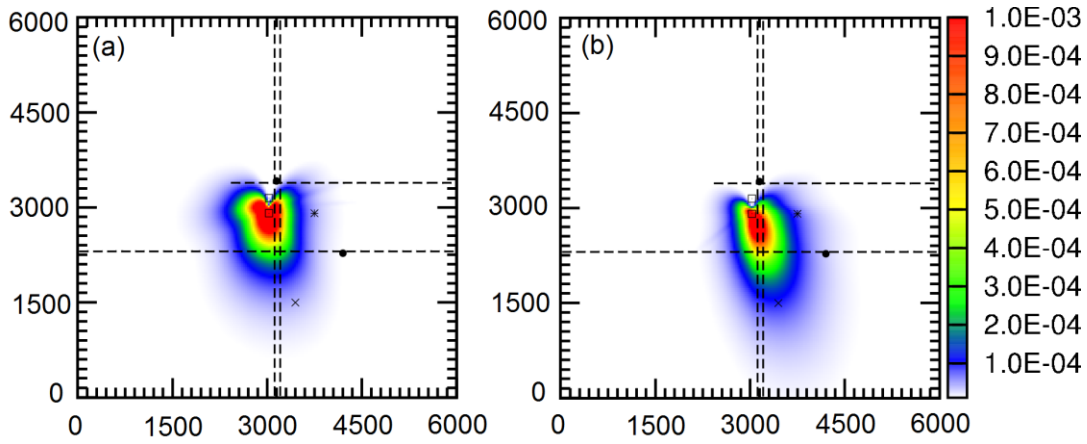

Figure 22 Averaged footprint function in the domain for (a) 0700-1200 and (b) 1300-1900 CST. Numbers on the x and y axes are distance in m. Maximum values are approximately 3.35×10^{-3} for grid cells close to the tower, which is located at center (3000 m, 3000 m). See Figure 17 for details of the major roadways and other emission sources.

4.3.2.1 Foam plastics industry emissions

To narrow the VOC emission rates from the foam plastics industry, only the data with wind directions between 100 and 170 degrees to the receptor location were considered in the analysis. This resulted in 123 samples which had non-negative flux contributions. Equation (4.7) was used to calculate the VOC emission factor of the foam plastics industry factor:

$$E_{pentane} = 10^{-6} S_I F_{pentane} \left(\sum_I \varphi \right)^{-1} \quad (4.7)$$

where $E_{pentane}$ is the VOC emission rate from the industrial source (kg h^{-1}); S_I is area (m^2) of the industrial source region, from which VOC emissions are released into the atmosphere; $F_{pentane}$ is the ME-2-resolved VOC flux (mg m^{-2} h^{-1}) for the industry; φ is the flux footprint probability at each grid cell; 10^{-6} converts the units from mg to kg; and the summation means summing the φ values for the grid cells within the industrial source region.

In order to estimate the uncertainty of the VOC emissions rate due to uncertainty in φ, a Monte Carlo technique was used with the underlying assumption that uncertainties in φ can be represented by the variation of φ in nearby grid cells. For each valid foam plastics industry emissions' flux data point, 4000 simulations were carried out. In each simulation, the emission source region was randomly moved around a fixed center location, assuming a normal distribution with a standard deviation of ±3 grid cells (i.e. ±90 m) in both x and y directions. The average VOC emissions rate for the pentane source for a flux data point was then calculated from these 4000 simulations. The number of necessary simulations was determined by incrementally increasing the number of simulations until the mean and standard deviation of the emission rate no longer changed. The number of grid cells that cover the emission source region and the shape of the source region remained constant in these simulations. Once mean emission rates of all data points were determined, extremely high and low hourly mean emission rates within the dataset were removed as outliers, which are defined as samples that fall outside 1.5 times the inter-quartile range of the data (Moore and McCabe, 1999). This resulted in removal of 19 samples (15%) from overall emission factor analysis. This

outlier removal procedure was also carried out for the analysis of other sources described in subsequent sections.

Half of the estimated emission factors had a relative standard deviation of less than 9.6% and 90% of the data had a relative standard deviation of less than 19.3%. This suggests that for most of the data points, the uncertainty in the individual emission rate due to uncertainty in φ was quite small. Statistical analysis of the data (table 8) showed a median of 15.7 kg h^{-1} with 95% confidence intervals [12.6, 18.8] kg h^{-1}, and a mean emission rate of 18.5 kg h^{-1}. Although the area of the source region is related with the plume size of emissions at the displacement height, which is unknown, it is not going to greatly affect $E_{pentane}$ because when S_I decreases $\sum_I \varphi$ also decreases. As long as there is a weak gradient of φ near the source region, $E_{pentane}$ will remain relatively constant. To verify this, the area of the source region was varied from 1 to 15 grid cells in a series of calculations similar to the approach described above but without using the Monte Carlo technique that varies the center of the source region. The resulting mean emission rate varied slightly between 17.1 and 18.7 kg h^{-1}. The average of the mean emission rates was 17.7 kg h^{-1}, which is very similar to the mean using 15 grid cells as the source area.

Table 8 Descriptive statistics for the hourly emission rates.

	Foam Plastics Industry source (kg h^{-1})	Vehicle exhaust emissions (g h^{-1} $vehicle^{-1}$)	Vehicle evaporate emissions (g h^{-1} $vehicle^{-1}$)
Number of data points	107	204	60
Minimum	0.2	0.1	0.1
1st quartile	7.6	5.7	0.5
Median	15.7	14.5	2.3
3rd quartile	27.5	23.9	5.3
Maximum	53.3	55.1	11.4
Lower 95% confidence limit for median	12.6	12.5	1.4
Upper 95% confidence limit for median	18.8	16.5	3.3
Mean	18.5	17.5	2.9
Standard deviation	13.6	14.2	0.8
Skewness	0.7	0.9	0.7

The company has a permit to emit 10.5 kg h^{-1}, with 45% of emissions from storage. Thus, the estimated mean and median emission factors were 40-60% higher than permitted emissions. However, summer, particularly June 2008 had above normal temperatures possibly enhancing emissions, and as comparisons of the Kormann and Meixner model to a more sophisticated back-trajectory footprint model suggest a systematically longer "tail" of the Kormann and Meixner model footprint function (Kljun et al., 2003), we cannot exclude a slight high bias in our estimate for this distant source. Additionally, the absence of pentane in vehicle related source profiles (figure 18) could have resulted in this over-prediction.

4.3.2.2 Vehicle exhaust

VOC emission factors for vehicle exhaust were also estimated using resolved vehicle exhaust flux and the footprint model. Hourly vehicle volume (Tables B7 and B8 in Appendix B) and speed (Tables B9 and B10 in Appendix B) data were collected on four major roadways for through-traffic (Hardy St., Elysian St., Collingsworth St. and Quitman St.; figure 17 and figure B3 in Appendix B) near YCT during March and November, 2011. Hardy and Elysian are north-south oriented multi-lane roadways one and two blocks east of YCT, respectively. Quitman and Collingsworth are normal two-lane east-west oriented streets, 7 blocks south, and 4 blocks north of YCT, respectively. In the emission factor calculation, nearby local streets within approximately 250 m of YCT were also included. Traffic data collected on Hays Street, which is the local east-west oriented street approximately 20 m north of the tower, were assumed to represent general traffic conditions in the surrounding local streets. The names and the locations of the eight nearby local streets included in the emission factor calculation are shown in figure B4 (Appendix B). As shown in figure B5 (Appendix B), these eight local streets and four thoroughfares encompass areas with significant footprint probability. Including additional local roadways further away from YCT is not expected to affect the estimated emission factor.

Hourly traffic density (number of driving vehicles per grid cell) for a typical weekday and weekend day, which is needed for the emission factor calculation, was calculated using the collected traffic data. Although traffic count data were not directly available for the current modeling period, it was assumed that traffic density did not change significantly within a few years in this relatively old neighborhood. This assumption is supported by a less than 1% change in annual average diurnal traffic (AADT) during 2008-2011 on the freeways surrounding the tower (http://www.txdot.gov/apps/statewide_mapping/StatewidePlanningMap.html). It was further assumed that vehicle density was uniform at the footprint grid cells of the same roadway, and that the vehicle fleet composition was the same everywhere in the domain so that the VOC emission factor is uniform throughout the domain.

The hourly emission factors were calculated using equation (4.8) based on the ME-2-apportioned vehicle VOC exhaust fluxes and the corresponding footprint values,

$$EF_{exhaust} = 10^{-3} F_{exhaust} \left(\sum_{i=1}^{N_x} \sum_{j=1}^{N_y} \varsigma_{i,j}^{road} k_{i,j} \varphi_{i,j} \right)^{-1} \tag{4.8}$$

where $EF_{exhaust}$ is the VOC emission factor for an average vehicle in the domain (g h^{-1} $vehicle^{-1}$), $F_{exhaust}$ is the ME-2 apportioned vehicle VOC flux at YCT (mg m^{-2} h^{-1}) for a specific hour; ς^{road} is the roadway mask function, which returns unity if a footprint grid cell belongs to one of the roadways otherwise it returns zero; k is the vehicle density of a grid cell (number of vehicles m^{-2}); φ is the average hourly footprint value at each grid cell; and 10^{-3} converts units to g h^{-1} $vehicle^{-1}$. Since the roadways and larger vehicle densities are located dominantly in the east and south directions of the tower, only hourly data with wind direction between 20 and 270 degrees were considered for the analysis. This resulted in 233 samples which had non-negative flux contributions from vehicle exhaust. The total emission rates of the 18 measured VOCs were converted to the total VOC emission rates using a weighing factor of 0.41±0.11 (mass of 18 measured VOCs/total of all VOC mass in a VOC speciation profile) based on the vehicle exhaust profiles available in the SPECIATE 4.2 chemical speciation data base (Hsu and Divita, 2008).

Similar to the foam plastics industry emission factor calculations, uncertainty in the vehicle exhaust due to k and φ was estimated using the Monte Carlo technique. For each data point, 20000 simulations were carried out. In each simulation, the vehicle density was calculated by randomly varying the vehicle speed and traffic volume based on normal distributions with mean and standard deviations shown in tables B7-B10 in Appendix B. Uncertainty in the footprint function was again estimated by randomly selecting φ values from grid cells with a normal distribution centered at the road grid points and a standard deviation of 3 grid cells in both x and y directions. 29 samples (approximately 12%) were removed as outliers from the analysis.

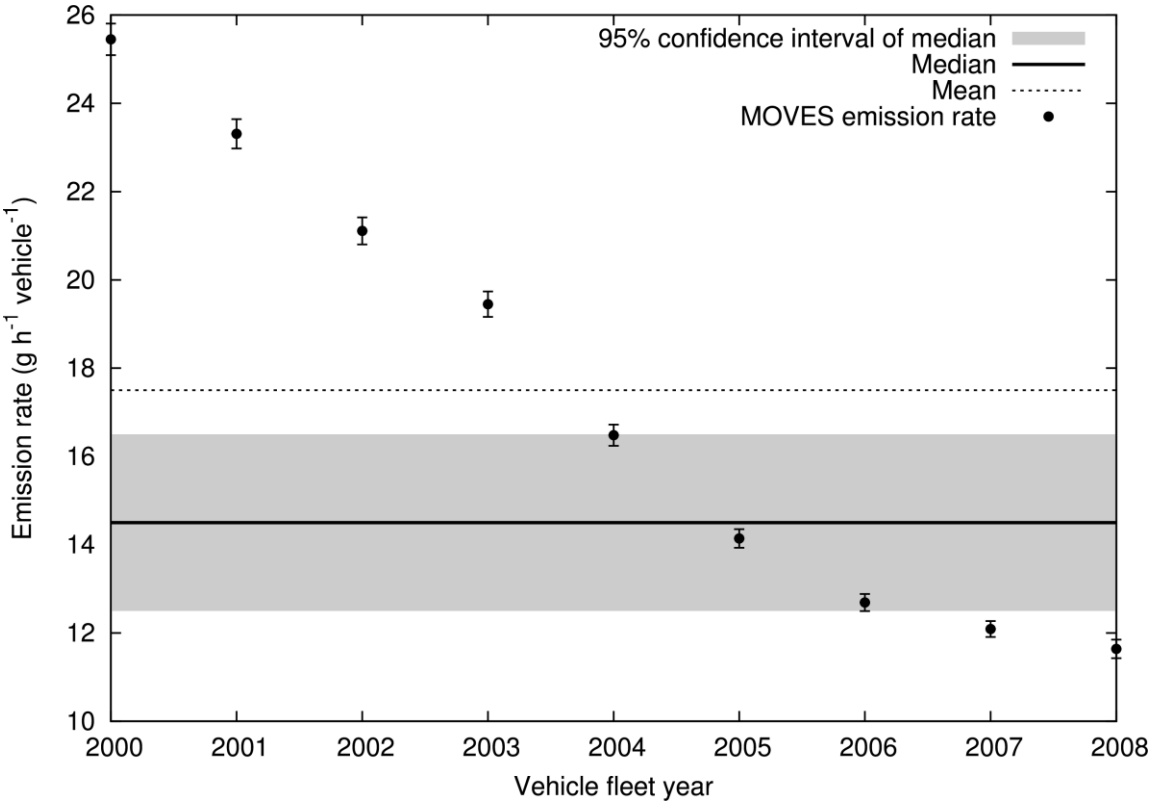

Figure 23 Comparison of vehicle exhaust emission rates estimated using the flux-footprint analysis and the MOVES model. Uncertainties of the MOVES emission are one standard deviation about the mean, estimated using a Monte-Carlo technique that considers the uncertainties in the vehicle volume and speed, as used in the flux-footprint calculations.

Half of the estimated emission factors had a relative standard deviation of less than 30% and 90% of the data had a relative standard deviation of less than 200%. Data points with larger uncertainties typically occurred when the wind was not from the south. The gradient of φ is significant near the north-south streets of Hardy and Elysian (figure 22), which explains some of the higher uncertainty in the estimated hourly emission rates. Table 8 shows the statistical analysis of the hourly data. The mean vehicle exhaust emission rate was 17.5 g h^{-1} $vehicle^{-1}$. The median emission rate was 14.5 g h^{-1} vehicle $^{-1}$, with a 95% confidence interval [12.5, 16.5] g h^{-1} $vehicle^{-1}$.

The calculated VOC emission factor from an average vehicle was next compared with the emission factors estimated by the Motor Vehicle Emission Simulator (MOVES) model. Calculating emission factors for an average vehicle using MOVES and traffic monitoring data has been described in detail in a separate manuscript (Kota et al., 2013a). Figure 23 shows the MOVES estimated emission factor for fleet years 2000 to 2008 and their comparison with the flux-footprint estimated emission factors. Variations in the predicted MOVES emission factors were smaller because, e.g., no footprint function is involved in the MOVES emission calculations. The MOVES emission factors for fleet year 2005 to 2008 were within the 95% confidence interval of the median emission factors estimated by the flux-footprint analysis, and the 2005 MOVES emission factor (14.1±0.2 g h^{-1} $vehicle^{-1}$) was closest to the median value (14.5 g h^{-1} $vehicle^{-1}$). However, the mean emission rate from the flux-footprint analysis (17.5 g h^{-1} $vehicle^{-1}$) was closest to the MOVES estimated emissions for fleet year 2004 (16.5 g h^{-1} $vehicle^{-1}$).

In addition to the major roads discussed in this study, two major freeways, US-59 and I-45 (both oriented roughly in north-south direction) are located at the edge of the footprint region 1270 m toward the east and 1740 m toward the west from the tower, respectively. I-45 and US-59 have 35.4 and 22.2 times higher vehicle traffic than Quitman (http://ttihouston.tamu.edu/hgac/trafficcountmap/). Despite these substantially higher traffic volumes, including the two freeways in the emission factor calculation resulted in only a 2.7% decrease in the average emission factor.

4.3.2.3 Evaporative fuel emissions

Although there are many potential sources that can contribute to evaporative fuel emissions, we are interested in limiting our analysis to the VOC evaporative flux from stopped and parked vehicles, mostly at or near YCT and its two major parking lots, located at 90-180 m southeast and 60-120 m northeast of YCT (figure 17). The number of parked taxi cars near the tower was estimated by counting the number of designated parking spots near the facility (240 and 120 vehicles in southeast and northeast parking lots, respectively). Since not all the parking spaces were occupied by vehicles, this may give a lower bound estimation of the actual evaporative emission rate. Parked vehicles on the streets in other grid cells can also contribute to the measured flux at the tower. The parked vehicle density in other grid cells was estimated to be 2 vehicles per grid cell based on Google Earth images for the year 2008. To reduce the uncertainty in the emission rates estimation, only samples with wind directions between 100-190 degrees (the southeast parking lot) and 20-80 degrees (the northeast parking lot) were included in the calculation. This resulted in 70 samples which had non-negative flux contributions from evaporative emissions. Contributions to evaporative fuel emissions from a gasoline transport company approximately 1.2 km to the east of the sampling site (figure 17) was estimated based on daily transport truck trips and the AP-42 refueling losses emission factor (see Supplementary Materials) and subtracted from total evaporative fuel emission rate.

The mean and standard deviation for each hourly vehicle evaporative emission factor were again estimated using the Monte-Carlo technique. 3000 simulations were undertaken by randomly varying parking lots and the gas transport company location with a standard deviation of 3 grid cells around the actual location of these facilities to account for uncertainties in φ. In addition, an uncertainty of 50% in the AP-42 truck refueling emission factor was assumed, and the number of truck trips per hour was assumed to have an uncertainty of 25%. Half of the estimated emission factors had a standard deviation of less than 17% and 90% of the data had a standard deviation of less

than 50%. The smaller uncertainty indicates that spatial variation of φ was relatively small near the source region. 10 samples (approximately 14%) were removed as outliers from the analysis. Table 8 shows the statistical analysis of the hourly data. The mean vehicle evaporative emission rate was found to be 2.9 g h^{-1} $vehicle^{-1}$; the median emission rate was 2.3 g h^{-1} vehicle $^{-1}$, with a 95% confidence interval of [1.3, 3.3] g h^{-1} $vehicle^{-1}$.

The evaporative fuel emission factor from the flux-footprint analysis was again compared with MOVES estimated values. The YCT site features a constant turnover of taxi cabs during daytime coming to and from headquarters, stopping or parking short-term near the tower, which is expected to contribute additional hot-soak emissions. The MOVES based average daytime emission factor for the parked vehicles (assuming half of the vehicles with peak hot soak emissions and the remaining half with average hot soak emissions) were 0.41 g h^{-1} $vehicle^{-1}$ and 0.55 g h^{-1} $vehicle^{-1}$ for year 2008 and 2000 vehicle fleets, respectively, which is approximately 18% and 24% of the median emission rate from the flux-footprint analysis. Thus, uncertainty in vehicle ages cannot explain the discrepancy and alternative explanations were explored.

Uncertainties in the estimation of number of parked vehicles in other areas in the footprint domain and emissions from two fuel service stations (gas stations), located at 480 m NNE and 1380 m SE of the tower, as shown in figure 17, were determined (see Supplementary Materials) to have very small effects on the evaporative fuel emission factor. Another potential source of evaporative emission is on-road vehicles. Based on vehicle density described in Section 3.2.2 and additional evaporative emission factors of running vehicles estimated using the MOVES model (approximately 0.06 g km^{-1} at 48 kmh^{-1}), a decrease of the evaporative fuel emission factor by approximately 10% was obtained, which still cannot explain the significant discrepancy between the obtained vehicle fuel emission factors based on the flux source apportionment data and the MOVES model. Possible explanations for the difference between flux-based and MOVES-based evaporative emission rates could be (i) evaporative fuel emissions from a large auto-repair workshop 100 m east to the tower, (ii) a few percent of poorly

maintained vehicles that could have evaporative emission rates hundreds of times higher than well-maintained vehicles, and/or (iii) a significant underestimation of evaporative emissions by the MOVES model in this environment, similar to previous results (Quigley, 2007). A more detailed inspection of the vehicle fleet condition would be needed to confirm the existence of the first two possibilities.

4.4 Conclusions

In this study, a receptor-oriented statistical model and an analytical flux-footprint model were utilized to analyze VOC flux data obtained from an urban area in Houston to determine the contributions of responsible sources of VOCs to observed flux and the VOC emission rates from these sources. Emission rates from a foam plastics industry source, running vehicle exhaust and evaporative emissions were calculated. Median VOC emissions from the industrial source were 15.7±3.1 kg h^{-1}, higher than officially permitted amounts, but potentially biased due to the large distance from the source and higher temperatures in the summer months. Estimated vehicle exhaust emissions, with a median emission rate of 14.5±2 g h^{-1} $vehicle^{-1}$, were similar to the estimates using the MOVES model and a vehicle fleet of year 2005 (14.1±0.2 g h^{-1} $vehicle^{-1}$), possibly representative of the vehicles used in the study domain. And finally, estimated evaporative emissions from parked vehicles, with a median emission rate of 2.3±1 g h^{-1} $vehicle^{-1}$, were significantly higher than the MOVES model predictions, suggesting either (i) the existence of poorly maintained vehicles with much higher evaporative emissions, (ii) other sources apart from vehicles contributing to the evaporative fuel emissions flux., and/or (iii) a significant underestimation of evaporative fluxes by MOVES. Based on this study, while the reported evaporative emission rates should be considered as an upper limit for parked vehicles in this area, more studies on evaporative fuel emissions appear to be needed to validate the accuracy of the emissions model.

The flux methodology used in this study can be used as an alternative approach to measure emission rates from sources for which direct emissions measurements are difficult or impossible. For example, if deployed to a tall tower downwind of

petrochemical industry regions in the Houston Ship Channel, it could be used to estimate emissions from these industrial sources, including fugitive and transient emissions, which are usually not reported accurately (Vizuete et al., 2008). The method used here could also be used more widely to determine real-world emissions from in-use vehicles and compare with estimations from emission factor models, with a goal of validation. The advantage of this method is that it naturally estimates the emission rate under real world driving and dilution conditions rather than under an artificial driving cycle and dilution ratio in typical vehicle emission testing. It can also provide more details on the chemical composition than remote sensing, which is limited in its ability in resolving chemical compositions (Singer et al., 1998). However, as demonstrated in this study, more details regarding the vehicle fleet composition, speeds and density are needed to improve the top-down versus bottom-up emissions comparison, and to effectively validate and improve vehicle emission factor models.

5. EVALUATION OF MEGAN PREDICTED BIOGENIC ISOPRENE EMISSIONS AT URBAN LOCATIONS USING A SOURCE-ORIENTED COMMUNITY MULTISCALE AIR QUALITY MODEL

Summertime isoprene emissions in urban Houston area predicted by the Model of Emissions of Gases and Aerosol from Nature (MEGAN) version 2.1 during the 2006 TexAQS study were evaluated using a source-oriented Community Multiscale Air Quality Model. Predicted isoprene concentrations at six surface sites operated by the Texas Commission of Environmental Quality (TCEQ) are significantly higher than observations during daytime hours when biogenic emissions dominate the total isoprene concentrations, with mean normalized bias (MNB) ranges from 2.01 to 5.96 and mean normalized error (MNE) ranges from 2.01 to 5.98. Predicted upper air isoprene and its first generation oxidation products of methacrolein (MACR) and methyl vinyl ketone (MVK) are also significantly higher (MNB=8.6, MNE=9.1) than observations made onboard of NOAA's WP-3 airplane which flew past the urban area. Over-prediction of isoprene and its oxidation products both at the surface and the upper air strongly suggests that biogenic isoprene emissions in urban Houston areas are significantly overestimated. Reducing the emission rates by approximately 2/3 is necessary to reduce the error between predictions and observations. Comparison of gridded leaf area index (LAI), plant functional type (PFT) and isoprene emission factor (EF) in the MEGAN input data and these from a field survey in an urban Houston area shows that the apparent isoprene over-prediction is likely caused by the combined effects of large overestimation of EF and underestimation of LAI in the urban Houston area in MEGAN. Although, predicted ozone concentrations in this region are not significantly affected by isoprene over-predictions, predicted isoprene SOA concentrations can be higher by as much as 50% using the higher isoprene emission rates.

5.1 Introduction

Plants emit significant amounts of biogenic volatile organic compounds (BVOCs) into the atmosphere (Guenther, 1995). Many of the BVOCs are highly reactive unsaturated alkenes, such as isoprene and terpenes, that can effectively react with hydroxyl radical (Zhang et al., 2000), ozone (Warneke et al., 2004) and nitrate radical (Brown et al., 2009; Brown et al., 2013) in atmospheric photochemical reactions. BVOCs are the dominant precursors to global secondary organic aerosol (SOA) loading and thus have significant impacts on global climate (Pacifico et al., 2009). In urban areas with significant biogenic influences, BVOCs can also contribute significantly to regional SOA concentrations (Kleeman et al., 2007; Zhang and Ying, 2011b). In addition to its major role in aerosol formation, BVOCs are important precursors of tropospheric ozone. For example, the incremental ozone reactivity of isoprene is approximately 20% higher than ethylene (Carter, 1994; Derwent et al., 1996). In a previous study, Ying and Krishnan (2010) showed that contributions of biogenic emissions to ozone formation is 20% higher than contributions of anthropogenic emissions in Southeast Texas.

Evaluation of the impacts on air quality and global climate due to biogenic emissions depends on accurate isoprene and other BVOC emissions estimations from different vegetation types. A number of models have been developed to estimate biogenic emissions in regional and global scales, such as the Biogenic Emission Inventory System (BEIS) (Pierce et al., 1998), the Model of Emissions of Gases and Aerosols from Nature (MEGAN) (Guenther et al., 2006; Guenther et al., 2012), and the Global Biosphere Emissions and Interactions System (GloBEIS3) (Yarwood et al., 2002). These emission models have been directly evaluated with leaf-level and ambient flux measures (Kaser et al., 2013; Langford et al., 2010a), and indirectly with observed concentrations. Model inter-comparison studies have also been reported. For example, Carlton and Baker (2011) used the Community Multiscale Air Quality (CMAQ) model to simulate concentrations of BVOCs and their oxidation products in a high emission region in central United States using BEIS and MEGAN, and found that while MEGAN significantly over-estimated isoprene and monoterpene emissions, BEIS under-estimated

them. Warneke et al. (2010) derived emission rates of isoprene from ambient measurements and compared with MEGAN and BEIS estimations, and came to similar conclusions.

While these studies provided important evaluations of the emission models, they are usually carried out over densely forested areas with rather uniform vegetation types and coverage. Capability of the biogenic emission models in heterogeneous urban/suburban regions with less vegetation cover has not been satisfactorily evaluated. In addition, recent studies have pointed out that the anthropogenic contributions to isoprene concentrations in urban and rural environment can be significant. For example, Borbon et al. (2001) used principal component analysis on measured hydrocarbons in an urban region and concluded that motor vehicle contributions to isoprene were non-negligible in summer and became more significant in winter. Song et al. (2008) studied the differences between observed and CAMx-predicted concentrations of isoprene in Southeast Texas using GloBEIS, and concluded that under-predictions of anthropogenic emissions might be a reason for under-predictions of isoprene at urban locations. Park et al. (2011) summarized past findings and concluded from urban isoprene measurements in Houston that traffic emissions can make non-negligible contributions to isoprene emissions, especially at nighttime and during the early morning rush hours. If anthropogenic emissions are a significant contributor to total isoprene concentrations, traditional observation and modeling based techniques, which use total isoprene concentrations from all sources, could not be directly used to evaluate the performance of the biogenic emission inventories in urban areas.

In this study, the capability of the most recent version of the MEGAN model (MEGAN2.1) in estimating isoprene emissions in Southeast Texas during a relatively wet summer ozone episode is evaluated using high temporal resolution isoprene concentration data collected at a number of urban sites as well as in the upper air near these urban locations. Uncertainties in the predicted isoprene concentrations due to emission factors, the plant functional types (PFTs) and leaf area index (LAI) are discussed.

5.2 Model Description

The Community Multiscale Air Quality Model (CMAQ, version 4.7.1) (Byun and Schere, 2006; Carlton et al., 2010; Foley et al., 2010) was used as a framework to incorporate a source-oriented version of the SAPRC-99 gas phase photochemical mechanism (Carter, 2000) to directly predict isoprene concentrations due to biogenic and anthropogenic emissions. In the source-oriented CMAQ model, emissions, transport, gas phase chemistry, dry/wet deposition of isoprene from biogenic sources are tracked separately from isoprene emitted from anthropogenic sources using two different isoprene species. The upwind isoprene entering the domain from model boundaries is lumped with the anthropogenic isoprene source category. Due to the short atmospheric lifetime, isoprene from upwind sources is not expected to travel long distance to affect concentrations at sites in the middle of the model domain.

While more detailed source-oriented SAPRC-99 mechanisms have been used in the past to track VOC sources (Ying and Krishnan, 2010; Zhang et al., 2013), the current version is greatly simplified to only track primary emissions of isoprene from two sources (biogenic and anthropogenic). This is sufficient for the purpose of this study to evaluate biogenic isoprene emission inventories and can greatly reduce simulation time and output file size. By separately tracking the isoprene from biogenic and anthropogenic emission sources, comparisons of observations with predictions can be made at times when predicted isoprene concentrations at monitoring sites are dominated by biogenic emissions. This allows a more strict evaluation of the performance of the underlying biogenic emission model. A similar approach was used in a previous study that evaluated vehicle emissions of CO and NO_x in Southeast Texas (Kota et al., 2014).

5.3 Model Application

The source-oriented CMAQ model was applied to predict the isoprene concentrations during a three-week summer ozone episode in Southeast Texas during the 2006 Texas Air Quality Study (TexAQS 2006), from August 25th to September 16, 2006. Hourly isoprene concentrations were measured at six ground based stations using automatic gas

chromatography (AutoGC) instruments operated by TCEQ. During this data intensive period, isoprene and its first oxidation products methacrolein (MACR) and methyl vinyl ketone (MVK) were also measured aboard the National Oceanic and Atmospheric Administration (NOAA) WP-3D aircraft using the Proton-Transfer Reaction Mass Spectrometry (PTR-MS). Three of the flight days, August 31st, September 11th and 13th, are within the simulation episode. As shown in figure 24, most of flight tracks were directly above the urban areas where the surface measurements are made. This upper air data were downloaded from the NOAA's website at http://esrl.noaa.gov/csd/projects/2006/. They can be directly used to evaluate the combined isoprene emission and CMAQ model performance.

CMAQ simulations were conducted using three-level nested domains, with horizontal grid resolutions of 36, 12 and 4 km. The vertical extent of the domain has 14 layers with a surface layer thickness of 42 m. The 36 and 12-km resolution domains cover the eastern United States (US) and the east Texas and neighboring states, respectively. The innermost 4-km domain centers on the Houston-Galveston-Brazoria and Beaumont-Port Author areas. A detailed map of the 4-km domain with the locations of AutoGC sites and flight paths is shown in figure 24. More detailed descriptions of the AutoGC sites are available from TCEQ (http://www.tceq.state.tx.us/cgi-bin/compliance/monops/site_info.pl). Barring the Beaumont site, all other sites are located in areas near downtown Houston. Beaumont, Deer Park, Milby Park and Channelview sites are located in urban residential areas. The Cesar Chavez and Clinton sites are located in commercial and industrial areas, respectively.

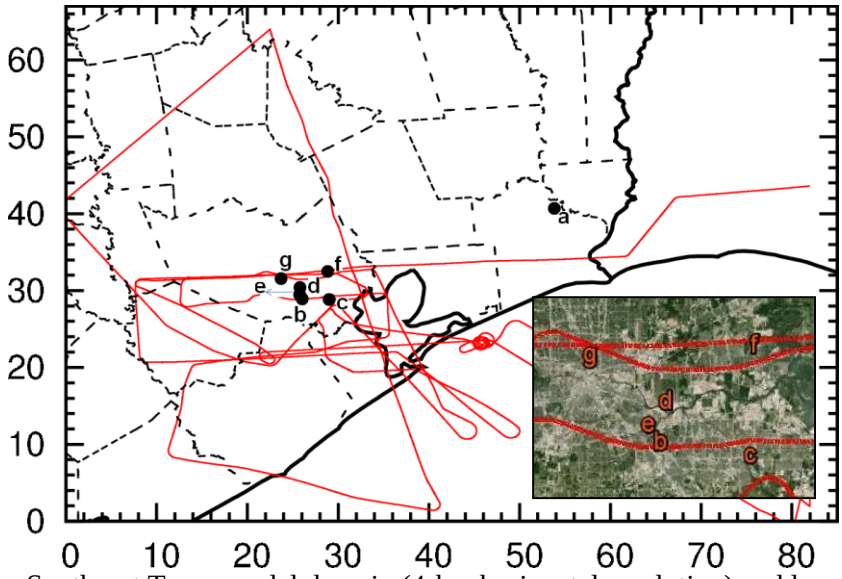

Figure 24 The Southeast Texas model domain (4-km horizontal resolution) and locations of isoprene monitoring sites. Sites (a) Beaumont (AQS code: 482450009, 30.036^0,-94.07^0), (b) Cesar Chavez (482016000, 29.68^0,-95.25^0), (c) Deer Park (482011039, 29.67,-95.12^0), (d) Clinton (482011035, 29.73^0,-95.25^0), (e) Milby Park (482010069, 29.71^0,-95.26^0) and (f) Channelview (482010026, 29.8^0,-95.12^0) are AutoGC sites operated by TCEQ. Site (g) is the Yellow Cab Tower (YCT) site where local LAI and PFT data are reported by Park et al. (2011). Blue line shows the NOAA WP-3D aircraft flight tracks. The inset is a satellite map of the urban area where the stations are located (from Google).

Details of the anthropogenic emissions and meteorological input preparation for the study episode have been documented previously (Kota et al., 2014; Zhang et al., 2013) and are only briefly summarized here. The meteorology inputs needed to drive the CMAQ model simulations were generated by TCEQ using the PSU/NCAR mesoscale model (MM5). The performance of the MM5 predictions for the modeling episode has been comprehensively evaluated in a previous study and shown to be able to reproduce the observed meteorological conditions (Ngan et al., 2012). The 2005 National Emission Inventory for 2005 (2005 NEI-v2) from the US EPA was processed using the Sparse Matrix Operator Kernel Emissions (SMOKE, version 2.5) model to generate anthropogenic emissions of gaseous and particulate pollutants.

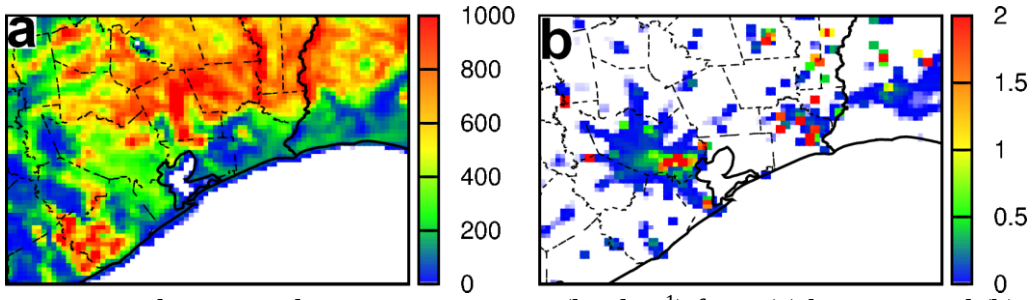

Figure 25 Episode averaged isoprene emissions (kg day^{-1}) from (a) biogenic and (b) anthropogenic sources.

The biogenic emissions were generated by TCEQ using MEGAN2.1. Leaf area index (LAI) was based on the eight-day averaged 1-km resolution LAI in the MCD15A2 product. LAI in the urban grid cells was set to a constant value of 0.4. The gridded LAI values were divided by the vegetation fraction in the same grid cell to estimate the LAI for the vegetated area (LAIv), which is used as input to the MEGAN model. MEGAN2.1 follows the 16 plant functional type (PFT) classification scheme used in the community land scale model (CLM, version 4) (Lawrence et al., 2011). In this study, the North America PFT dataset provided by Alex Guenther was used directly without modifications. Temperature and photosynthetically active radiation (PAR) were based on a TCEQ internal WRF simulation for the same 2006 TexAQS episode. Since TCEQ now uses an expanded air quality model domain, and all inputs are prepared based on this domain, it is not possible to use the MM5 model results used in this study to drive MEGAN calculations. Reduction of isoprene emissions due to potential soil moisture limitations was not considered when running the MEGAN model. Episode-averaged daily emission rates of isoprene from biogenic (domain total: 1691.5 ton d^{-1}) and anthropogenic sources (140 kg d^{-1}) in the 4-km domain are shown in figure 25.

Table 9 Percentage of four dominant vegetative types, total vegetative fraction (TPFT) and LAI at the site location.

Site	PFT1 (%)	PFT7 (%)	PFT10 (%)	PFT14 (%)	Overall Vegetation Cover (%)	LAI
Beaumont	12	19	8	8	50	1.2
Cesar Chavez	11	17	4	6	48	0.42
Deer Park	7	12	4	5	36	0.47
Clinton	11	17	3	5	43	0.4
Milby Park	11	17	4	6	48	0.43
Channelview	12	19	7	6	52	1.29

Figure 26(a) shows the averaged LAI_v during the simulation period. In the urban Houston area, the LAI_v value ranges from 0.5-1.0. LAI_v values are highest in the northeast part of the domain, with a maximum value of 0.93. Percentage vegetation cover based on the sum of the all PFT values in a grid cell is shown in figure 26(b). Vegetation coverage in the urban area is approximately 20-50%. Spatial distribution of the top four major PFTs are shown in panels (c)-(f), representing temperate needle leaf evergreen tree (PFT1), temperate broadleaf deciduous tree (PFT7), temperate broadleaf deciduous shrubs (PFT10) and C4 grass (PFT14), respectively. Contributions of other PFTs to total vegetation cover are small. In the northeast part of the domain where LAI_v values are highest, the percentage contribution of temperate needle leaf tree is also high, reaching 35-50%. Temperate broadleaf deciduous shrubs and C4 grass contributions are highest along the coastal areas. Table 9 lists these properties at the AutoGC sites. LAI_v input values ranged from 0.8 at the Milby Park site to 2.4 at the Channelview site in the Houston area. Total vegetation coverage at these sites was considered constant for the study period, ranging from 36% at the Deer Park site to 52% at the Channelview.

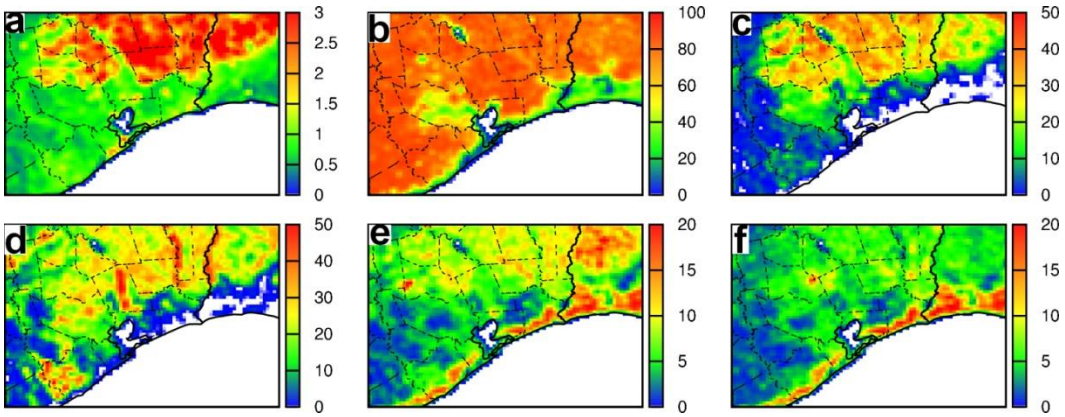

Figure 26 (a) Leaf area index for vegetated areas within each grid cell (LAI_v), (b) Fraction of cell covered by vegetation (based on the sum of all fractional plant functional type (PFT) data), (c-f) Percentage of major vegetation types: (c) temperate needle leaf evergreen tree, (d) temperate broadleaf deciduous tree, (e) temperate broadleaf deciduous shrubs, and (f) C_4 grass in the Southeast Texas domain.

Table 10 Performance statistics of predicted hourly isoprene concentrations at six TCEQ operated AutoGC sites.

Site	MFB*	MFE	MNB	MNE	Np (%)#
Beaumont	0.96 (1.30)^	1.18 (1.32)	4.61 (5.96)	4.75 (5.98)	74
Cesar Chavez	0.68 (0.99)	0.98 (1.03)	2.93 (3.75)	3.13 (3.78)	67
Deer Park	0.53 (0.79)	0.94 (0.98)	2.35 (2.84)	2.60 (2.93)	71
Clinton	0.32 (0.55)	0.96 (0.90)	1.46 (1.73)	1.83 (1.94)	85
Milby Park	0.92 (1.14)	1.1 (1.16)	3.72 (4.41)	3.83(4.42)	75
Channelview	0.48 (0.85)	1.03 (1.17)	2.32 (2.98)	2.65 (3.08)	75

*$MFB=2/N*\Sigma(P_i-O_i)/(P_i+O_i)$, $MFE=2/N*\Sigma abs(P_i-O_i)/(P_i+O_i)$, $MFB=1/N*\Sigma(P_i-O_i)/(O_i)$, and $MNE=1/N*\Sigma abs(P_i-O_i)/(O_i)$ where N is the total number of data points, P is prediction, O is observations and subscript i represents the i^{th} data point.

^ The numbers in the parenthesis are based on the hours when predicted isoprene from biogenic emissions accounts for more than 90% of the total isoprene concentration.

Percentage of data points that biogenic isoprene accounts for 90% of the total concentration.

5.4 Results and Discussion

5.4.1 MEGAN over-predicts biogenic isoprene emissions

Total (anthropogenic + biogenic) isoprene concentrations predicted by the model were compared to the AutoGC measurements made at six surface TCEQ stations (see figure 24), as shown in figure 27. In general, predictions were able to reproduce the observed diurnal and day-to-day variation patterns of the concentrations. However, predicted

concentrations are significantly higher than the observed concentrations. Detailed statistical analysis of the model performance at the sites is shown in table 10. The mean fractional bias (MFB), mean fractional error (MFE), mean normalized bias (MNB) and mean normalized error (MNE) for all the stations are 0.67, 1.0, 3.0 and 3.2, respectively, suggesting an average over-prediction of approximately 300%. The model performance is worst at Beaumont, which has an input LAI value of 1.2 and total vegetative fraction of 50%. Comparatively better performance was achieved at Clinton, which has the lowest input LAI (0.4) and second lowest total PFT (43%) among the sites.

As the monitoring sites are located in urban regions, contributions of on-road vehicles and industries might be non-negligible. The source-oriented CMAQ is capable of determining the contributions of biogenic emissions to total isoprene explicitly to provide a more direct evaluation of the biogenic isoprene emission inventory. Figure 28 shows the relative contributions of biogenic and anthropogenic sources to total isoprene concentrations at the six surface monitoring sites. Isoprene emissions from biogenic sources dominate the total isoprene concentrations during the day but anthropogenic emission contributions are much more important at night, when the total concentration of isoprene is low. The CMAQ model performance of isoprene is further analyzed by only including data points in which biogenic emissions contribute to at least 90% of total isoprene. As shown in table 10, the model performance is even worse under these conditions. The MFB, MFE, MNB and MNE for the biogenic emission dominated data points from all stations are 0.9, 1.1, 3.6 and 3.7 respectively, which are approximately 10-20% higher than the corresponding parameters that are based on all data points.

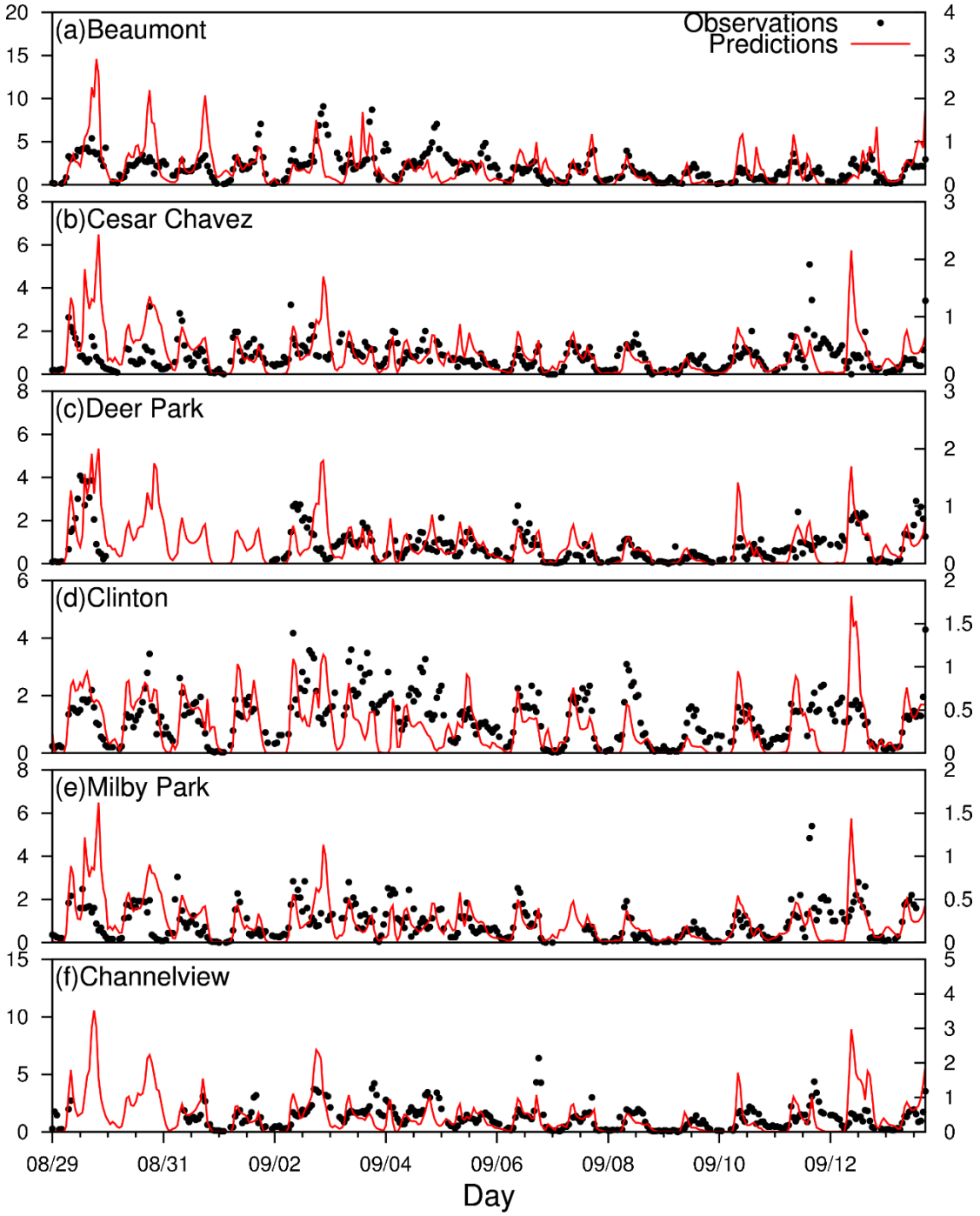

Figure 27 Time series of predicted and observed isoprene concentrations (ppb) at the six TCEQ operated AutoGC sites. Predictions and observations are shown using left and right y-axis, respectively.

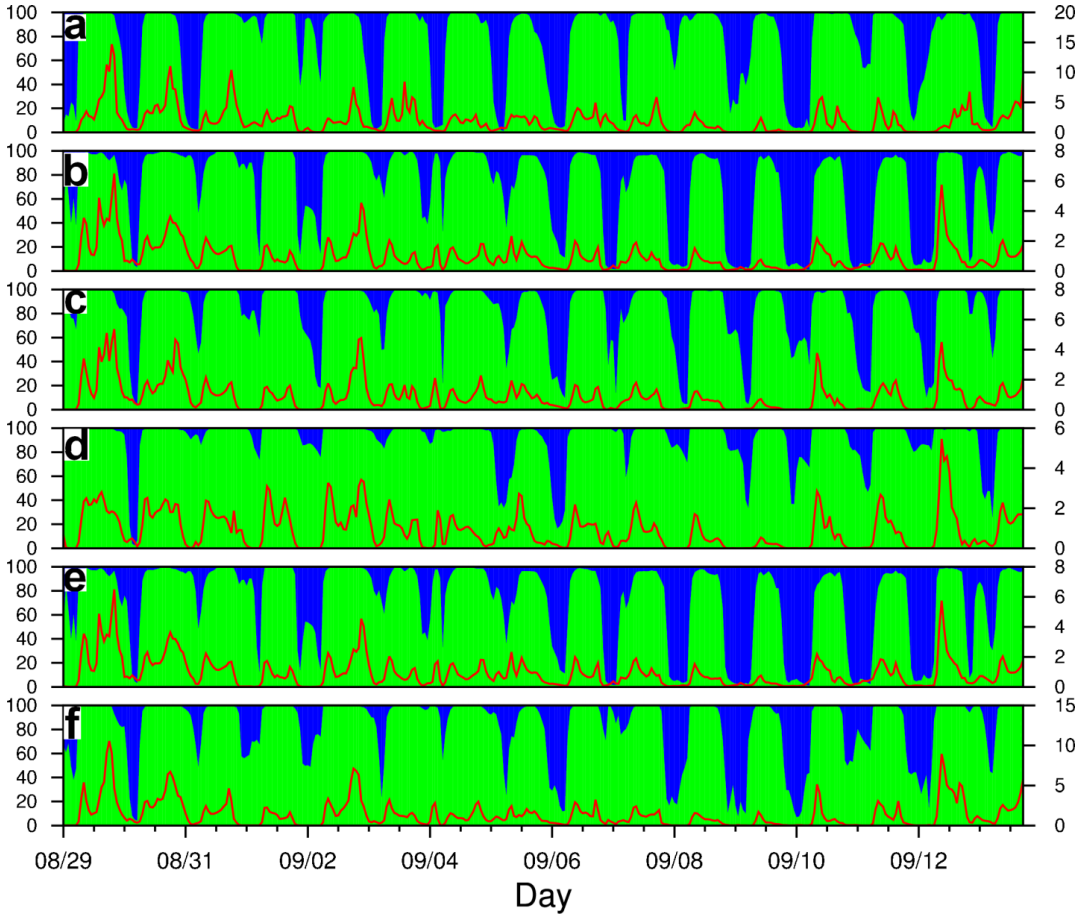

Figure 28 Time series of relative source contributions (biogenic and other sources are indicated by green and blue, respectively) to total isoprene at (a) Beaumont, (b) Cesar Chavez, (c) Deer Park, (d) Clinton, (e) Milby Park and (f) Channelview. The red lines indicate total predicted isoprene concentrations (ppb) (secondary y-axis).

Predicted isoprene and MACR+MVK concentrations at higher elevations were compared with upper air concentrations. Figure 29(a) and (b) show the comparison of observed and predicted isoprene and the sum of MACR and MVK concentrations along the flight tracks. Again, only data points with more than 90% of the biogenic emissions contributions are included in the analysis. Results indicate significant over-predictions of both isoprene and MACR+MVK concentrations across all elevations. The observed MACR+MVK concentrations show good correlation with observations (r^2=0.7). The MNB and MNE values are 4.5 and 4.6, respectively. The over-prediction of isoprene in

the upper air further supports the notion that the overestimation is unlikely due to errors in the model's transport calculations of species. If the emissions were close to reality but the model predicted less vertical dilution to cause the over-estimation at the surface, one would expect under-predictions of isoprene and its first generation oxidation products at higher elevations. Song et al. (2008) demonstrated that while vertical diffusion schemes have significant impacts on surface isoprene concentrations, they have less impact on the predicted isoprene concentrations aloft. The isoprene concentrations were less affected by the horizontal wind due to slow surface wind speed during the study episode (~2 m s^{-1}) and the short life time of isoprene. The over-prediction of MACR+MVK provides further evidence that the isoprene over-estimation is not due to a lack of oxidation capacity of the simulated atmosphere. If the oxidation capacity (i.e. hydroxyl radical concentrations) was significantly under-predicted, the concentrations of the first generation oxidation products in the upper air would typically be under-predicted as well.

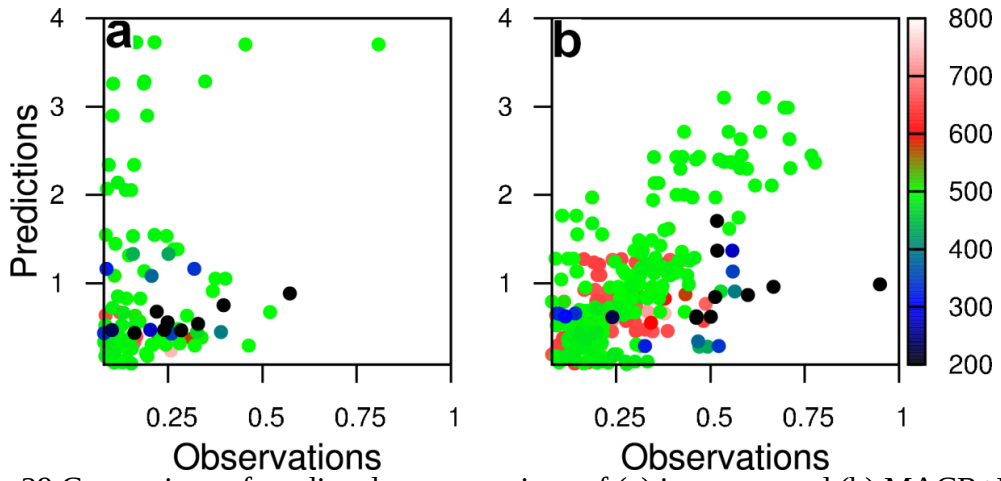

Figure 29 Comparison of predicted concentrations of (a) isoprene, and (b) MACR+MVK with observations collected on NOAA P-3 aircraft during TEXAQS-2006 study. Data points are color-coded by their measurement height (m).

Combining the time series of isoprene at the surface sites and the statistical analysis of the model performance at surface and higher elevations, it can be concluded that isoprene emissions from urban Houston areas are likely strongly overestimated by the current MEGAN model. In order to estimate the magnitude of over-estimation, several emission scaling simulations that reduces biogenic isoprene emissions by 33%, 50% and 66% were conducted. Figure 30 shows the episode averaged hourly predicted isoprene concentrations for the base case along with the simulations with a uniform emission reduction of 66% and the observed isoprene concentrations. Model performance of isoprene at the surface stations was improved with reduced emissions, as shown in table 11. Apart from Clinton Drive, the model performance in terms of MFE, MNB and MNE for the case with 66% reduction is better than the base case and other two scaling cases, i.e. 33% and 50%. For example, at Beaumont, MFE for the 66% reduction case is much better than the base case, 50% reduction and 33% reduction cases by 90%, 58% and 32% respectively. In addition to surface concentrations, predicted upper air concentrations of isoprene and MVK+MACR are also improved. The next question that needs to be investigated is what causes the over-estimation of isoprene emissions. In the following sections, uncertainties in the emissions due to vegetation type and fractional cover estimation in urban areas are discussed.

Table 11 Performance statistics of predicted hourly isoprene concentrations for cases with scaled emissions (by 33, 50 and 66%).

	MFB			MFE			MNB			MNE		
Site	33%	50%	66%	33%	50%	66%	33%	50%	66%	33%	50%	66%
Beaumont	0.72	0.51	0.18	0.98	0.82	0.62	2.59	1.64	0.71	2.76	1.64	1.00
Cesar Chavez	0.39	0.20	-0.08	0.81	0.73	0.67	1.50	0.90	0.30	1.80	1.27	0.83
Deer Park	0.23	0.01	-0.3	0.8	0.73	0.71	1.17	0.62	0.08	1.54	1.10	0.74
Clinton	-0.1	-0.27	-0.60	0.82	0.78	0.82	0.50	0.10	-0.27	1.01	0.02	0.59
Milby Park	0.64	0.44	-0.13	0.85	0.71	0.58	2.03	1.30	0.59	1.54	1.10	0.74
Channelview	0.17	-0.04	0.36	0.86	0.79	0.78	1.1	0.58	0.06	1.53	1.1	0.77
Upper Air isoprene	-0.25	-0.44	-0.71	1.27	1.24	1.25	3.66	2.30	1.02	4.48	3.22	2.1
Upper Air MACR+MVK	0.12	-0.09	-0.41	0.96	0.86	0.83	1.72	0.97	0.26	2.19	1.52	1.01

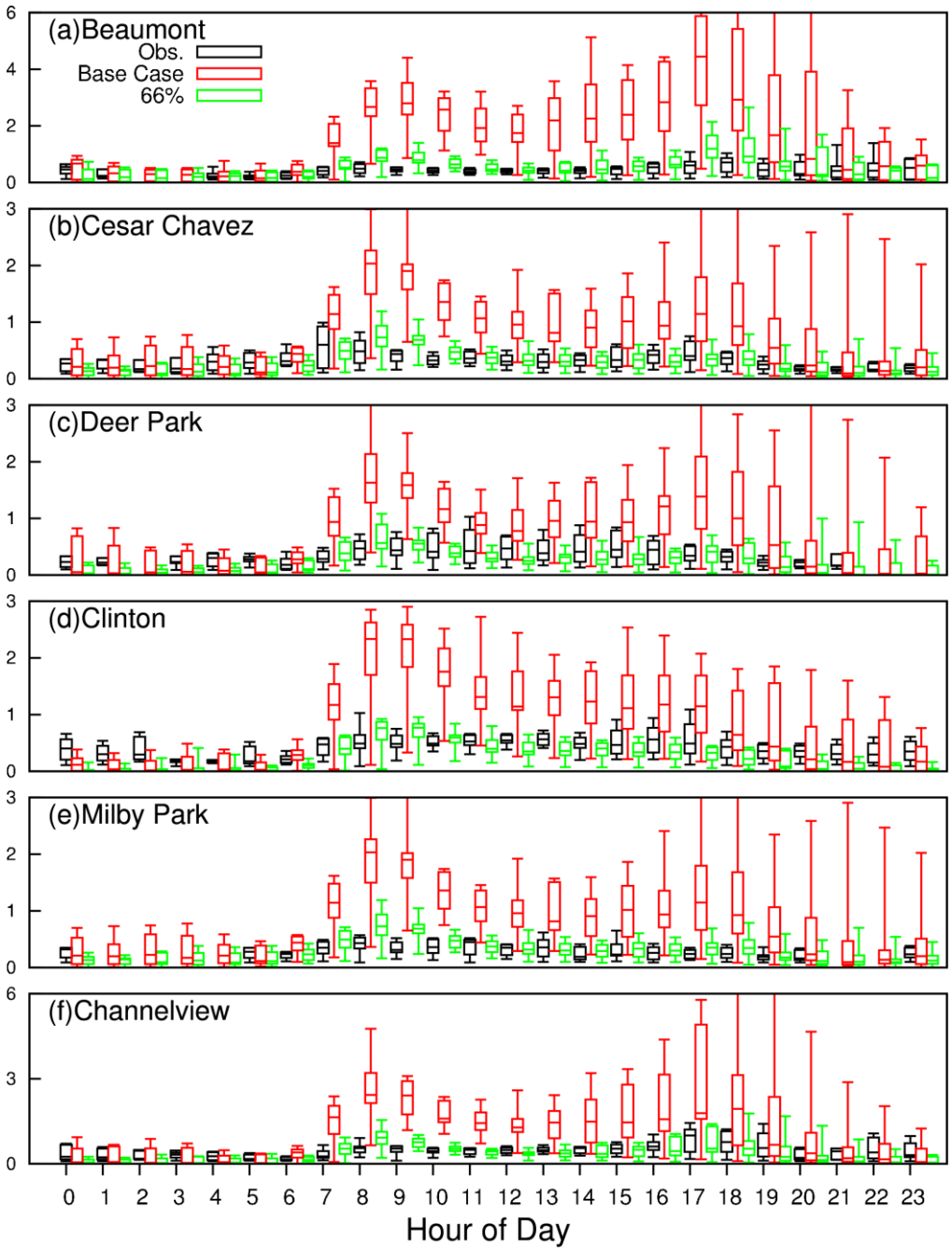

Figure 30 Episode averaged observations, base case and 66% (66% reduction of biogenic emissions) predictions as a function of hour of a day. The Box-Whisker plot shows the maximum, minimum, upper and lower quartiles, and the median.

5.4.2 What causes the overestimation of isoprene emissions

In a simplified representation, emission rate (F) of isoprene in each model grid cell (μg h^{-1}) can be calculated by equation (5.1):

$$F = \gamma \times LAI_v \times EF \times A \quad (5.1)$$

where γ is a lumped correction factor (unit-less) that includes corrections for radiation, temperature, soil moisture, leaf age, and CO_2 level; LAI_v is the leaf area index for the vegetated surface (m^2 of leaf area per m^2 of vegetated surface area); *EF* is the emission factor of isoprene at standard conditions (μg $h^{-1} \times m^2$ of vegetation area/(m^2 of leaf area×m^2 of ground area)); and *A* is the area of the grid cell (m^2). In the default configuration, MEGAN2.1 uses a gridded EF map for isoprene emissions. The EF map was prepared based on fractional areal coverage of vegetation species (χ, in units of m^2 vegetation surface per m^2 of ground surface) in a grid cell and species-specific emission factors at standard condition (ε, in units of μg of VOC per hour per m^2 of leaf surface area), based on equation (5.2):

$$EF = \sum_{i=1}^{N} \varepsilon_i \cdot \chi_i \quad (5.2)$$

where i is the vegetation type index, and N and is the total number of vegetation types in a grid cell. As an alternative to the offline prepared EF maps using detailed vegetation cover information, the EF map can also be calculated during a MEGAN simulation using PFT distributions and PFT-specific emission factors (Guenther et al. 2012). In that case, ε is the PFT-specific emission rate and χ is the fractional PFT in a grid cell.

The accuracy of the PFT, EF and LAI data can significantly affect the prediction of emissions and ambient concentrations of isoprene (Pfister et al., 2008). Although the accuracy of the inputs used in calculating the correction factor γ can also affect isoprene emissions estimations, a consistent positive scale factor in the predicted isoprene concentrations suggests that other parameters needs to be examined more carefully first. Uncertainties of LAI and PFT in urban areas can be greater than in forested areas, potentially leading to large uncertainties in emission estimations. Remote sensing determination of LAI in urban areas is largely constrained by spatial heterogeneity

within the resolved satellite pixel (Jensen and Hardin, 2005). Determination of PFT in urban areas is more uncertain because multiple satellite products are often involved (Poulter et al., 2011). In the following, the MEGAN input data (LAI, PFT and EF) are compared with a field survey of tree distributions in a residential area surrounding the Yellow Cab Tower (YCT) (see figure 24) as reported by Park et al. (2011).

The estimated respective PFT distributions from that field survey are 5% PFT1, 25% PFT7 (including live oak), 2% PFT10 and 10% PFT13/14 (PFT13 represents C3 grass), with a normalized total vegetation coverage (accounting for tree overlap with impervious and grassy areas) of 35-40%. Oak trees in PFT7 are the most important isoprene emitters. As listed in Park et al. (2011), major oak trees in this area are live oak (26% of all oaks), water oak (23%), post oak (23%), willow oak (16%) and white oak (6%). Using above canopy flux measurements, Park et al. (2011) obtained a standard emission rates of 400 $\mu g\ m^{-2}\ h^{-1}$, reasonably matching a local isoprene emissions model. This is much lower than the MEGAN gridded isoprene EF of 5700 $\mu g\ m^{-2}\ h^{-1}$ for a 1-km grid that includes the YCT.

To understand what causes the higher EF in the MEGAN input file, the alternative approach calculating EF using PFT distributions and PFT-specific EF (Guenther et al., 2012) was also attempted. The PFT distributions from the gridded MEGAN PFT input file (re-gridded to the 4-km domain) at the YCT location are 19% PFT1, 30% PFT7, 2% PFT10 and 3% PFT14, and total vegetation coverage is 58%. The percentage of PFT7, the category that includes tree species with maximum isoprene emission factors, is similar in both the field survey and the gridded input file. Using these PFT distributions and the PFT-specific EF, the calculated isoprene EF at standard conditions (using equation 5.2) is 3380 $\mu g\ m^{-2}\ h^{-1}$. This much larger estimated isoprene EF than obtained from the field data is mainly due to over-estimation of EF for PFT7. Based on Guenther et al. (2012), EF for PFT7 (EF7) is 10000 $\mu g\ m^{-2}\ h^{-}1$, and this large value is applied to all tree species in PFT7. However, the actual EF7 includes many non-emitting tree species; at the YCT site more than $2/3^{rds}$ of the PFT7 trees are non-emitters, meaning MEGAN assumes a much too high fraction of isoprene emitting trees in PFT7 than what

appears appropriate for the urban Houston area. In addition, the isoprene emission factor of coastal live oak is relatively small compared to most other oak tree species. So, it is likely that EF7 was over-estimated due to both higher fractions of isoprene-emitting trees, and higher emitting oak trees. Also, EF7 might be estimated by assuming a higher fraction of isoprene emitting trees in PFT7 than what is appropriate for the urban Houston area. Lastly, the difference between calculated EF using PFT-specific EFs and gridded EF is not clearly understood. However, since 5700×0.58=3306, which is very close to 3380, leads to suspicions that when preparing gridded EF, it was inadvertently divided by the fraction of vegetation area in the grid cell.

In summary, the above analysis suggests that using PFT and PFT-specific EF can lead to significant errors in isoprene emission estimations, especially in urban environments. Such over-estimations may be inadvertently corrected, however, by additional incorrect input data, such as LAI.

The LAI_v in full sun estimated from the field survey was approximately 3.75 (i.e., 1.5/40%). The gridded 4-km resolution LAI input data is approximately 0.69 (i.e. 0.4/58%), which is only 18.4% of the field survey data. Even though the larger gridded area includes more impervious land compared to the field study area, this indicates that LAI of 0.4 used for urban grids is an under-estimate and should be increased to a value closer to 1. Ignoring the LAI dependence of the radiation correction factor (considering only leaves in full sun), the ratio of MEGAN calculated emission rates (F_{MEGAN}) at YCT to the emission rates based on field survey (F_{field}) can be estimated using Equation (5.3):

$$\frac{F_{MEGAN}}{F_{field}} \approx \frac{LAI_{v,MEGAN}}{LAI_{v,\,field}} \times \frac{EF_{MEGAN}}{EF_{field}} = \frac{0.69}{3.75} \times \frac{5700}{400} = 2.62 \qquad (5.3)$$

This indicates that MEGAN over-estimated the isoprene emissions by a factor of 2.62 at this location. This is in good agreement with the emission scaling runs (see section 5.4.1), which suggested that isoprene emissions in urban Houston are likely overestimated by a factor of 3. The above analyses suggest that the over-estimation of isoprene emissions in urban Houston maybe due to combined effects of underestimation

of LAI_v and over-estimation of EF. Accurate vegetation cover and species-specific emissions should be used when estimating isoprene emissions.

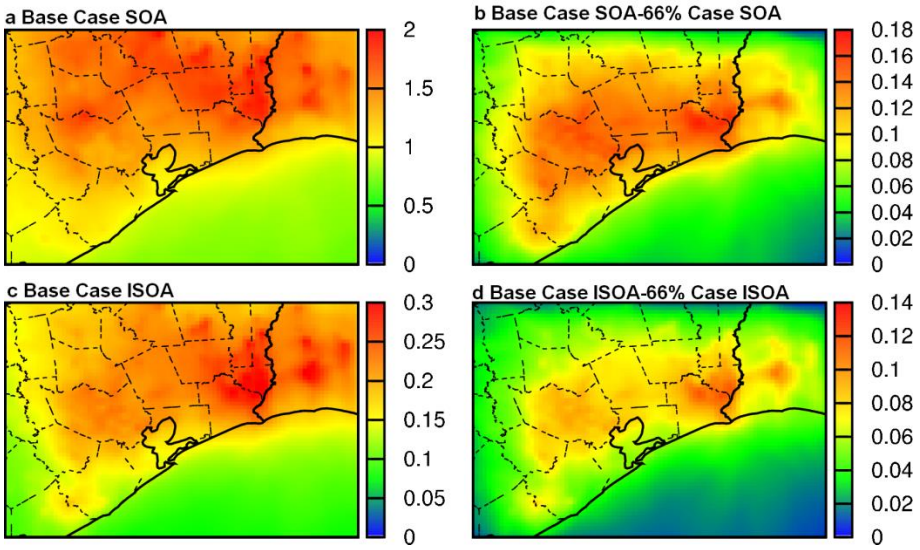

Figure 31 Predicted average (a) total secondary organic aerosol (SOA) and (d) SOA from isoprene (ISOA) concentrations during the simulation period. Changes in predicted SOA and ISOA in the 66% isoprene reduction case are shown in Panels (b,d) respectively. The scales are different to better illustrate spatial distributions. Units are µg m^{-3}.

5.4.3 Impacts on surface ozone and SOA concentrations

Overestimation of biogenic emissions may also impact ozone and SOA formation. Analyses of ozone time series and its model performance show little impact on ozone concentrations at ozone monitors in the Houston-Galveston-Brazoria area (see figure C1 and table C1 in Appendix C). This is consistent with a previous study which shows gradual ozone buildup in air parcels as they are transported towards to receptor sites. The air parcels usually started in rural areas with large isoprene emissions and ozone formation in these areas are limited by NO_x availability. As they reach the urban areas industrial and transportation related emissions are more important in ozone formation (Ying and Krishnan 2010). Thus the changes in the emissions of isoprene have a smaller than expected impact on the observed ozone concentration at the monitor sites.

However, overestimation of isoprene leads to significantly higher estimations of SOA from isoprene and also leads to slightly higher predictions of other SOA components, as shown in figure 31. Predicted SOA concentration due to isoprene in the base case simulation is approximately 0.2-0.3 μg m^{-3}, and total SOA is approximately 1.5-2 μg m^{-3}. In the 66% emission reduction case, isoprene SOA concentrations are decreased by approximately 0.1 μg m^{-3}. Comparatively, decrease in total SOA is slightly higher, as shown in figure 31(b) and (c), suggesting that changes in isoprene emissions can change the oxidation capacity of the atmosphere and lead to changes in SOA from other precursors.

5.5 Conclusions

In this study, MEGAN2.1 estimations of biogenic emissions in an urban area in Southeast Texas were evaluated by comparing predicted isoprene concentrations by a source-oriented CMAQ model with isoprene measurements at six surface sites equipped with Auto-GC during the summer TexAQS 2006 episode. In addition, predicted isoprene and MACR+MVK in the upper air are compared with measurements made by PTR-MS on NOAA's WP-3D aircraft. The source-oriented model confirms that even in urban areas biogenic isoprene dominates the daytime ambient isoprene concentrations. However, the predicted biogenic isoprene mixing ratios are much higher than observations at both surface sites (MNB=2.01-5.96, MNE=2.21-5.98) and in the upper air (MNB=8.6, MFE=9.1). Upper air MACR+MVK concentrations are also significantly over-estimated (MNB=3.6 and MFE=3.8). Due to relatively short life time of isoprene during the day and slow wind speeds in the modeling episode, it can be concluded that biogenic emissions are significantly over estimated by the MEGAN model in this study. Uniform emission reduction simulations suggest that a reduction of isoprene emissions by approximately 66% is necessary to make the predictions close to observations. Although simultaneously predicted ozone concentrations in this region and episode are not significantly affected by isoprene over-predictions, predicted isoprene SOA

concentrations are can by higher by as much as 50% with the higher isoprene emission rates.

Comparison of PFT distributions, isoprene EF at standard conditions and LAI data from a field survey with the gridded input data at an urban location shows that gridded PFT distributions at the urban sites are close to the field data. However, over-prediction of isoprene EF at standard conditions could be a major reason for the discrepancy in predicted and observed concentrations. The comparison with field data also indicates that the representative LAI used in urban grids in this study is likely lower than what is present in the field. These warrant getting more field data for better prediction of species-specific EF and LAI to improve biogenic isoprene estimations in urban areas using MEGAN.

6. CONCLUSION

6.1 Summary

The overall objective of this study is to evaluate vehicle and biogenic emission inventories in Southeast Texas. While sections 2 to 4 discuss regarding the evaluation of vehicle emission inventories with respect to CO, NO_x and VOCs emissions, section 5 includes evaluation of biogenic emission inventory.

In section 2, TAMNROM-3D model with SAPRC99 photochemical mechanism, and MOVES generated emissions, was used to predict the concentrations of pollutants near a rural highway at Austin. Results indicate that there are significant uncertainties in MOVES NO_x estimations, pointing to a significant over-prediction of atleast 15%. Additionally, MOVES NO_2/NO_x ratio of 9% is an under-representation, and the model performance of NO_2 indicates that a ratio of 29%, estimated from the curb side measurements, is necessary. To further probe the influence of using curbside ratio of 29% instead of traditional practice of using 5%, a regional simulation using CMAQ for Southeast Texas was carried out. Results indicated an increase of 6 ppb in 8-hour averaged ozone due to the usage of 29% ratio. This indicates that sufficient care should be taken while using MOVES in a near-road environment, especially in the absence of adequate observations.

In section 3, on-road vehicle emission inventories in Southeast Texas during 2006 for CO and NO_x were evaluated using a source-oriented CMAQ model with MM5 generated meteorology. Clear trends in FB were observed when the data were grouped based on the vehicle contributions to total CO and NO_x. While over-prediction of NO_x by both vehicles and other sources is observed, an under prediction of CO by other sources but over prediction by vehicles is observed. However, further analysis is required in studying the performance of other sources. Results indicate that MOVES generated NEI over predicts CO and NO_x by a factor of 2 and 1.7 respectively. This indicates necessity of significant reductions in CO and NO_x emission predictions by MOVES. To analyze the influence of meteorology models on conclusions, an additional

simulation using WRF generated meteorology was performed. Eventhough, relatively poorer performance of WRF generated meteorology resulted in greater FB ranges the trends were similar in both simulations. This indicates that future regional air quality studies should carefully evaluate and improve performance of meteorology models.

In section 4, fluxes of 18 VOCs collected during May to July 2008 on a 60m tower in an urban Houston residential area were analyzed using ME-2. Two vehicle related profiles, one representing exhaust and dominated with toluene and xylenes, the other representing evaporative emissions and dominated by isopentane, were observed. The diurnal variation of vehicle contributions, indicate a morning rush hour peak around 7AM-9AM, with average median flux of 0.76 mg m^{-2} h^{-1}. Evaporative emissions had higher contributions than vehicle exhaust, but did not show a morning rush hour peak. EdiRe, an analytical flux-footprint model, along with the contributions estimated by ME-2, was used to resolve daytime source specific emissions rates. The estimated vehicle exhaust emissions, with a median emission rate of 14.5±2 g h^{-1} $vehicle^{-1}$, were similar to the MOVES model predictions for a vehicle fleet of year 2005 (14.1±0.2 g h^{-1} $vehicle^{-1}$). This possibly is representative of the vehicles used in the study domain. However, the estimated evaporative emission rate of 2.3±1 g h^{-1} $vehicle^{-1}$ was around 7 times higher than MOVES predictions. This could either be due to presence of poorly maintained vehicles in the locality, or presence of other evaporative fuel emissions source in the locality, or significant under-prediction of evaporative emissions by MOVES. Thus, more studies are required to analyze performance of MOVES in estimating evaporative emissions.

In section 5, MEGAN estimated biogenic emissions in an urban area in Southeast Texas were evaluated using a source-oriented CMAQ model. The predicted concentrations were compared with isoprene measurements at six surface sites operated by TCEQ, and NOAA's WP-3D aircraft during the summer TexAQS 2006 episode. The predicted biogenic isoprene was much higher than observations at surface with MNB in the range of 2.01 to 5.96. Similarly, the upper air MNB was 8.6, indicating an over-prediction. A clear over-prediction of the upper air concentrations of isoprene's

oxidation products, MACR+MVK, with a MNB=3.6 was also observed. This indicates that biogenic emissions are substantially over estimated by the MEGAN model. Sensitivity simulations indicated that reduction of isoprene emissions by approximately 66% is necessary to achieve a reasonable model-measurement match. To understand the accuracy of input vegetation data, detailed field observations at a location in the domain were compared to the gridded LAI and PFT input data. Although the analysis indicated inconsequential difference in PFT distribution, the emission factor for the critical PFT7 was drastically overestimated, seemingly assuming a very different PFT composition (many high isoprene emitting trees) than present in Houston (few, including low isoprene emitting tree species). These differences likely explain the drastic over-estimation of urban isoprene concentrations.

6.2 Recommendations for Future Research

Section 2 indicates that MOVES over estimates NO_x emissions. However, due to less vehicle density on the roadway in the study proper conclusions regarding MOVES CO estimations could not be achieved. Thus, this analysis should be repeated in a case with higher vehicle density roadway. Additionally, this section indicated that using curb side NO_2/NO_x ratio in emissions resulted in better model performance. However, as MOVES predicts tail pipe emissions, the higher curbside ratio could be due to conversion of NO to NO_2 from tail pipe to curbside. Thus, this should be explored further.

Sections 2, 3 and 4 concentrate on evaluation of MOVES performance in estimating gaseous pollutants from vehicles. However, in addition to gaseous pollutants, particulate matter (PM) emissions from vehicular traffic are also of health concerns (Anderson et al., 2001; Curtis et al., 2006). Studies also showed high ultrafine particle number concentrations near roadways (e.g. Zhu et al. (2002)). Thus it is necessary to model size resolved particle number and mass concentrations near roadways. In addition to speciated PM2.5 and PM10, MOVES has the ability to predict emissions of metals from vehicles. Moreover, unlike previous USEPA emission factor models, which were insensitive to vehicle speed MOVES PM and EC/OC emission factors change with

vehicle speed (Kota et al., 2012). Thus it would be interesting to evaluate the performance of MOVES in predicting PM.

In section 3, the estimated vehicle exhaust emission factor in this study was compared to MOVES predictions. Eventhough transient operating modes of vehicles on the surrounding roadways for every minute were available in this study, only MOVES predictions at average speed was only considered. So in future the exploration of modal version of MOVES is recommended. Additionally, the procedure used in section 3 should be repeated for particle fluxes measured on the tower. This would help in direct evaluation of MOVES PM emission factor estimations.

Receptor oriented statistical analysis used in section 3, resulted in identification and quantification of pentane emissions from a point source in the locality. This method can be further used in regions where under-reporting or non-reporting of emissions from industries is common.

The accuracy of source-oriented model, used in section 4, is a must for the policy makers while analyzing the results. However, in this dissertation only influence of meteorology models on model performance was only studied. Thus effects of horizontal and vertical grid resolutions, dispersion parameterizations should be explored in future. Additionally, this source-oriented model can also be used in estimating the effect of different vehicle fleet compositions on predicted concentrations. This can help the policy makers by suggesting possible regulations on certain fleet for environmental benefits.

Moreover, section 4 suggests NO_x emission control only. But due to non-linearity of VOC and NO_x reactions resulting in the formation of ozone, both NO_x and VOCs emitted from vehicles should be tracked together in future, to suggest effective control strategy for ozone in Southeast Texas.

REFERENCES

Alessio, G.A., Estiarte, M., Llusia, J., Peñuelas, J., 2008. Contrasting species-specific, compound-specific, seasonal, and interannual responses of foliar isoprenoid emissions to experimental drought in a mediterranean shrubland. International Journal of Plant Sciences 169, 637-645.

Amato, F., Pandolfi, M., Escrig, A., Querol, X., Alastuey, A., Pey, J., Perez, N., Hopke, P.K., 2009. Quantifying road dust resuspension in urban environment by multilinear engine: A comparison with PMF2. Atmos. Environ. 43, 2770-2780.

Anderson, H.R., Bremner, S.A., Atkinson, R.W., Harrison, R.M., Walters, S., 2001. Particulate matter and daily mortality and hospital admissions in the west midlands conurbation of the United Kingdom: associations with fine and coarse particles, black smoke and sulphate. Occupational and Environmental Medicine 58, 504-510.

Atkinson, R., 2000. Atmospheric chemistry of VOCs and NOx. Atmos. Environ. 34, 2063-2101.

Badman, D.G., Jaffe, E.R., 1996. Blood and air pollution: State of knowledge and research needs. Otolaryngology - Head and Neck Surgery 114, 205-208.

Banta, R., Senff, C., Nielsen-Gammon, J., Darby, L., Ryerson, T., Alvarez, R., Sandberg, S., Williams, E., Trainer, M., 2005. A bad air day in Houston. Bulletin of the American Meteorological Society 86, 657-669.

Barad, M.L., 1958. Project Prairie Grass: A field program in diffusion, Geophys. Res. Paper No. 59(ii) TR-58-235(ii). Air Force Cambridge Research Centre, Bedford, Massachusetts.

Bäumer, D., Vogel, B., Fiedler, F., 2005. A new parameterisation of motorway-induced turbulence and its application in a numerical model. Atmos. Environ. 39, 5750-5759.

Berkowicz, R., 2000. OSPM - A parameterised street pollution model. Environmental Monitoring and Assessment 65, 323-331.

Borbon, A., Fontaine, H., Veillerot, M., Locoge, N., Galloo, J.C., Guillermo, R., 2001. An investigation into the traffic-related fraction of isoprene at an urban location. Atmos. Environ. 35, 3749-3760.

Boriboonsomsin, K., Barth, M., 2007. Evaluating air quality benefits of freeway high-occupancy vehicle lanes in southern California. Transportation Research Record: Journal of the Transportation Research Board 2011, 137-147.

Brioude, J., Kim, S.W., Angevine, W.M., Frost, G.J., Lee, S.H., McKeen, S.A., Trainer, M., Fehsenfeld, F.C., Holloway, J.S., Ryerson, T.B., Williams, E.J., Petron, G., Fast, J.D., 2011. Top-down estimate of anthropogenic emission inventories and their interannual variability in Houston using a mesoscale inverse modeling technique. Journal of Geophysical Research-Atmospheres 116, D20305.

Brown, S.G., Reid, S.B., Roberts, P.T., Buhr, M.P., Funk, T.H., Kim, E., Hopke, P.K., 2004. Reconciliation of the VOC and NOx emission inventory with ambient data in the Houston, Texas region, 13th International Emission Inventory Conference "Working for Clean Air in Clearwater", Clearwater, FL.

Brown, S.S., deGouw, J.A., Warneke, C., Ryerson, T.B., Dube, W.P., Atlas, E., Weber, R.J., Peltier, R.E., Neuman, J.A., Roberts, J.M., Swanson, A., Flocke, F., McKeen, S.A., Brioude, J., Sommariva, R., Trainer, M., Fehsenfeld, F.C., Ravishankara, A.R., 2009. Nocturnal isoprene oxidation over the northeast United States in summer and its impact on reactive nitrogen partitioning and secondary organic aerosol. Atmospheric Chemistry and Physics 9, 3027-3042.

Brown, S.S., Dube, W.P., Bahreini, R., Middlebrook, A.M., Brock, C.A., Warneke, C., de Gouw, J.A., Washenfelder, R.A., Atlas, E., Peischl, J., Ryerson, T.B., Holloway, J.S., Schwarz, J.P., Spackman, R., Trainer, M., Parrish, D.D., Fehshenfeld, F.C., Ravishankara, A.R., 2013. Biogenic VOC oxidation and organic aerosol formation in an urban nocturnal boundary layer: aircraft vertical profiles in Houston, TX. Atmospheric Chemistry and Physics 13, 11317-11337.

Brunekreef, B., Janssen, N.A.H., deHartog, J., Harssema, H., Knape, M., vanVliet, P., 1997. Air pollution from truck traffic and lung function in children living near motorways. Epidemiology 8, 298-303.

Burnett, R.T., Dales, R.E., Brook, J.R., Raizenne, M.E., Krewski, D., 1997. Association between ambient carbon monoxide levels and hospitalizations for congestive heart failure in the elderly in 10 Canadian cities. Epidemiology 8, 162-167.

Burnett, R.T., Smith-doiron, M., Stieb, D., Cakmak, S., Brook, J.R., 1999. Effects of particulate and gaseous air pollution on cardiorespiratory hospitalizations. Archives of Environmental Health: An International Journal 54, 130-139.

Buzcu, B., Fraser, M.P., 2006. Source identification and apportionment of volatile organic compounds in Houston, TX. Atmos. Environ. 40, 2385-2400.

Buzcu Guven, B., Olaguer, E.P., 2011. Ambient formaldehyde source attribution in Houston during TexAQS II and TRAMP. Atmos. Environ. 45, 4272-4280.

Byun, D., Schere, K.L., 2006. Review of the governing equations, computational algorithms, and other components of the models-3 community multiscale air quality (CMAQ) modeling system. Applied Mechanics Reviews 59, 51-77.

CARB, 2007. EMFAC2007. Calculating emission inventories for vehicles in California, user guide. California Air Resource Board, Sacramento, California.

Carlton, A.G., Baker, K.R., 2011. Photochemical modeling of the Ozark isoprene volcano: MEGAN, BEIS, and their impacts on air quality predictions. Environmental Science & Technology 45, 4438-4445.

Carlton, A.G., Bhave, P.V., Napelenok, S.L., Edney, E.D., Sarwar, G., Pinder, R.W., Pouliot, G.A., Houyoux, M., 2010. Model representation of secondary organic aerosol in CMAQv4.7. Environmental Science & Technology 44, 8553-8560.

Carslaw, D.C., 2005. Evidence of an increasing NO2/NOX emissions ratio from road traffic emissions. Atmos. Environ. 39, 4793-4802.

Carter, W.P.L., 1994. Development of ozone reactivity scales for volatile organic-compounds. Journal of the Air & Waste Management Association 44, 881-899.

Carter, W.P.L., 2000. Documentation of the SAPRC-99 chemical mechanism for VOC reactivity assessment, report to the California air resources board. California Air Resources Board, Sacramento, California.

Carvalho, J.C., Vilhena, M.T., Moreira, D.M., 2007. Comparison between Eulerian and Lagrangian semi-analytical models to simulate the pollutant dispersion in the PBL. Applied Mathematical Modelling 31, 120-129.

Castellanos, P., Marufu, L.T., Doddridge, B.G., Taubman, B.F., Schwab, J.J., Hains, J.C., Ehrman, S.H., Dickerson, R.R., 2011. Ozone, oxides of nitrogen, and carbon monoxide during pollution events over the eastern United States: An evaluation of emissions and vertical mixing. Journal of Geophysical Research: Atmospheres 116, D16307.

Chang, T.-Y., Huang, K.-H., Liu, C.-S., Shie, R.-H., Chao, K.-P., Hsu, W.-H., Bao, B.-Y., 2010. Exposure to volatile organic compounds and kidney dysfunction in thin film transistor liquid crystal display (TFT-LCD) workers. Journal of Hazardous Materials 178, 934-940.

Chauhan, A.J., Krishna, M.T., Frew, A.J., Holgate, S.T., 1998. Exposure to nitrogen dioxide (NO2) and respiratory disease risk. Reviews on Environmental Health 13, 73-90.

Choi, D., Koupal, J., 2011. MOVES validation, MOVES workshop, Ann Arbor, Michigan.

Clements, A.L., Jia, Y., Denbleyker, A., McDonald-Buller, E., Fraser, M.P., Allen, D.T., Collins, D.R., Michel, E., Pudota, J., Sullivan, D., Zhu, Y., 2009. Air pollutant concentrations near three Texas roadways, part II: Chemical characterization and transformation of pollutants. Atmos. Environ. 43, 4523-4534.

Cook, R., Isakov, V., Touma, J.S., Benjey, W., Thurman, J., Kinnee, E., Ensley, D., 2008. Resolving local-scale emissions for modeling air quality near roadways. Journal of the Air & Waste Management Association 58, 451-461.

Costa, C.P., Vilhena, M.T., Moreira, D.M., Tirabassi, T., 2006. Semi-analytical solution of the steady three-dimensional advection-diffusion equation in the planetary boundary layer. Atmos. Environ. 40, 5659-5669.

CRC, 2004. Evaluation of the US EPA MOBILE6 highway vehicle emission factor model. Final report CRC Project E-64. ENVIRON International Corp, Novato, California.

Curtis, L., Rea, W., Smith-Willis, P., Fenyves, E., Pan, Y., 2006. Adverse health effects of outdoor air pollutants. Environment International 32, 815-830.

Czader, B.H., Byun, D.W., Kim, S.T., Carter, W.P.L., 2008. A study of VOC reactivity in the Houston-Galveston air mixture utilizing an extended version of SAPRC-99 chemical mechanism. Atmos. Environ. 42, 5733-5742.

Daniel, J.S., Solomon, S., 1998. On the climate forcing of carbon monoxide. Journal of Geophysical Research: Atmospheres 103, 13249-13260.

Degrazia, G.A., Anfossi, D., Carvalho, J.C., Mangia, C., Tirabassi, T., Campos Velho, H.F., 2000. Turbulence parameterisation for PBL dispersion models in all stability conditions. Atmos. Environ. 34, 3575-3583.

Derwent, R.G., Jenkin, M.E., Saunders, S.M., 1996. Photochemical ozone creation potentials for a large number of reactive hydrocarbons under European conditions. Atmos. Environ. 30, 181-199.

EEA, 2007. COPERT4. Computer programme to calculate emissions from road transport, user manual. European Topic Center on Air and Climate Change, Europe.

Eskridge, R.E., Hunt, J.C.R., 1979. Highway modeling .1. Prediction of velocity and turbulence fields in the wake of vehicles. Journal of Applied Meteorology 18, 387-400.

FHWA, 2001. Traffic monitoring guide. Section 4: Vehicle classification monitoring. U.S. Department of transportation, Washington, District of Columbia.

Finkelstein, M.M., Jerrett, M., Sears, M.R., 2004. Traffic air pollution and mortality rate advancement periods. American Journal of Epidemiology 160, 173-177.

Foken, T., Wichura, B., 1996. Tools for quality assessment of surface-based flux measurements. Agricultural and Forest Meteorology 78, 83-105.

Foley, K.M., Roselle, S.J., Appel, K.W., Bhave, P.V., Pleim, J.E., Otte, T.L., Mathur, R., Sarwar, G., Young, J.O., Gilliam, R.C., Nolte, C.G., Kelly, J.T., Gilliland, A.B., Bash, J.O., 2010. Incremental testing of the community multiscale air quality (CMAQ) modeling system version 4.7. Geoscientific Model Development 3, 205-226.

Franco, V., Kousoulidou, M., Muntean, M., Ntziachristos, L., Hausberger, S., Dilara, P., 2013. Road vehicle emission factors development: A review. Atmos. Environ. 70, 84-97.

Fuentes, J.D., Lerdau, M., Atkinson, R., Baldocchi, D., Bottenheim, J.W., Ciccioli, P., Lamb, B., Geron, C., Gu, L., Guenther, A., Sharkey, T.D., Stockwell, W., 2000. Biogenic hydrocarbons in the atmospheric boundary layer: A review. Bulletin of the American Meteorological Society 81, 1537-1575.

Fujita, E.M., Campbell, D.E., Zielinska, B., Chow, J.C., Lindhjem, C.E., DenBleyker, A., Bishop, G.A., Schuchmann, B.G., Stedman, D.H., Lawson, D.R., 2012. Comparison of the MOVES2010a, MOBILE6.2, and EMFAC2007 mobile source emission models with on-road traffic tunnel and remote sensing measurements. Journal of the Air & Waste Management Association 62, 1134-1149.

Fujita, E.M., Lu, Z., Sagebiel, J., Robinson, N.F., Watson, J.G., 1995. VOC source apportionment for the coast oxidant assessment for southeast Texas. Texas Natural Resource Conservation Commission, Desert Research Institute, Austin, Texas.

Garratt, J.R., 1994. The atmospheric boundary layer. Press Syndicate of the University of Cambridge, New York.

Gauderman, W.J., Vora, H., McConnell, R., Berhane, K., Gilliland, F., Thomas, D., Lurmann, F., Avol, E., Kunzli, N., Jerrett, M., Peters, J., 2007. Effect of exposure to traffic on lung development from 10 to 18 years of age: A cohort study. The Lancet 369, 571-577.

Gentner, D.R., Harley, R.A., Miller, A.M., Goldstein, A.H., 2009. Diurnal and seasonal variability of gasoline-related volatile organic compound emissions in Riverside, California. Environmental Science & Technology 43, 4247-4252.

Geron, C.D., Nie, D., Arnts, R.R., Sharkey, T.D., Singsaas, E.L., Vanderveer, P.J., Guenther, A., Sickles, J.E., Kleindienst, T.E., 1997. Biogenic isoprene emission: Model evaluation in a southeastern United States bottomland deciduous forest. Journal of Geophysical Research: Atmospheres 102, 18889-18901.

Gryning, S.E., Lyck, E., 1984. Atmospheric dispersion from elevated sources in an urban area: Comparison between tracer experiments and model calculations. Journal of climate and applied meteorology 23, 651-660.

Guenther, A., 1995. A global model of natural volatile organic compound emissions. Journal of Geophysical Research 100, 8873-8892.

Guenther, A., Karl, T., Harley, P., Wiedinmyer, C., Palmer, P.I., Geron, C., 2006. Estimates of global terrestrial isoprene emissions using MEGAN (Model of emissions of gases and aerosols from nature). Atmospheric Chemistry and Physics 6, 3181-3210.

Guenther, A.B., Hills, A.J., 1998. Eddy covariance measurement of isoprene fluxes. Journal of Geophysical Research: Atmospheres 103, 13145-13152.

Guenther, A.B., Jiang, X., Heald, C.L., Sakulyanontvittaya, T., Duhl, T., Emmons, L.K., Wang, X., 2012. The model of emissions of gases and aerosols from nature version 2.1 (MEGAN2.1): an extended and updated framework for modeling biogenic emissions. Geoscientific Model Development 5, 1471-1492.

Guo, H., So, K.L., Simpson, I.J., Barletta, B., Meinardi, S., Blake, D.R., 2007. C1–C8 volatile organic compounds in the atmosphere of Hong Kong: Overview of atmospheric processing and source apportionment. Atmos. Environ. 41, 1456-1472.

Gustafson, W.I., Yu, S., 2012. Generalized approach for using unbiased symmetric metrics with negative values: normalized mean bias factor and normalized mean absolute error factor. Atmospheric Science Letters 13, 262-267.

Harley, P., Guenther, A., Zimmerman, P., 1996. Effects of light, temperature and canopy position on net photosynthesis and isoprene emission from sweetgum (Liquidambar styraciflua) leaves. Tree Physiology 16, 25-32.

Harley, P., Guenther, A., Zimmerman, P., 1997. Environmental controls over isoprene emission in deciduous oak canopies. Tree Physiology 17, 705-714.

Harley, R.A., Russell, A.G., McRae, G.J., Cass, G.R., Seinfeld, J.H., 1993. Photochemical modeling of the southern California air-quality study. Environmental Science & Technology 27, 378-388.

Held, T., Chang, D.P.Y., Niemeier, D.A., 2003. UCD 2001: An improved model to simulate pollutant dispersion from roadways. Atmos. Environ. 37, 5325-5336.

Henry, R.C., Spiegelman, C.H., Collins, J.F., Park, E., 1997. Reported emissions of organic gases are not consistent with observations. Proceedings of the National Academy of Sciences of the United States of America 94, 6596-6599.

Hoek, G., Brunekreef, B., Goldbohm, S., Fischer, P., van den Brandt, P.A., 2002. Association between mortality and indicators of traffic-related air pollution in the Netherlands: A cohort study. Lancet 360, 1203-1209.

Hoffmann, B., Moebus, S., Stang, A., Beck, E.M., Dragano, N., Mohlenkamp, S., Schmermund, A., Memmesheimer, M., Mann, K., Erbel, R., Jockel, K.H., Heinz Nixdorf, R.S.I., 2006. Residence close to high traffic and prevalence of coronary heart disease. Eur. Heart J. 27, 2696-2702.

Hsu, Y., Divita, F., 2008. SPECIATE 4.2 Speciation database development documentation. Draft Report. Prepared for Office of Research and Development, U.S. Environmental Protection Agency. E.H. Pechan & Associates, Inc., Research Triangle Park, North Carolina.

Isaksen, I.S.A., Hov, Ø., 1987. Calculation of trends in the tropospheric concentration of O3, OH, CO, CH4 and NOx. Tellus B 39B, 271-285.

Jacobson, M.Z., 1998. Fundamentals of atmospheric modeling. Cambridge University Press, New York.

Jensen, R.R., Hardin, P.J., 2005. Estimating urban leaf area using field measurements and satellite remote sensing data. Journal of Arboriculture 31, 21-27.

Kalthoff, N., Bäumer, D., Corsmeier, U., Kohler, M., Vogel, B., 2005. Vehicle-induced turbulence near a motorway. Atmos. Environ. 39, 5737-5749.

Karl, T., Apel, E., Hodzic, A., Riemer, D.D., Blake, D.R., Wiedinmyer, C., 2009. Emissions of volatile organic compounds inferred from airborne flux measurements over a megacity. Atmospheric Chemistry and Physics 9, 271-285.

Karl, T., Guenther, A., Jordan, A., Fall, R., Lindinger, W., 2001. Eddy covariance measurement of biogenic oxygenated VOC emissions from hay harvesting. Atmos. Environ. 35, 491-495.

Kaser, L., Karl, T., Guenther, A., Graus, M., Schnitzhofer, R., Turnipseed, A., Fischer, L., Harley, P., Madronich, M., Gochis, D., Keutsch, E.N., Hansel, A., 2013. Undisturbed and disturbed above canopy ponderosa pine emissions: PTR-TOF-MS measurements and MEGAN 2.1 model results. Atmospheric Chemistry and Physics 13, 11935-11947.

Kastner-Klein, P., Berkowicz, R., Plate, E.J., 2000. Modelling of vehicle-induced turbulence in air pollution studies for streets. International Journal of Environment and Pollution 14, 496-507.

Kenty, K.L., Poor, N.D., Kronmiller, K.G., McClenny, W., King, C., Atkeson, T., Campbell, S.W., 2007. Application of CALINE4 to roadside NO/NO2 transformations. Atmos. Environ. 41, 4270-4280.

Kim, E., Brown, S.G., Hafner, H.R., Hopke, P.K., 2005. Characterization of non-methane volatile organic compounds sources in Houston during 2001 using positive matrix factorization. Atmos. Environ. 39, 5934-5946.

Kim, E., Hopke, P.K., Paatero, P., Edgerton, E.S., 2003. Incorporation of parametric factors into multilinear receptor model studies of Atlanta aerosol. Atmos. Environ. 37, 5009-5021.

Kim, J.J., Smorodinsky, S., Lipsett, M., Singer, B.C., Hodgson, A.T., Ostro, B., 2004. Traffic-related air pollution near busy roads: The east bay children's respiratory health study. Am. J. Respir. Crit. Care Med. 170, 520-526.

Kim, S.W., McKeen, S.A., Frost, G.J., Lee, S.H., Trainer, M., Richter, A., Angevine, W.M., Atlas, E., Bianco, L., Boersma, K.F., Brioude, J., Burrows, J.P., de Gouw, J., Fried, A., Gleason, J., Hilboll, A., Mellqvist, J., Peischl, J., Richter, D., Rivera, C., Ryerson, T., Hekkert, S.T.L., Walega, J., Warneke, C., Weibring, P., Williams, E., 2011. Evaluations of NOx and highly reactive VOC emission inventories in Texas and their implications for ozone plume simulations during the Texas air quality study 2006. Atmospheric Chemistry and Physics 11, 11361-11386.

Kirchstetter, T.W., Singer, B.C., Harley, R.A., Kendall, G.R., Chan, W., 1996. Impact of oxygenated gasoline use on California light-duty vehicle emissions. Environmental Science & Technology 30, 661-670.

Kite, C., 2011. Preliminary comparison between MOVES and MOBILE6 Houston/Galveston/Brazoria (HGB) on-road emission inventories for 2006 and 2018. Texas Commision on Environmental Quality, Austin, Texas.

Kleeman, M.J., Ying, Q., Lu, J., Mysliwiec, M.J., Griffin, R.J., Chen, J.J., Clegg, S., 2007. Source apportionment of secondary organic aerosol during a severe photochemical smog episode. Atmos. Environ. 41, 576-591.

Kleinman, L.I., Daum, P., Imre, D., Lee, Y.N., Nunnermacker, L., Springston, S., Weinstein-Lloyd, J., Rudolph, J., 2002. Ozone production rate and hydrocarbon reactivity in 5 urban areas: A cause of high ozone concentration in Houston. Geophysical Research Letters 29, 105-101-105-104.

Kleinman, L.I., Daum, P.H., Lee, Y.N., Nunnermacker, L.J., Springston, S.R., Weinstein-Lloyd, J., Rudolph, J., 2005. A comparative study of ozone production in five U.S. metropolitan areas. Journal of Geophysical Research: Atmospheres 110, D02301.

Kljun, N., Calanca, P., Rotach, M., Schmid, H., 2004. A simple parameterisation for flux footprint predictions. Boundary-Layer Meteorology 112, 503-523.

Kljun, N., Kormann, R., Rotach, M.W., Meixer, F.X., 2003. Comparison of the Langrangian footprint model LPDM-B with an analytical footprint model. Boundary-Layer Meteorology 106, 349-355.

Kljun, N., Rotach, M.W., Schmid, H.P., 2002. A three-dimensional backward Lagrangian footprint model for a wide range of boundary-layer stratifications. Boundary-Layer Meteorology 103, 205-226.

Kormann, R., Meixner, F., 2001. An analytical footprint model for non-neutral stratification. Boundary-Layer Meteorology 99, 207-224.

Kota, S.H., Ying, Q., Schade, G.W., 2012. MOVES vs. MOBILE6.2: Differences in emission factors and regional air quality predictions, Transportation Research Board Annual Meeting, Washington, District of Columbia.

Kota, S.H., Ying, Q., Zhang, Y., 2010. TAMNROM-3D. Three-dimensional Eulerian model to simulate air quality near highways. Transportation Research Record: Journal of the Transportation Research Board 2158, 61-68.

Kota, S.H., Ying, Q., Zhang, Y., 2013a. Simulating near-road reactive dispersion of gaseous air pollutants using a three-dimensional Eulerian model. Science of the Total Environment 454-455, 348-357.

Kota, S.H., Zhang, H., Chen, G., Schade, G.W., Ying, Q., 2014. Evaluation of on-road vehicle CO and NOx national emission inventories using an urban-scale source-oriented air quality model. Atmos. Environ. 85, 99-108.

Kota, S.H., Zhang, H., Ying, Q., Schade, G., W., 2013b. Evaluation of CO and NOx emissions from MOVES and MOBILE6.2 in southeast Texas using a source-oriented regional air quality model Transportation Research Board Annual Meeting, Washington, District of Columbia.

Kroll, J.H., Seinfeld, J.H., 2008. Chemistry of secondary organic aerosol: Formation and evolution of low-volatility organics in the atmosphere. Atmos. Environ. 42, 3593-3624.

Kuhns, H.D., Mazzoleni, C., Moosmüller, H., Nikolic, D., Keislar, R.E., Barber, P.W., Li, Z., Etyemezian, V., Watson, J.G., 2004. Remote sensing of PM, NO, CO and HC

emission factors for on-road gasoline and diesel engine vehicles in Las Vegas, NV. Science of The Total Environment 322, 123-137.

Kukkonen, J., Härkönen, J., Walden, J., Karppinen, A., Lusa, K., 2001. Evaluation of the CAR-FMI model against measurements near a major road. Atmos. Environ. 35, 949-960.

Langford, B., Davison, B., Nemitz, E., Hewitt, C.N., 2009. Mixing ratios and eddy covariance flux measurements of volatile organic compounds from an urban canopy (Manchester, UK). Atmospheric Chemistry and Physics 9, 1971-1987.

Langford, B., Misztal, P.K., Nemitz, E., Davison, B., Helfter, C., Pugh, T.A.M., MacKenzie, A.R., Lim, S.F., Hewitt, C.N., 2010a. Fluxes and concentrations of volatile organic compounds from a south-east Asian tropical rainforest. Atmospheric Chemistry and Physics 10, 8391-8412.

Langford, B., Nemitz, E., House, E., Phillips, G.J., Famulari, D., Davison, B., Hopkins, J.R., Lewis, A.C., Hewitt, C.N., 2010b. Fluxes and concentrations of volatile organic compounds above central London, UK. Atmospheric Chemistry and Physics 10, 627-645.

Laothawornkitkul, J., Taylor, J.E., Paul, N.D., Hewitt, C.N., 2009. Biogenic volatile organic compounds in the Earth system. New Phytologist 183, 27-51.

Lawrence, D.M., Oleson, K.W., Flanner, M.G., Thornton, P.E., Swenson, S.C., Lawrence, P.J., Zeng, X., Yang, Z.-L., Levis, S., Sakaguchi, K., Bonan, G.B., Slater, A.G., 2011. Parameterization improvements and functional and structural advances in version 4 of the community land model. Journal of Advances in Modeling Earth Systems 3, M03001.

Lee, A., Schade, G.W., Holzinger, R., Goldstein, A.H., 2005. A comparison of new measurements of total monoterpene flux with improved measurements of speciated monoterpene flux. Atmospheric Chemistry and Physics 5, 505-513.

Lee, G., You, S., Ritchie, S.G., Saphores, J.-D., Jayakrishnan, R., Ogunseitan, O., 2012. Assessing air quality and health benefits of the clean truck program in the Alameda corridor, CA. Transportation Research Part A: Policy and Practice 46, 1177-1193.

Leuchner, M., Rappenglück, B., 2010. VOC source–receptor relationships in Houston during TexAQS-II. Atmos. Environ. 44, 4056-4067.

Li, G., Zhang, R., Fan, J., Tie, X., 2007. Impacts of biogenic emissions on photochemical ozone production in Houston, Texas. Journal of Geophysical Research: Atmospheres 112, D10309.

Mandal, P.K., 2005. Dioxin: A review of its environmental effects and its aryl hydrocarbon receptor biology. Journal of Comparative Physiology B: Biochemical, Systemic, and Environmental Physiology 175, 221-230.

McGaughey, G.R., Desai, N.R., Allen, D.T., Seila, R.L., Lonneman, W.A., Fraser, M.P., Harley, R.A., Pollack, A.K., Ivy, J.M., Price, J.H., 2004. Analysis of motor vehicle emissions in a Houston tunnel during the Texas Air Quality Study 2000. Atmos. Environ. 38, 3363-3372.

McKeen, S., Grell, G., Peckham, S., Wilczak, J., Djalalova, I., Hsie, E.Y., Frost, G., Peischl, J., Schwarz, J., Spackman, R., Holloway, J., de Gouw, J., Warneke, C., Gong, W., Bouchet, V., Gaudreault, S., Racine, J., McHenry, J., McQueen, J., Lee, P., Tang, Y., Carmichael, G.R., Mathur, R., 2009. An evaluation of real-time air quality forecasts and their urban emissions over eastern Texas during the summer of 2006 second Texas air quality study field study. Journal of Geophysical Research: Atmospheres 114, D00F11.

Miller, S.M., Matross, D.M., Andrews, A.E., Millet, D.B., Longo, M., Gottlieb, E.W., Hirsch, A.I., Gerbig, C., Lin, J.C., Daube, B.C., Hudman, R.C., Dias, P.L.S., Chow, V.Y., Wofsy, S.C., 2008. Sources of carbon monoxide and formaldehyde in North America determined from high-resolution atmospheric data. Atmospheric Chemistry and Physics 8, 7673-7696.

Mills, N.J., 2007. Foamed thermoplastics: Microstructure and processing. Butterworth-Heinemann, Oxford.

Moore, D.S., McCabe, G.P., 1999. Introduction to the pratice of statistics, 3rd ed. W. H. Freeman, New York.

Nam, J., Kimura, Y., Vizuete, W., Murphy, C., Allen, D.T., 2006. Modeling the impacts of emission events on ozone formation in Houston, Texas. Atmos. Environ. 40, 5329-5341.

Ngan, F., Byun, D., Kim, H., Lee, D., Rappengluck, B., Pour-Biazar, A., 2012. Performance assessment of retrospective meteorological inputs for use in air quality modeling during TexAQS 2006. Atmos. Environ. 54, 86-96.

Norris, G.A., R. Vedantham, K. Wade, P. Zhan, S. Brown, P. Pentti, S. I. Eberly, and C. Foley, 2009. Guidance document for PMF applications with the multilinear engine. U.S. Environmental Protection Agency, Washington, District of Columbia.

Pacifico, F., Harrison, S.P., Jones, C.D., Sitch, S., 2009. Isoprene emissions and climate. Atmos. Environ. 43, 6121-6135.

Park, C., Schade, G.W., Boedeker, I., 2010. Flux measurements of volatile organic compounds by the relaxed eddy accumulation method combined with a GC-FID system in urban Houston, Texas. Atmos. Environ. 44, 2605-2614.

Park, C., Schade, G.W., Boedeker, I., 2011. Characteristics of the flux of isoprene and its oxidation products in an urban area. Journal of Geophysical Research: Atmospheres 116, D21303.

Parrish, D.D., 2006. Critical evaluation of US on-road vehicle emission inventories. Atmos. Environ. 40, 2288-2300.

Pfister, G.G., Emmons, L.K., Hess, P.G., Lamarque, J.F., Orlando, J.J., Walters, S., Guenther, A., Palmer, P.I., Lawrence, P.J., 2008. Contribution of isoprene to chemical budgets: A model tracer study with the NCAR CTM MOZART-4. Journal of Geophysical Research: Atmospheres 113, D05308.

Pierce, T., Geron, C., Bender, L., Dennis, R., Tonnesen, G., Guenther, A., 1998. Influence of increased isoprene emissions on regional ozone modeling. Journal of Geophysical Research: Atmospheres 103, 25611-25629.

Pierce, T.E., Waldruff, P.S., 1991. PC-BEIS: A personal computer version of the biogenic emissions inventory system. Journal of the Air & Waste Management Association 41, 937-941.

Polissar, A.V., Hopke, P.K., Paatero, P., Malm, W.C., Sisler, J.F., 1998. Atmospheric aerosol over Alaska: 2. Elemental composition and sources. Journal of Geophysical Research: Atmospheres 103, 19045-19057.

Polissar, A.V., Hopke, P.K., Poirot, R.L., 2001. Atmospheric aerosol over Vermont: Chemical composition and sources. Environmental Science & Technology 35, 4604-4621.

Potosnak, M.J., LeStourgeon, L., Pallardy, S.G., Hosman, K.P., Gu, L., Karl, T., Geron, C., Guenther, A.B., 2014. Observed and modeled ecosystem isoprene fluxes from an oak-dominated temperate forest and the influence of drought stress. Atmos. Environ. 84, 314-322.

Poulter, B., Ciais, P., Hodson, E., Lischke, H., Maignan, F., Plummer, S., Zimmermann, N.E., 2011. Plant functional type mapping for earth system models. Geoscientific Model Development 4, 993-1010.

Quigley, C.J., 2007. Refueling and evaporative emissions of volatile organic compounds from gasoline powered motor vehicles, Civil Engineering. University of Texas, Austin, p. 198.

Ramadan, Z., Eickhout, B., Song, X.-H., Buydens, L.M.C., Hopke, P.K., 2003. Comparison of positive matrix factorization and multilinear engine for the source apportionment of particulate pollutants. Chemometrics and Intelligent Laboratory Systems 66, 15-28.

Rao, K.S., 2002. ROADWAY-2: A model for pollutant dispersion near highways. Water, Air, & Soil Pollution: Focus 2, 261-277.

Rappenglück, B., Lubertino, G., Alvarez, S., Golovko, J., Czader, B., Ackermann, L., 2013. Radical precursors and related species from traffic as observed and modeled at an urban highway junction. Journal of the Air & Waste Management Association 63, 1270-1286.

Reid, S.B., Chinkin, L.R., Penfold, B.M., Gilliland, E.K., 2000. Emissions inventory validation and improvement: A central California case study. Sonama Technology, Inc., Petaluma, California.

Roy, S., Hegde, M.S., Madras, G., 2009. Catalysis for NOx abatement. Applied Energy 86, 2283-2297.

Rubin, J.I., Kean, A.J., Harley, R.A., Millet, D.B., Goldstein, A.H., 2006. Temperature dependence of volatile organic compound evaporative emissions from motor vehicles. Journal of Geophysical Research: Atmospheres 111, D03305.

Sahlodin, A.M., Sotudeh-Gharebagh, R., Zhu, Y., 2007. Modeling of dispersion near roadways based on the vehicle-induced turbulence concept. Atmos. Environ. 41, 92-102.

Samet, J.M., Dominici, F., Curriero, F.C., Coursac, I., Zeger, S.L., 2000. Fine particulate air pollution and mortality in 20 US Cities, 1987-1994. N. Engl. J. Med. 343, 1742-1749.

Schauer, J.J., Rogge, W.F., Hildemann, L.M., Mazurek, M.A., Cass, G.R., Simoneit, B.R.T., 1996. Source apportionment of airborne particulate matter using organic compounds as tracers. Atmos. Environ. 30, 3837-3855.

Scora, G., Barth, M., 2006. Comprehensive modal emissions model(CHEM), version 3.01. University of California, Riverside, California.

Seigneur, C., Pun, B., Pai, P., Louis, J.-F., Solomon, P., Emery, C., Morris, R., Zahniser, M., Worsnop, D., Koutrakis, P., White, W., Tombach, I., 2000. Guidance for the performance evaluation of three-dimensional air quality modeling systems for particulate matter and visibility. Journal of the Air & Waste Management Association 50, 588-599.

Seinfeld, J.H., Pandis, S.N., 2006. Atmospheric chemistry and physics. From air pollution to climate change, 2 ed. John Wiley & Sons,Inc., Hoboken, New Jersey.

Sharkey, T.D., Singsaas, E.L., Lerdau, M.T., Geron, C.D., 1999. Weather effects on isoprene emission capacity and applications in emissions algorithms. Ecological Applications 9, 1132-1137.

Simon, H., Baker, K.R., Phillips, S., 2012. Compilation and interpretation of photochemical model performance statistics published between 2006 and 2012. Atmos. Environ. 61, 124-139.

Simon, H., Phillips, S., Possiel, N., Pouliot, G., Koupal, J., Zubrow, A., Eyth, A., Mason, R., 2011. Evaluation of CMAQ NOx performance using onroad vehicle emissions inputs from two mobile source emissions models, 2011 CMAS Conference, the Friday Center, UNC-Chapel Hill, North Carolina.

Singer, B.C., Harley, R.A., Littlejohn, D., Ho, J., Vo, T., 1998. Scaling of infrared remote sensor hydrocarbon measurements for motor vehicle emission inventory calculations. Environmental Science & Technology 32, 3241-3248.

Song, J., Vizuete, W., Chang, S., Allen, D., Kimura, Y., Kemball-Cook, S., Yarwood, G., Kiournourtzoglou, M.A., Atlas, E., Hansel, A., Wisthaler, A., McDonald-Buller, E., 2008. Comparisons of modeled and observed isoprene concentrations in southeast Texas. Atmos. Environ. 42, 1922-1940.

Spirig, C., Neftel, A., Ammann, C., Dommen, J., Grabmer, W., Thielmann, A., Schaub, A., Beauchamp, J., Wisthaler, A., Hansel, A., 2005. Eddy covariance flux measurements of biogenic VOCs during ECHO 2003 using proton transfer reaction mass spectrometry. Atmospheric Chemistry and Physics 5, 465-481.

Tingey, D.T., Manning, M., Grothaus, L.C., Burns, W.F., 1979. The influence of light and temperature on isoprene emission rates from live oak. Physiologia Plantarum 47, 112-118.

USEPA, 2003. User's guide to MOBILE6 and MOBILE6.2. Mobile source emission factor model. U.S. Environmental Protection Agency, Washington, District of Columbia.

USEPA, 2008. EPA positive matrix factorization (PMF) 3.0. Fundamentals and user guide. U.S. Environmental Protection Agency, Research Triangle Park, North Carolina.

USEPA, 2010a. Transportation conformity guidance for quantitative hot-spot analyses in PM2.5 and PM10 nonattainment and maintenance areas. Transportation and Regional Programs Division, Office of Transportation and Air Quality ,U.S. Environmental Protection Agency, Washington, District of Columbia.

USEPA, 2010b. User guide for motor vehicle emission simulator MOVES2010a U.S. Environmental Protection Agency, Washington, District of Columbia.

Uysal, N., Schapira, R.M., 2003. Effects of ozone on lung function and lung diseases. Current Opinion in Pulmonary Medicine 9, 144-150.

Vallamsundar, S., Lin, J., 2011. MOVES Versus MOBILE. Transportation Research Record: Journal of the Transportation Research Board 2233, 27-35.

Vardoulakis, S., Fisher, B.E.A., Pericleous, K., Gonzalez-Flesca, N., 2003. Modelling air quality in street canyons: a review. Atmos. Environ. 37, 155-182.

Velasco, E., Pressley, S., Grivicke, R., Allwine, E., Coons, T., Foster, W., Jobson, B.T., Westberg, H., Ramos, R., Hernandez, F., Molina, L.T., Lamb, B., 2009. Eddy covariance flux measurements of pollutant gases in urban Mexico City. Atmospheric Chemistry and Physics 9, 7325-7342.

Vizuete, W., Kim, B.U., Jeffries, H., Kimura, Y., Allen, D.T., Kioumourtzoglou, M.A., Biton, L., Hendersona, B., 2008. Modeling ozone formation from industrial emission events in Houston, Texas. Atmos. Environ. 42, 7641-7650.

Wallace, H.W., Jobson, B.T., Erickson, M.H., McCoskey, J.K., VanReken, T.M., Lamb, B.K., Vaughan, J.K., Hardy, R.J., Cole, J.L., Strachan, S.M., Zhang, W., 2012. Comparison of wintertime CO to NOx ratios to MOVES and MOBILE6.2 on-road emissions inventories. Atmos. Environ. 63, 289-297.

Wang, Y.J., DenBleyker, A., McDonald-Buller, E., Allen, D., Zhang, K.M., 2011. Modeling the chemical evolution of nitrogen oxides near roadways. Atmos. Environ. 45, 43-52.

Wang, Y.J., Nguyen, M.T., Steffens, J.T., Tong, Z., Wang, Y., Hopke, P.K., Zhang, K.M., 2013. Modeling multi-scale aerosol dynamics and micro-environmental air quality near a large highway intersection using the CTAG model. Science of The Total Environment 443, 375-386.

Warneke, C., de Gouw, J.A., Del Negro, L., Brioude, J., McKeen, S., Stark, H., Kuster, W.C., Goldan, P.D., Trainer, M., Fehsenfeld, F.C., Wiedinmyer, C., Guenther, A.B., Hansel, A., Wisthaler, A., Atlas, E., Holloway, J.S., Ryerson, T.B., Peischl, J., Huey,

L.G., Hanks, A.T.C., 2010. Biogenic emission measurement and inventories determination of biogenic emissions in the eastern United States and Texas and comparison with biogenic emission inventories. Journal of Geophysical Research: Atmospheres 115, D00F18.

Warneke, C., de Gouw, J.A., Goldan, P.D., Kuster, W.C., Williams, E.J., Lerner, B.M., Jakoubek, R., Brown, S.S., Stark, H., Aldener, M., Ravishankara, A.R., Roberts, J.M., Marchewka, M., Bertman, S., Sueper, D.T., McKeen, S.A., Meagher, J.F., Fehsenfeld, F.C., 2004. Comparison of daytime and nighttime oxidation of biogenic and anthropogenic VOCs along the New England coast in summer during New England air quality study 2002. J. Geophys. Res.-Atmos. 109, D10309.

Wegmann, M., Fehrenbach, A., Heimann, S., Fehrenbach, H., Renz, H., Garn, H., Herz, U., 2005. NO2-induced airway inflammation is associated with progressive airflow limitation and development of emphysema-like lesions in C57BL/6 mice. Experimental and Toxicologic Pathology 56, 341-350.

Weiss, M., Bonnel, P., Hummel, R., Provenza, A., Manfredi, U., 2011. On-road emissions of light-duty vehicles in Europe. Environmental Science & Technology 45, 8575-8581.

Wu, C.-f., Larson, T.V., Wu, S.-y., Williamson, J., Westberg, H.H., Liu, L.J.S., 2007. Source apportionment of PM2.5 and selected hazardous air pollutants in Seattle. Science of The Total Environment 386, 42-52.

Xie, Y., Berkowitz, C.M., 2006. The use of positive matrix factorization with conditional probability functions in air quality studies: An application to hydrocarbon emissions in Houston, Texas. Atmos. Environ. 40, 3070-3091.

Yarwood, G., Wilson, G., Shepaed, S., 2002. User's guide to the global biosphere emissions and interactions system (GloBEIS) version3. ENVIRON International Corporation, Novato, California.

Ying, Q., Kleeman, M.J., 2006. Source contributions to the regional distribution of secondary particulate matter in California. Atmos. Environ. 40, 736-752.

Ying, Q., Krishnan, A., 2010. Source contributions of volatile organic compounds to ozone formation in southeast Texas. Journal of Geophysical Research: Atmospheres 115, D17306.

Zavala, M., Herndon, S.C., Slott, R.S., Dunlea, E.J., Marr, L.C., Shorter, J.H., Zahniser, M., Knighton, W.B., Rogers, T.M., Kolb, C.E., Molina, L.T., Molina, M.J., 2006. Characterization of on-road vehicle emissions in the Mexico city metropolitan area using a mobile laboratory in chase and fleet average measurement modes during the MCMA-2003 field campaign. Atmospheric Chemistry and Physics 6, 5129-5142.

Zavala, M., Herndon, S.C., Wood, E.C., Onasch, T.B., Knighton, W.B., Marr, L.C., Kolb, C.E., Molina, L.T., 2009. Evaluation of mobile emissions contributions to Mexico city's emissions inventory using on-road and cross-road emission measurements and ambient data. Atmospheric Chemistry and Physics 9, 6305-6317.

Zhang, H., Li, J., Ying, Q., Guven, B.B., Olaguer, E.P., 2013. Source apportionment of formaldehyde during TexAQS 2006 using a source-oriented chemical transport model. Journal of Geophysical Research: Atmospheres 118, 1525-1535.

Zhang, H., Ying, Q., 2011a. Contributions of local and regional sources of NOx to ozone concentrations in southeast Texas. Atmos. Environ. 45, 2877-2887.

Zhang, H., Ying, Q., 2011b. Secondary organic aerosol formation and source apportionment in southeast Texas. Atmos. Environ. 45, 3217-3227.

Zhang, H., Ying, Q., 2012. Secondary organic aerosol from polycyclic aromatic hydrocarbons in southeast Texas. Atmos. Environ. 55, 279-287.

Zhang, R.Y., Suh, I., Lei, W., Clinkenbeard, A.D., North, S.W., 2000. Kinetic studies of OH-initiated reactions of isoprene. Journal of Geophysical Research-Atmospheres 105, 24627-24635.

Zhu, Y., Hinds, W.C., Kim, S., Shen, S., Sioutas, C., 2002. Study of ultrafine particles near a major highway with heavy-duty diesel traffic. Atmos. Environ. 36, 4323-4335.

Zhu, Y., Pudota, J., Collins, D., Allen, D., Clements, A., DenBleyker, A., Fraser, M., Jia, Y., McDonald-Buller, E., Michel, E., 2009. Air pollutant concentrations near three Texas roadways, Part I: Ultrafine particles. Atmos. Environ. 43, 4513-4522.

APPENDIX A

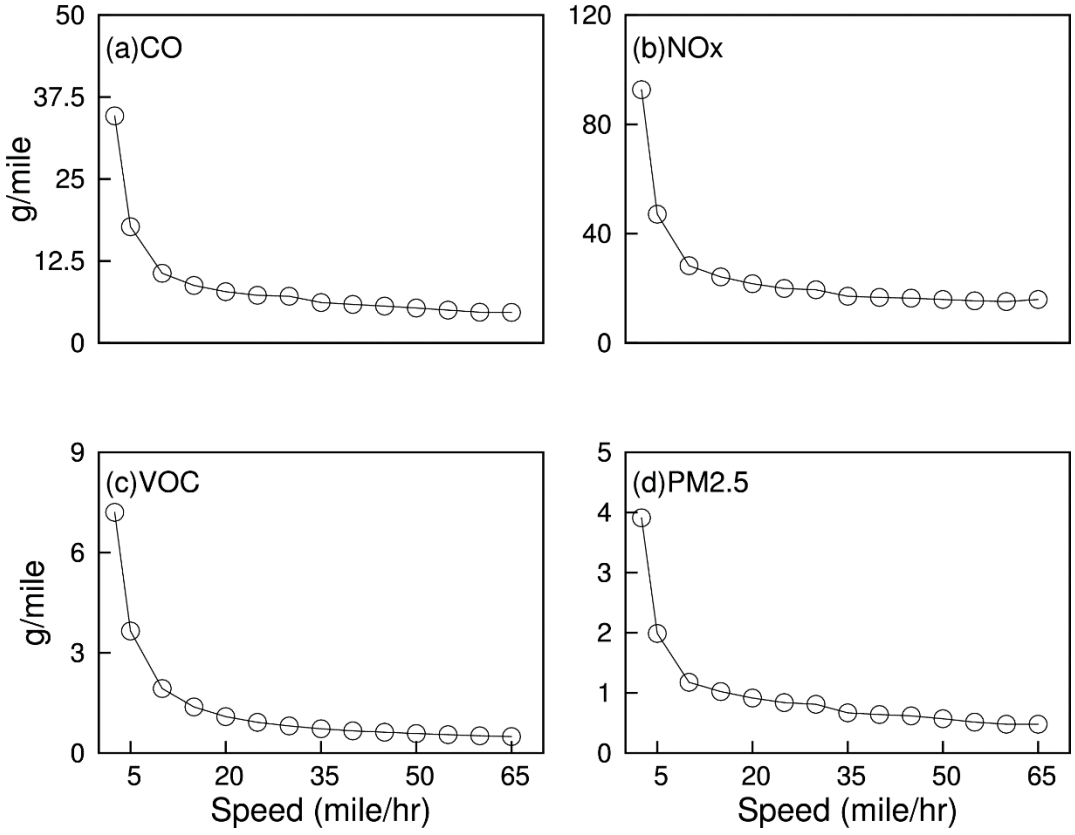

Figure A1 Emission factors for lumped Class B vehicle as a function of vehicle speed based on the 2007 US national fleet from MOVES.

Performance of TAMNROM 3-D under parallel winds in the same field study was evaluated using the NOx observations from Wang et al. (2011). During the simulation episode average wind speed and temperature were 2.71 m s^{-1} and 29.4 ^{0}C respectively. The emissions from roadways were calculated based on an average traffic volume of 12.9 vehicles per minute (28% of which are considered as Class B vehicles) moving at speed of 35 mph during the model episode (Wang et al., 2011). Figure A1 shows the dilution of NO_x with parallel winds (0 degrees) and with near parallel winds (348 degrees). Results indicate that TAMNROM-3D can also well predicts the dilution of pollutants under parallel wind condition.

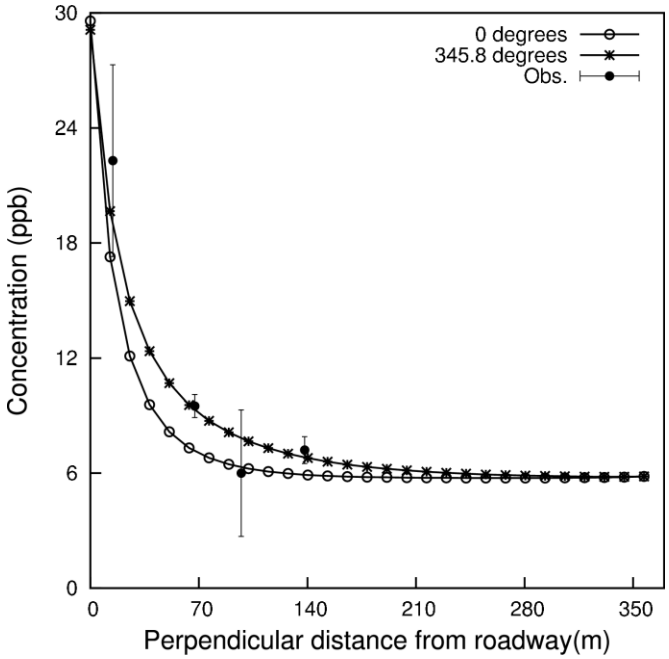

Figure A2 Predicted NO_x as a function of downwind distances for the cases where wind is exactly parallel to roadway and for the case with wind direction 345.8 degrees (from north, the angel between the road and wind direction is 14.2 degrees).

To study the sensitivity of the grid size to results, a new simulation with a horizontal grid size of 2.125×2.125m and a vertical height of 80 m was conducted. The vertical domain was divided into 24 layers with a vertical spacing of grid cells varies from 1 m near the surface to 20 m at the top. Figure A3 (a) shows that surface NO_x profiles in the base case and the higher resolution case are almost identical. Figure A3 (b) shows that using a finer resolution in the vertical direction leads to very small differences in the vertical concentration profile of NO_x.

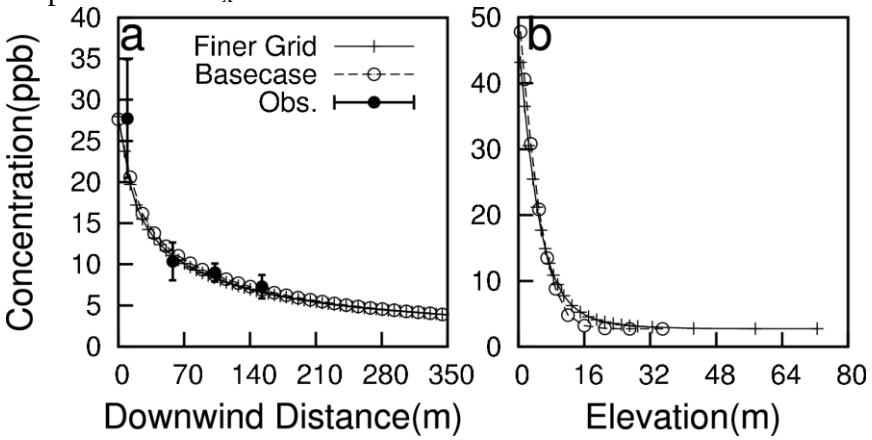

Figure A3 Predicted NOx horizontal (a)and vertical profiles (b) based on the original grid setup and a finer grid.

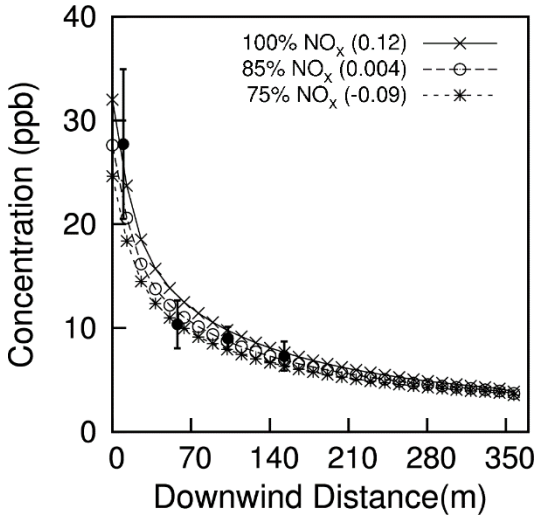

Figure A4 Change in NO_x concentrations as a function of distance for the case with original MOVES emissions (100% NO_x), base case (85% NO_x) and a case where MOVES emission factor has been scaled by 75% (75% NO_x). Mean Fractional Bias (MFB) is included in the brackets. MFB=2(P-O)/(P+O), where P and O are corresponding observation and prediction at a distance.

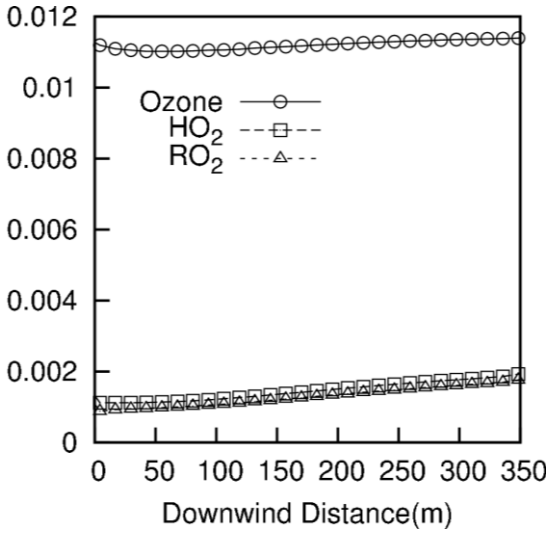

Figure A5 (a) Pseudo first order reaction rate coefficients (k') of NO conversion due to O_3, HO_2 and RO_2 (for X=O_3 and HO_2, k'=k*[X]; for RO_2, $k' = \sum_{i=1}^{n} k_i [RO_{2,i}]$; n is the number of RO_2 radical species in the mechanism, k is the reaction rate of the compounds with NO) as function of downwind distance.

APPENDIX B

B.1 Source Apportionment of Concentration Data

A subset of the concentration data matching the available flux data was used in the analysis. Although the concentration data themselves need not be screened based on u* and non-stationarity as applied to the flux data, selecting matching time periods for the flux and concentration data allows a more reasonable comparison between the concentration and flux source apportionment results.

The concentration data were analyzed using Multilinear Engine version 2 (ME-2) assuming four, five and six factors. In the four-factor model, two profiles (vehicle exhaust and residential and commercial solvent emissions) were not separated. In the six-factor model two similar profiles both identified as consumer and commercial solvent use emissions were observed. The five-factor model (with an f_{peak} value of 1) yielded reasonable source profiles and was used in subsequent analyses. In order to corroborate the ME-2 analysis, the measured concentrations were also analyzed using the Unmix model, which also resulted in the same five sources. Bootstrap analysis was used for both ME-2 and Unmix analyses to ensure the robustness of the chemical composition of the profiles. 100 bootstrap runs with minimum correlation R-value of 0.6 were conducted.

The resultant factor profiles from both multivariate methods are shown in Figure B1. The first source is dominated by C4 alkanes, which accounts for 57% (by mass) of the VOCs in the PMF profile and 49% of the VOCs in the Unmix profile. Both PMF and Unmix profiles match a number of consumer and commercial solvent use emissions VOC profiles in the SPECIATE database (θ=97.5% for PMF profile and θ=95% for Unmix profile). The second source representing emissions from a foam plastics industry is dominated by pentane (C5H12), which accounts for 79% of the VOCs in the PMF profile and 77% of the VOCs in the Unmix profile. The third source predominantly includes toluene (TOLU, 20% of the VOCs in the PMF profile and 16% of the VOCs in the Unmix profile) and m/p xylenes (MPXYL, 25% and 15% of VOCs in the PMF and Unmix profiles, respectively). In addition to toluene and m/p-xylenes, the profiles also have a significant amount of benzene (BENZ), ethylbenzene (EBENZ) and o-xylene (OXYL). The profiles match several similar vehicle exhaust profiles in the SPECIATE database (θ=94% for PMF and 95% for Unmix). The fourth source matches with several similar evaporative fuel emissions profiles in the SPECIATE database (θ=91.8% for PMF and 92% for Unmix). This profile is dominated by isopentane, (IC5H12, 19% and 24% of the VOCs in the PMF and Unmix profiles, respectively) and C4 alkanes (18% and 24% of the VOCs in the PMF and Unmix profiles, respectively). The last source includes isoprene (C5H8) as the major VOC species (35% and 17% of the VOCs in ME-2 and Unmix profiles, respectively). The profile matches a biogenic emissions profile in the SPECIATE database (θ=83% for PMF and θ=77% for Unmix).

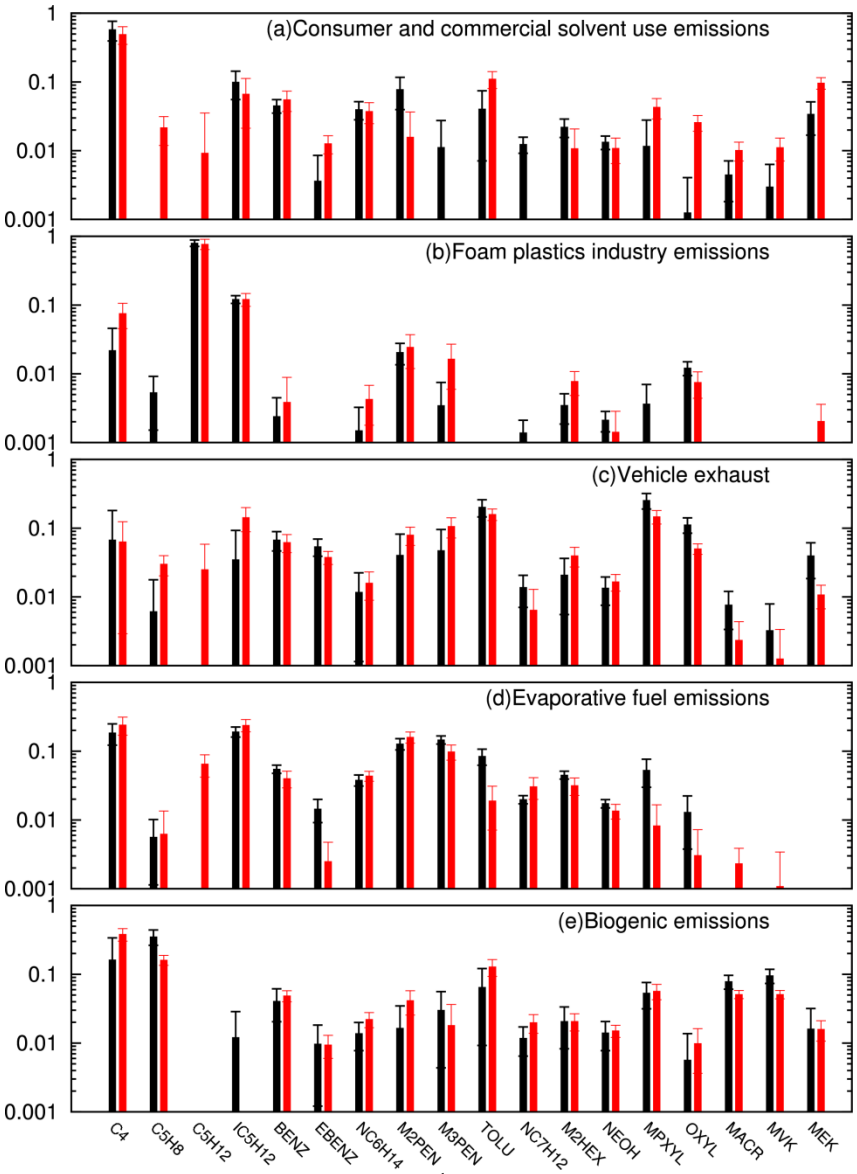

Figure B1: Predicted source profiles (mg mg^{-1}) by ME-2 (black) and Unmix (red) based on the concentration data. Error bars are standard deviations estimated using bootstrap analyses.

A comparison of reconstructed concentrations of species from ME-2 with measured concentrations is shown in Figure B2. In general, the ME-2 model reproduces the observed concentrations well. Table B3 shows normalized mean bias factor (NMBF) and for each VOC species. For species with lower concentrations such as MVK and MACR, a slight under-prediction is observed. That is expected as these species are mostly secondary products from isoprene oxidation, and their formation rates vary by different emissions as driven by meteorological conditions.

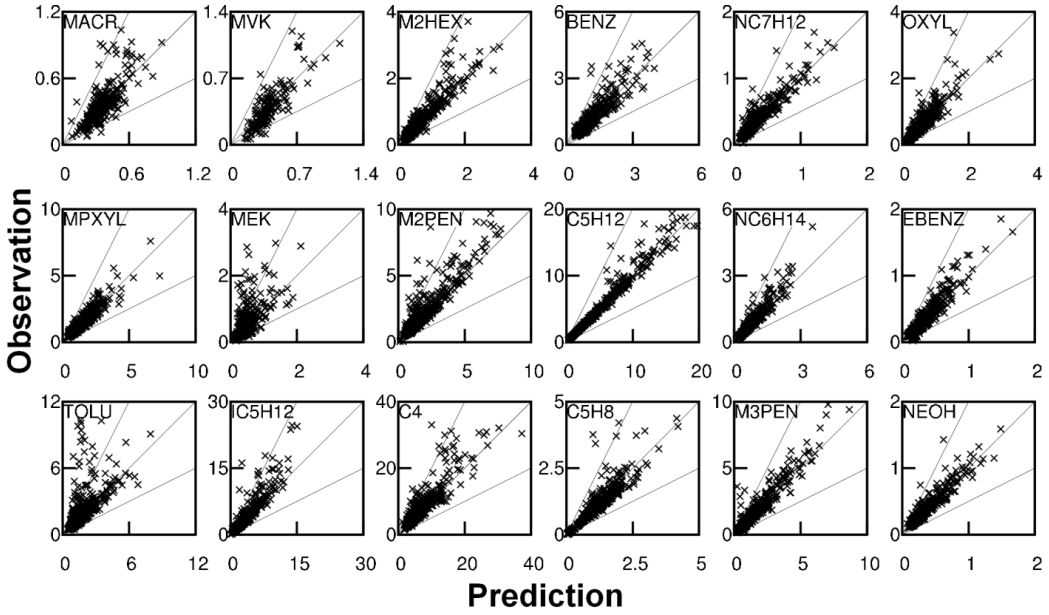

Figure B2: ME-2 reconstructed and observed concentrations of VOC species measured at the Yellow Cab Tower. Units are μg/m^3.

Table B1 shows the percentage of missing fluxes and concentrations for each species. Most of the species had less than 20% negative flux data points within the entire data set. The negative fluxes were generally much smaller in magnitude compared to the positive fluxes and were mostly due to noise associated with the measured concentrations in the up and downdrafts. However, some of the absolute values of negative fluxes were significantly negative, and possibly indicative of advective effects due to source heterogeneity.

Table B1 Percentage of negative fluxes and missing fluxes and concentrations

Abbreviation of Species	Percentage of negative fluxes (%)	Percentage of missing* fluxes or concentrations (%)
C4	9.5	1.5
C5H8	13.1	15.1
C5H12	12.9	5
IC5H12	18.1	1.8
BENZ	22.1	0.1
EBENZ	19.8	1.3
NC6H14	17.1	2.3
M2PEN	19.8	2.1
M3PEN	37.8	5.4
TOLU	11.8	1.7
NC7H12	14.9	1.4
M2HEX	19.4	3.4
NEOH	14.6	3.3

MPXYL	9.6	1.4
OXYL	26.5	1.3
MACR	12.3	45.3
MVK	36.3	8.05
MEK	16.5	49.4

Note: Here 'missing' denotes fluxes with one or both of the GC-FID channels had concentration below MDL.

B.2 Selection of the FPEAK parameter for flux data

Different possible FPEAK parameters were explored in this study. As negative FPEAK parameters showed convergence issues (Around 10% of their bootstrap runs did not converge), their results are not shown here. The results of three FPEAK cases 0, 3, 4 and 5 are discussed in detail here. $Q/Q_{expected}$ was 1.12, 1.14, 1.15 and 1.6 for 0, 3, 4 and 5 FPEAK cases respectively. 83.1, 83.8, 83.7 and 83.3% of total VOC was reproduced for 0, 3, 4 and 5 FPEAK cases respectively. From Table B2, it is clear that compared to selected FPEAK case (FPEAK=4) percentage of dominant species are similar with FPEAK 3 and 5 cases, but higher than FPEAK 0. For example, biogenic emissions are dominated by isoprene by 15%, 40%, 44% and 43% for 0, 3, 4 and 5 FPEAK cases respectively. The comparison of predicted and observed fluxes of different species is shown in Table B3. Results indicate that for most of the species normalized mean bias factor (NMBF) for FPEAK 3, 4 and 5 cases were similar, unlike for FPEAK case 0. Only 4 species in FPEAK cases 0 showed better results than selected FPEAK (FPEAK =4) case.

Table B2: Comparison of percentage of dominant species for FPEAK cases 0, 3, 4 and 5

Percentage of dominant species in the source profile	**FPEAK=0**	**FPEAK=3**	**FPEAK=4**	**FPEAK=5**
Consumer and commercial solvent use emissions	28%	42%	43%	43%
Foam Plastic industry emissions	36%	58%	60%	59%
Vehicle exhaust	13%	23%	24%	24%
Evaporative emissions	23%	30%	30%	30%
Biogenic emissions	15%	40%	44%	43%

Table B3 Normalized Mean Bias Factor (NMBF), calculated for different species for five factor solution. NMBF for FPEAK values of 0, 3, 4 and 5 are shown.

Abbreviation	Fpeak=0	Fpeak=3	Fpeak=4	Fpeak=5
C4	-0.36	-0.34	-0.34	-0.34
C5H8	-0.06	-0.02	-0.02	-0.02
C5H12	-0.16	-0.17	-0.19	-0.21
IC5H12	-0.1	-0.1	-0.1	-0.1
BENZ	-0.38	-0.38	-0.38	-0.38
EBENZ	-0.08	-0.07	-0.07	-0.07
NC6H14	-0.1	-0.09	-0.08	-009
M2PEN	-0.01	-0.003	-0.002	-0.004
M3PEN	-0.26	-0.26	-0.25	-0.25
TOLU	-0.41	-0.42	-0.42	-0.43
NC7H12	-0.12	-0.12	-0.12	-0.13
M2HEX	-0.07	-0.06	-0.06	-0.06
NEOH	-0.07	-0.06	-0.05	-0.06
MPXYL	-0.1	-0.08	-0.08	-0.09
OXYL	0.003	0.007	0.008	0.008
MACR	-0.97	-0.9	-0.89	-0.9
MVK	-3.6	-3.4	-3.4	-3.4
MEK	-0.5	-0.47	-0.47	-0.48

***** Definitions and brief explanations of NMBF can be found in the paragraph below Table B5.

B.3 Comparison of concentration and flux source apportionment results

Table B4 Matching profile names, profile id in parentheses, in the SPECIATE 4.2 database for concentration and flux data along with their θ values.

Source	Concentration	Flux
Consumer and commercial solvent use emissions	Consumer and commercial products: Household products (8514); θ=97.5% Consumer and Commercial Products: Household Products (8511); θ=97.5% Consumer and Commercial Products: Household Products: Hard Surface Cleaners (8512); θ=97.4% Consumer and Commercial Products: Personal Care Products (8501); θ=97.3% Consumer and Commercial Products: Miscellaneous Products (8531); θ=97.3%	Consumer and commercial products: Household products (8514); θ=97.4% Consumer products: Rubber and vinyl protectants (3021); θ=97.3% Consumer products: Household products (3146); θ=97.1% Consumer products: Personal care products (3147); θ=96.9% Consumer and commercial products:

		Household products (8512); θ=96.9% Consumer and commercial products: Miscellaneous products (8539); θ=96.9%
Foam plastics industry emissions source	Pentane* (1198); θ=100%	Pentane (1198); θ=100%
Vehicle tailpipe exhaust	Vehicle exhaust (2492); θ=94.1% Vehicle Exhaust (2510); θ=91.8% Vehicle Exhaust (2499); θ=90.7% Vehicle Exhaust (2520); θ=90.3% Light-Duty Gasoline Vehicles – Exhaust (1203); θ=89.4%	Vehicle exhaust (2510);θ=91.8% Light-Duty Gasoline Vehicles – Exhaust (1203); θ=90% Vehicle Exhaust (2492); θ=88.2% Vehicle Exhaust (2499); θ=87.5% Vehicle Exhaust (2491); θ=86%
Evaporative emissions	Gasoline headspace vapor-Exxon Grade 93 (4471); θ=91.8% Gasoline Headspace Vapor - Shell Grade 93 (8571); θ=90.4% Gasoline Headspace Vapor - Circle K Grade 93 (8614); θ=89.8% Gasoline Headspace Vapor - Exxon Grade 89 (4530); θ=89.3% Gasoline Headspace Vapor – Super America Grade 87 (4503); θ=89.3%	Gasoline vapor 'Hot-Soak' (2452), θ=93.6% Gasoline headspace vapor-Conoco grade 89 (8550), θ=92.3% Gasoline headspace vapor-Shell grade 89 (4482), θ=91.0% Gasoline Headspace Vapor - Exxon Grade 89 (8541); θ=90.1% Gasoline Headspace Vapor - Chevron Grade 89 (8541); θ=89%
Biogenic emissions	Isoprene (1148); θ=83%	Isoprene (1148); θ=91%

Note: In the 'pentane' profile (1198), pentane is the only species.

Table B5 Normalized mean bias factor (NMBF) and normalized mean absolute error factor (NMAEF) calculated for different species.

Abbreviation	**Concentration**		**Flux**	
	NMBF	NMAEF	NMBF	NMAEF
C4	-0.08	0.19	-0.34	0.70
C5H8	0.07	0.18	-0.02	0.17
C5H12	-0.40	0.08	-0.19	0.28
IC5H12	-0.15	0.22	-0.10	0.58
BENZ	-0.08	0.18	-0.38	0.89
EBENZ	-0.06	0.18	-0.07	0.58
NC6H14	-0.07	0.16	-0.08	0.44
M2PEN	-0.13	0.21	-0.002	0.56
M3PEN	-0.08	0.17	-0.25	0.45
TOLU	-0.16	0.28	-0.42	0.74
NC7H12	-0.08	0.18	-0.12	0.55
M2HEX	-0.05	0.15	-0.06	0.43
NEOH	-0.03	0.13	-0.05	0.32
MPXYL	-0.03	0.17	-0.08	0.40
OXYL	-0.07	0.23	0.008	0.74
MACR	0.002	0.21	-0.89	1.20
MVK	-0.003	0.26	-3.40	10.6
MEK	-0.22	0.45	-0.47	1.00

Definitions and interpretation of NMBF and NMAEF

$$NMBF = \begin{cases} \left|\bar{P}/\bar{O}\right| - 1 & \text{if } \left|\bar{P}\right| \geq \left|\bar{O}\right| \\ 1 - \left|\bar{O}/\bar{P}\right| & \text{if } \left|\bar{P}\right| < \left|\bar{O}\right| \end{cases}$$

$$NMAEF = \begin{cases} \left|\overline{P-O}\right| \Big/ \left|\bar{O}\right| & \text{if } \left|\bar{P}\right| \geq \left|\bar{O}\right| \\ \left|\overline{P-O}\right| \Big/ \left|\bar{P}\right| & \text{if } \left|\bar{P}\right| < \left|\bar{O}\right| \end{cases}$$

The above definitions are valid when $\left|\bar{P}\right| / \left|\bar{O}\right| = \bar{P} / \bar{O}$, i.e. the signs of predicted mean ($\bar{P}$) and observed mean ($\bar{O}$) should be the same. If the signs are different, NMBF and NMAEF are undefined. This did not occur for any species in the current study. The sign of NMBF indicates whether $\bar{P}$ is under (<0) or overestimated (>0) relative to the observed mean ($\bar{O}$). The magnitude of NMBF indicates the factor of the under or overestimation. NMAEF is always positive and varies from 0 to ∞. It represents the ratio of the mean absolute gross error and mean prediction or observation. Based on NMBF and NMAEF in Table B5, both observed concentrations and fluxes were under-predicted by ME-2 analysis. While the NMBF for concentration and flux data are similar for many species, flux data in general have larger NMAEF values. This is reflected by

more scattered data shown in figure 19 for fluxes than data in Figure B2 for concentrations.

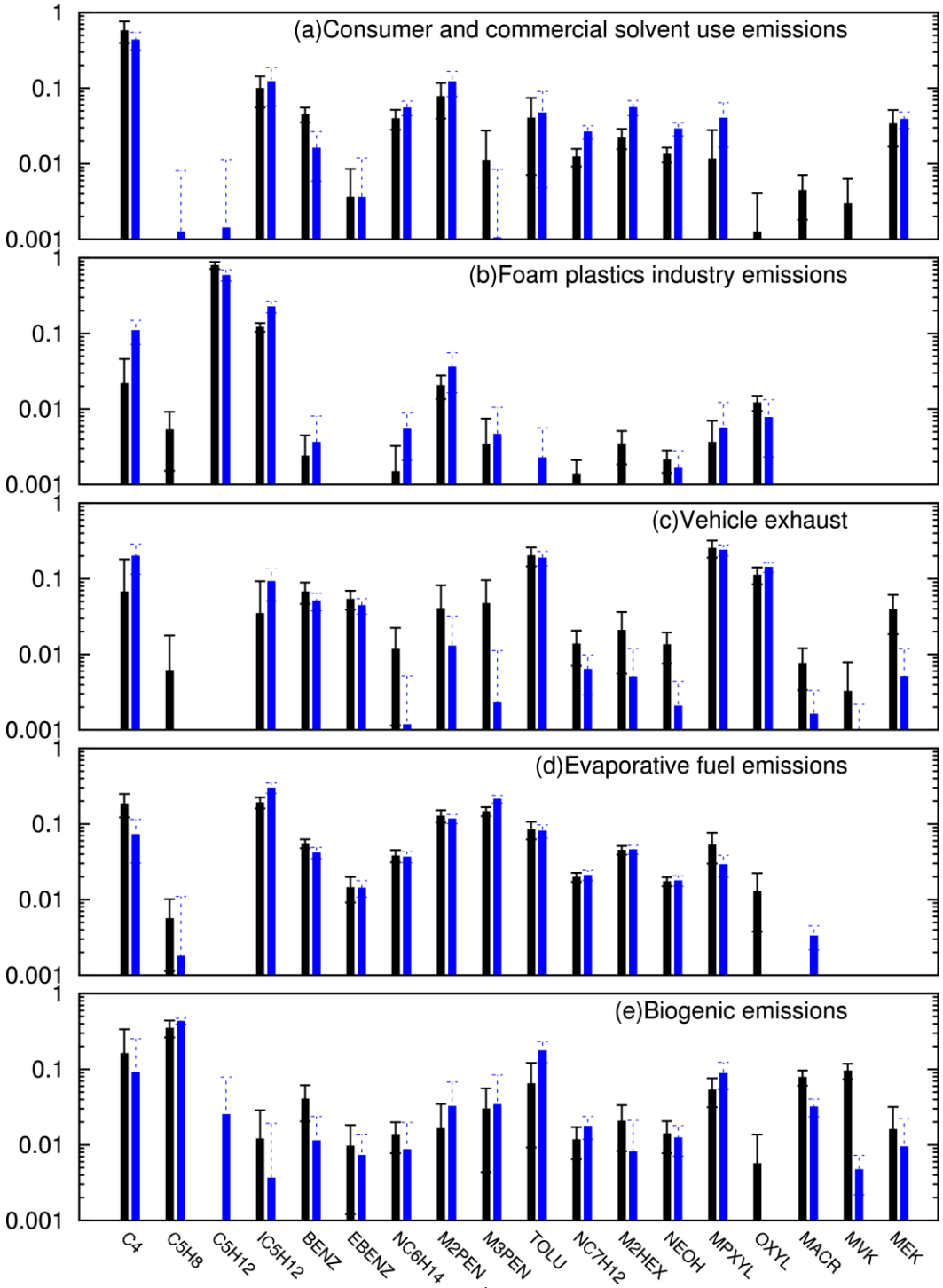

Figure B3: Predicted source profiles (mg mg^{-1}) for concentrations (black) and fluxes (blue). Error bars are standard deviations estimated using bootstrap analyses.

Table B6 shows a comparison of the average relative contributions of each source to total VOCs for the flux and concentration data. Contributions due to biogenic, consumer and commercial solvent use emissions and vehicle exhaust were quite similar. For the concentration data, evaporative emissions have higher contributions than the foam plastics industry emissions but for the flux data the foam plastics industry source has higher contributions. This is an expected result since the foam plastics industry source is a localized point source (and of known location) in the tower's footprint, while the evaporative source is a large area source, likely to be found all over Houston.

Table B6 Comparison of average relative contributions of each source (percentage) to total VOCs for concentration and flux data.

Source	Concentration	Flux
Consumer and commercial solvent use emissions	27.8%	21.5%
Foam plastics industry emissions	23%	32%
Vehicle exhaust	8.8%	12%
Evaporative emissions	30.5%	23.3%
Biogenic emissions	10%	11.2%

B.4 More details on evaporative emissions

B.4.1 Emissions from gasoline transport facility

A gasoline transport company approximately 1.2 km to the east of the sampling site (Figure 17) operates gasoline transport trucks that accumulate 30-40 trips per day, and might also contribute to the measured flux at YCT. Each truck can transport approximately 33 m^3 of fuel. The evaporation of gasoline during refueling of these trucks, estimated using the US EPA's Air Pollutant Emission factors (AP-42) (http://www.epa.gov/ttn/chief/ap42/index.html) for refueling losses, is 212 mg L^{-1}. Flux-footprint values were used to calculate the contributions to the measured flux at the tower.

B.4.2 Emission from fuel service stations

There are two fuel service stations (gas stations), located at 480 m NNE and 1380 m SE of the tower, as shown in Figure 17. It was estimated that an average of 4000 gallons of fuel was sold per day, according to National Association of Convenience and Refueling Stores annual report 2011. Assuming 167 gallons of fuel per hour were sold in those stations, however, only a decrease of less than 1% was observed in the vehicle evaporative emission factor.

B.4.3 Parked vehicle density

If the parked vehicle density in other areas was higher than what was expected, the evaporative emission factors would accordingly be lower. However, it would require a vehicle density of more than 40 vehicles per grid cell to arrive at an emission factor on the order of 0.4 g h^{-1} $vehicle^{-1}$. Such a high density of vehicles (approximately two times higher than vehicle density in the YC parking lots) in the surrounding area is unrealistic.

B.5 Other Supporting Data

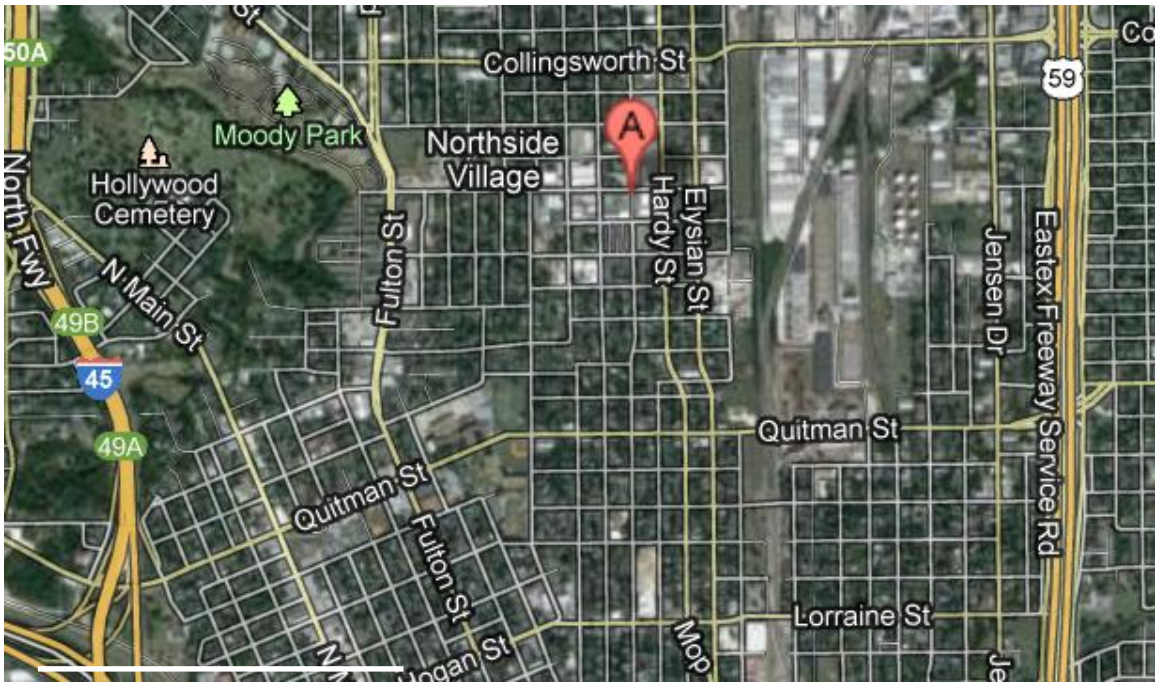

Figure B4: Yellow Cab Tower (YCT) and surround areas (Google Map image). White line on the figure represents approximately 1 km. 'A' is the location of YCT.

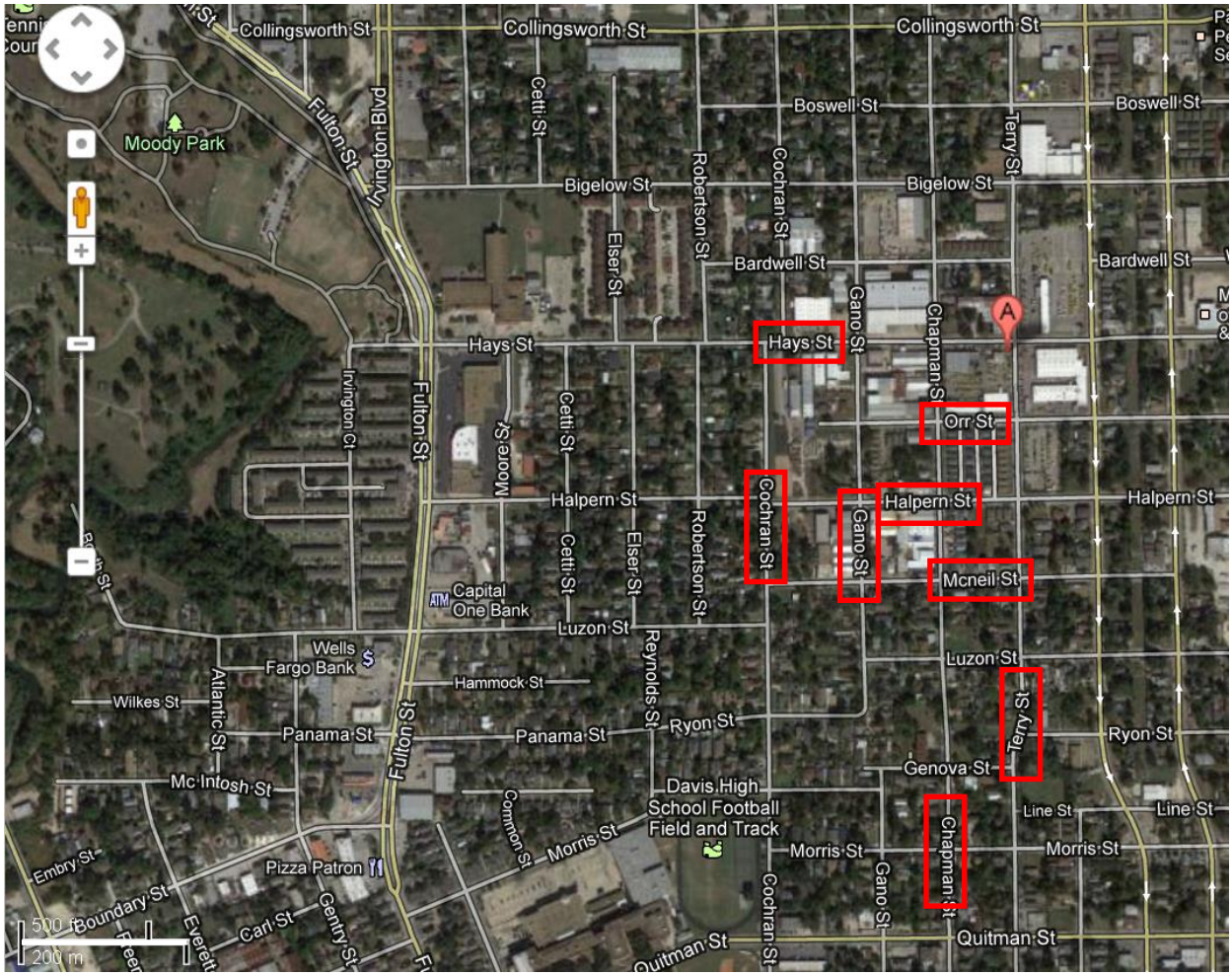

Figure B5: Local streets (marked with red boxes) included in the vehicle exhaust emission factor calculation (Google Map image). 'A' represents the Yellow Cab Tower. Streets with north/south bound traffic arrows are Elysian and Hardy, respectively. Collingsworth and Quitman are near the north and south boundary of the figure. White bar in the lower-left represents approximately 200 m.

Table B7 Mean and standard deviation (SD) of number of vehicles observed, on weekdays, during March and November 2011 as a function of time for Elysian, Hardy, Quitman, Collingworth and Hays streets.

	Elysian		**Hardy**		**Quitman**		**Collingsworth**		**Hays**	
Hour	Mean	SD	Mean	SD	Mean	SD	Mean	SD	Mean	SD
0	23	5	26	5	28	4	30	12	12	4
1	15	11	12	3	16	5	23	11	8	3
2	13	7	10	3	15	5	20	6	6	2
3	10	4	12	3	12	4	23	10	7	3
4	16	5	22	5	25	9	25	6	12	6
5	39	10	67	14	71	13	65	23	47	8
6	87	7	281	52	173	12	133	42	64	7
7	182	26	845	149	453	71	233	71	288	60
8	148	11	610	108	306	26	187	32	109	17
9	139	9	233	39	237	15	177	19	108	7
10	154	11	170	26	217	30	169	44	110	11
11	180	10	177	34	223	19	203	56	120	12
12	198	16	196	33	241	25	272	31	168	36
13	202	13	194	30	245	35	233	13	122	10
14	235	24	194	32	229	24	238	24	136	19
15	378	34	280	45	308	32	279	32	248	27
16	533	35	256	38	292	43	317	35	185	20
17	646	108	264	43	363	28	323	39	178	17
18	340	85	224	36	333	25	270	34	177	18
19	183	25	167	25	246	30	210	47	129	12
20	105	27	125	19	178	17	156	37	90	11
21	96	26	95	14	122	11	127	30	65	11
22	74	22	74	12	83	12	101	28	50	11
23	53	17	43	13	59	12	67	23	32	6

Table B8 Mean and standard deviation (SD) of number of vehicles observed, on weekends, during March and November 2011 as a function of time for Elysian, Hardy, Quitman, Collingworth and Hays streets.

	Elysian		**Hardy**		**Quitman**		**Collingsworth**		**Hays**	
Hour	Mean	SD	Mean	SD	Mean	SD	Mean	SD	Mean	SD
0	57	13	53	10	77	14	54	10	28	2
1	40	18	38	7	49	12	44	7	17	4
2	51	25	33	6	46	15	44	5	17	7
3	23	5	21	4	25	4	23	4	17	4
4	18	4	16	4	21	4	18	4	7	2
5	24	5	30	7	36	6	33	9	20	7
6	35	8	57	13	69	14	55	20	23	5
7	62	20	91	23	144	36	83	20	32	8
8	87	13	101	21	184	22	122	15	51	13
9	112	13	129	23	226	17	165	17	76	25
10	125	6	143	27	219	12	203	15	77	21
11	133	19	149	29	235	29	221	12	89	18
12	156	43	163	30	261	41	227	23	97	17
13	153	48	168	25	258	41	236	15	97	15
14	156	47	173	29	241	50	237	24	102	23
15	150	52	160	29	242	37	239	13	109	19
1**6**	154	30	161	28	255	43	259	13	105	18
17	165	21	163	27	247	12	243	17	106	20
18	146	22	163	27	262	14	231	24	93	10
19	131	17	132	19	238	11	187	17	87	10
20	106	7	121	18	189	15	154	21	70	13
21	94	19	111	17	146	11	143	9	68	17
22	87	24	111	17	126	22	102	16	45	11
23	67	16	73	15	79	19	71	16	27	10

Table B9 Mean and standard deviation (SD) of observed vehicle speeds (m s^{-1}) on weekdays during March and November 2011 as a function of time for Elysian, Hardy, Quitman, Collingworth and Hays streets.

	Elysian		**Hardy**		**Quitman**		**Collingsworth**		**Hays**	
Hour	Mean	SD	Mean	SD	Mean	SD	Mean	SD	Mean	SD
0	15.6	3.6	14.4	3.6	10.4	2.5	13.4	2.3	12.9	4.7
1	15.2	3.7	14.3	3.8	10.3	1.9	12.2	3.1	12.3	3.0
2	15.1	3.4	14.5	4.1	10.1	1.7	10.6	3.8	12.8	2.9
3	16.1	2.8	14.1	3.7	10.8	2.6	11.4	4.7	11.5	4.1
4	15.4	3.2	14.9	3.5	10.1	2.4	13.2	2.5	13.7	3.0
5	14.7	4.1	15.0	3.9	10.3	2.5	14.4	2.2	14.1	2.7
6	16.0	3.2	16.6	3.4	10.1	2.5	13.4	2.0	12.3	3.1
7	15.7	3.3	16.9	3.1	9.1	2.4	11.0	2.3	10.8	2.9
8	15.7	3.2	16.6	3.0	9.7	2.6	12.5	2.5	12.0	3.0
9	15.6	3.2	16.6	3.3	9.7	2.3	13.0	2.2	11.8	2.9
10	15.6	3.1	15.8	3.5	9.7	2.2	12.7	2.5	11.7	2.9
11	15.7	3.0	15.0	3.5	10.1	2.1	12.8	2.5	11.9	3.2
12	15.8	2.8	14.8	3.2	10.1	2.0	12.9	2.2	11.5	2.8
13	16.1	3.1	14.9	3.4	9.8	2.1	12.9	2.4	11.8	2.6
14	16.1	3.1	15.2	3.3	10.1	2.0	12.2	2.6	12.0	2.8
15	16.2	2.8	15.1	3.5	9.4	2.1	11.4	2.5	10.4	2.6
16	16.9	2.6	15.1	3.1	9.8	2.1	11.2	3.1	11.8	2.9
17	16.8	2.4	15.0	3.1	9.2	2.2	12.0	2.6	11.7	2.9
18	16.5	2.6	15.2	3.2	9.1	2.1	12.5	2.0	11.8	2.9
19	15.8	2.9	14.8	3.2	9.3	2.0	12.8	2.1	11.9	2.9
20	15.4	3.0	14.2	3.3	9.5	2.0	13.0	2.0	11.6	2.9
21	15.5	3.0	14.2	3.1	9.8	2.0	13.1	2.1	11.9	3.0
22	15.3	3.2	14.3	3.4	10.0	2.1	12.9	2.1	12.1	3.1
23	15.9	2.7	14.6	3.2	10.0	1.9	13.1	2.0	12.2	3.9

Table B10 Mean and standard deviation (SD) of observed vehicle speeds (m s^{-1}) on weekends during March and November 2011 as a function of time for Elysian, Hardy, Quitman, Collingworth and Hays streets.

	Elysian		**Hardy**		**Quitman**		**Collingsworth**		**Hays**	
Hour	Mean	SD	Mean	SD	Mean	SD	Mean	SD	Mean	SD
0	15.5	3.1	14.2	3.4	10.0	2.2	12.8	2.4	11.5	2.4
1	15.2	3.4	15.4	5.0	10.1	2.3	13.2	2.6	11.4	3.2
2	14.8	3.5	15.2	4.4	10.6	1.7	13.6	3.0	12.2	2.0

3	16.1	3.0	15.6	3.2	9.9	1.7	13.1	2.8	13.8	3.3
4	15.4	3.8	14.9	3.9	10.1	2.2	13.5	2.2	11.3	3.2
5	14.7	3.8	13.5	4.6	10.0	2.3	14.2	2.1	13.6	3.4
6	16.2	3.8	15.0	5.1	10.1	2.3	14.0	2.7	13.3	3.6
7	15.7	3.2	15.2	3.6	10.0	2.3	12.9	2.6	12.6	3.5
8	15.7	3.3	15.9	3.2	9.8	2.1	12.8	2.5	11.5	3.7
9	16.0	3.1	15.3	3.4	9.6	2.0	12.7	2.7	11.4	4.3
10	15.7	3.3	15.4	3.6	10.3	2.1	12.7	2.5	11.1	3.5
11	16.0	2.9	14.9	3.3	10.0	1.9	12.6	2.5	11.6	3.0
12	16.1	3.3	14.9	3.6	9.9	2.0	12.3	2.8	11.9	3.3
13	16.0	3.0	14.8	3.4	9.8	2.0	12.6	2.3	11.6	2.7
14	16.2	3.3	15.0	3.1	10.1	2.1	12.5	2.4	12.3	3.4
15	15.9	3.1	14.6	3.5	9.9	2.0	12.7	2.5	12.4	2.8
16	15.8	3.1	14.3	3.5	9.9	2.0	11.3	3.3	12.4	3.1
17	15.8	2.9	15.0	3.2	9.1	2.2	11.5	2.7	12.3	3.3
18	15.6	3.6	15.0	3.4	9.3	2.2	12.6	2.2	12.2	3.6
19	15.5	2.8	14.2	3.2	9.5	2.1	12.7	2.0	11.4	2.7
20	15.4	3.0	14.8	3.1	9.9	2.0	12.5	1.9	11.5	2.7
21	15.7	3.0	14.5	3.2	9.8	2.2	12.9	2.2	11.6	2.6
22	15.6	2.7	14.0	3.6	9.8	2.0	12.8	1.9	12.4	2.7
23	15.1	3.0	14.1	3.3	9.8	2.2	13.1	2.0	11.9	2.7

APPENDIX C

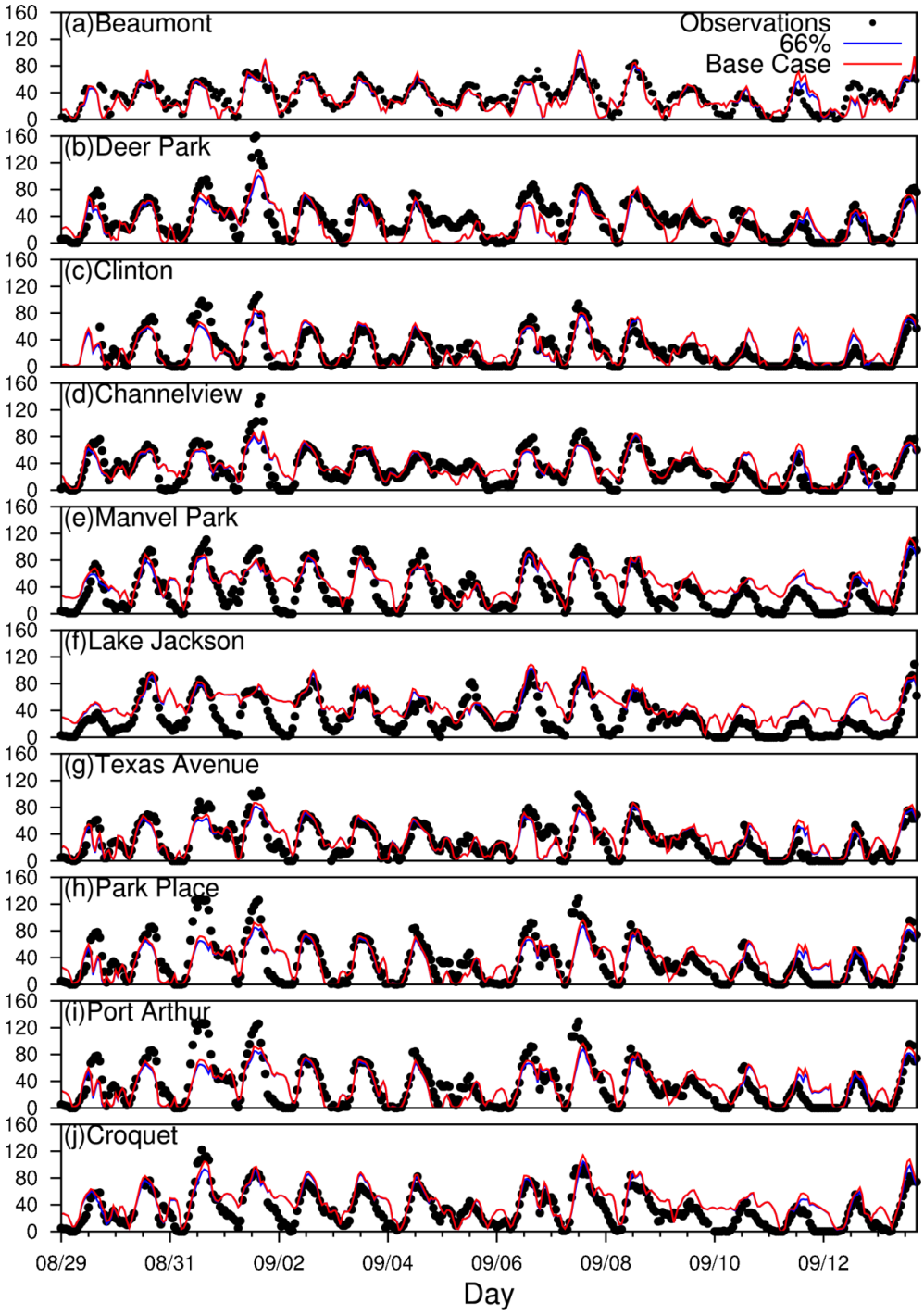

Figure C1 Comparison of predicted and observed hourly concentrations of ozone.

Table C1 Performance statistics of predicted hourly ozone concentrations for base case (BC) and case with biogenic emissions reduced by 66% at TCEQ operated stations.

		MFB		MFE		MNB		MNE	
Site	EPA Site No.	BC	66%	BC	66%	BC	66%	BC	66%
Manvel park	480391004	-0.08	-0.13	0.12	0.15	-0.07	-0.12	0.11	0.14
Lake Jackson	480391016	0.03	-0.02	0.13	0.12	0.04	-0.01	0.13	0.11
Groves	481670014	-0.02	-0.05	0.12	0.13	-0.01	-0.04	0.12	0.12
Aldine	482010024	-0.13	-0.16	0.16	0.18	-0.11	-0.14	0.15	0.16
Channelview	482010026	-0.13	-0.18	0.17	0.20	-0.11	-0.15	0.15	0.18
Northwest Harris	482010029	-0.16	-0.18	0.18	0.19	-0.14	-0.16	0.16	0.17
Houston North	482010046	-0.04	-0.08	0.13	0.14	-0.03	-0.06	0.13	0.13
Lang	482010047	-0.01	-0.05	0.13	0.14	0.01	-0.03	0.13	0.13
Croquet	482010051	0.09	0.03	0.15	0.14	0.11	0.04	0.17	0.15
Pecan valley	482010055	-0.06	-0.12	0.14	0.17	-0.05	-0.10	0.13	0.15
Monroe	482010062	-0.06	-0.13	0.17	0.20	-0.04	-0.10	0.16	0.17
Hou. Westhollow	482010066	-0.07	-0.12	0.15	0.18	-0.05	-0.10	0.14	0.15
Polk Avenue	482010070	-0.18	-0.24	0.23	0.27	-0.14	-0.19	0.19	0.22
Texas Avenue	482010075	-0.11	-0.17	0.17	0.20	-0.09	-0.14	0.16	0.18
Park Place	482010416	-0.24	-0.31	0.27	0.32	-0.19	-0.24	0.22	0.25
Lynchburg	482011015	-0.21	-0.26	0.23	0.26	-0.17	-0.21	0.19	0.21
Hou. East	482011034	-0.15	-0.19	0.19	0.21	-0.12	-0.16	0.17	0.19
Clinton	482011035	-0.19	-0.25	0.21	0.26	-0.16	-0.21	0.18	0.21
Deer Park	482011039	-0.17	-0.24	0.20	0.26	-0.14	-0.20	0.17	0.21
Seabrook	482011050	-0.04	-0.09	0.13	0.14	-0.03	-0.07	0.12	0.13
Beaumont	482450009	-0.05	-0.10	0.18	0.19	-0.02	-0.06	0.17	0.17
Port Arthur	482450011	-0.13	-0.18	0.17	0.20	-0.11	-0.15	0.15	0.17
Jefferson	482450018	0.05	0.02	0.05	0.04	0.05	0.02	0.05	0.04
Hamshire	482450022	-0.11	-0.13	0.15	0.16	-0.09	-0.11	0.14	0.15
Sabine Pass	482450101	-0.06	-0.10	0.14	0.15	-0.04	-0.08	0.13	0.14
SETPRC Port Arthur	482450628	-0.10	-0.16	0.19	0.22	-0.07	-0.12	0.17	0.19
Conroe	483390078	-0.14	-0.14	0.14	0.14	-0.13	-0.13	0.13	0.13
West Orange	483611001	-0.04	-0.06	0.21	0.22	0.01	-0.01	0.22	0.23
Maurice Ville	483611100	-0.02	-0.05	0.13	0.12	-0.01	-0.04	0.13	0.12